UC San Diego

Title

Construction of Dynamic DNA Structures for Drug Delivery

Permalink

Author

Dong, Xiangyi

Publication Date

2021

UNIVERSITY OF CALIFORNIA SAN DIEGO

Construction of Dynamic DNA Structures for Drug Delivery

A dissertation submitted in partial satisfaction of the
requirements for the degree
Doctor of Philosophy

in

Nanoengineering

by

Xiangyi Dong

Committee in charge:

Professor Liangfang Zhang, Chair
Professor Yi Chen, Co-Chair
Professor Shaochen Chen
Professor Stephen Howell
Professor Jerry Yang

2021

The dissertation of Xiangyi Dong is approved, and it is acceptable in quality and form for publication on microfilm and electronically.

University of California San Diego

2021

DEDICATION

This dissertation is dedicated to the researchers, no matter in the college or in industry, who have the common dream to make progress on human life science.

EPIGRAPH

Try to learn something about everything

and everything about something.

—Thomas Henry Huxley

TABLE OF CONTENTS

LIST OF FIGURES

LIST OF TABLES

ACKNOWLEDGEMENTS

I would like to acknowledge Professor Yi Chen for your instructions during my Ph. D study as my advisor and co-chair. I won't forget every time you gave me suggestions and led me on the right way.

I would like to acknowledge Professor Liangfang Zhang for your support and guidance during my Ph. D study as committee chair. Your support encourages me to work through the darkest I have ever met.

I would like to acknowledge my parents for your love, encouragement, and unconditional support through my life and Ph. D study. The encourage you give me provides infinite energy for me to overcome everything.

I would like to acknowledge Pei-Chia Chen for your support during years in my Ph. D study and I learned a lot from you on how to arrange classes and give lectures.

I would also like to acknowledge my lab mates for collaboration on my research, positively help on the difficulties and accompany my Ph. D years.

I would like also to acknowledge to my committee members: Professor Shaochen Chen, Professor Jerry Yang, and Professor Stephen Howell, for all your kind support and advices.

I would like also to acknowledge to my department and the faculty/staff working there, for providing the knowledge that leads me to scientific thinking and research and for helping me through all the problems that I met, especially Dana Jimenez, for all your kind help.

Chapter 1, in part, is a reprint of the publication in Advanced Healthcare Materials, 2018, Chava A; Sibai X; Mingxuan K; Xiangyi Dong; Yi Chen. The dissertation author was the coauthor of this paper.

Chapter 2, in full, has been submitted to Small Method for publication. Xiangyi Dong, Sibai Xie, Mingxuan Kai, Yi Chen. The dissertation author was the primary investigator and author of this paper.

Chapter 3, in full, is currently in the process of manuscripts preparation for publication.

Xiangyi Dong, Jinhyung Lee, Yi Chen. The dissertation author was the primary investigator and co-first author with Jinhyung Lee of this paper.

Chapter 4.1, in part, is currently in the process of manuscripts preparation for publication. Xiangyi Dong, Yi Chen. The dissertation author was the primary investigator and author of this paper.

Chapter 4.2 is a partial of a paper which is submitted for publication. Sibai Xie, Xiangyi Dong, Mingxuan Kai, Yi Chen. The dissertation author was the primary investigator of the simulation part and co-author of this paper.

VITA

2012	B. S. in Materials Science and Engineering, University of Science and Technology Beijing.
2014	M. S. E in Materials Science and Engineering, University of Pennsylvania.
2014-2021	Ph. D. in NanoEngineering, University of California San Diego
2014-2021	Teaching Assistant, University of California San Diego
2014-2021	Research Assistant, University of California San Diego
2018	Ph. D Intern, Regeneron Pharmaceuticals Inc

PUBLICATIONS

Angell, Chava, Mingxuan Kai, Sibai Xie, Xiangyi Dong, and Yi Chen. "Bioderived DNA Nanomachines for Potential Uses in Biosensing, Diagnostics, and Therapeutic Applications.", *Advanced healthcare materials*, 2018.

Xiangyi Dong, Sibai Xie, Mingxuan Kai, Yi Chen. "Virus-mimic pH-responsive DNA nanogel for drug delivery", *Submitted to Small Method*, 2021.

Xiangyi Dong, Yi Chen. "Size-reversible DNA nanogel Triggered by pH for drug delivery", *Manuscript in preparation*, 2021.

Xiangyi Dong, Jinhyung Lee, Yi Chen. "Protein captured DNA nanogel for drug delivery", *Manuscript in preparation*, 2021.

Sibai Xie, Xiangyi Dong, Mingxuan Kai, Yi Chen. "2D-3D reversible transition of DNA nanostructures", *Manuscript in preparation*, 2021.

ABSTRACT OF THE DISSERTATION

Construction of Dynamic DNA Structures for Drug Delivery

by

Xiangyi Dong

Doctor of Philosophy in Nanoengineering

University of California San Diego, 2021

Professor Liangfang Zhang, Chair
Professor Yi Chen, Co-Chair

Deoxyribonucleic acid (DNA) nanotechnology is a novel field that utilizes self-assembling DNA strands to create stable structures, including two-dimensional (2D) and three-dimensional (3D) structures. Dynamic DNA structures could be achieved through accurate design. Previous research has reported two major interactions in nature: the Watson–Crick and the Hoogsteen base pairs. Most DNA structures are based on the Watson–Crick base pair, which could perform a conformational change through strand displacement. Another means of carrying out conformational change is to make use of Hoogsteen bonding, which causes the

C-rich strands to form Hoogsteen bonds under acidic conditions and gives rise to a Watson–Crick interaction under higher pH conditions. DNA nanotechnology offers the advantages of biocompatibility and programmability, which could be utilized in the drug delivery field. Inspired by a pH-triggered virus dissociation during endocytosis, we made use of dynamic DNA structures to design a DNA nanogel system that can serve as a carrier with a pH-triggered release property. This dissertation presents a robust DNA nanogel platform that could load both small molecules like Doxorubicin and large molecules like proteins, with the advantages of easy synthesis, fast pH response, and self-assembly. Instead of the Watson–Crick interaction, we used G-quadruplex secondary structures as cross-linkers to form the DNA nanogel. When a Hoogsteen-related design (i-motif) was integrated, an acid-dissociated DNA nanogel platform was created, which could form a DNA nanogel under physiological conditions while dissociating under acidic conditions. When a triplex structure design was integrated into the framework, a size-reversible DNA nanogel that swells under acidic conditions and shrinks back to normal size under physiological conditions was fabricated. When applied to in vitro cell cytotoxicity experiments, during cellular uptake, the pH decreased to 4–6 during the endocytosis process, which provided the controlled release condition and caused conformational change in the DNA nanogel. This was followed by drug release inside the cell, resulting in higher cytotoxicity to the targeted cancer cell line. Aside from small-molecule drugs like Doxorubicin, our DNA nanogel platform can also capture protein drugs. Compared with the platforms of existing protein-loading methods, the DNA encapsulation of protein provides a novel non-covalent interaction-based method of loading protein drugs, which could preserve the protein function. Moreover, a Watson–Crick interaction-based dynamic DNA structure was investigated to construct a 2D-3D DNA dynamic

structure by importing strand displacement. We successfully investigated the different designs of DNA conformational change. To further study conformation changes at the molecular level, the OxDNA software was used to perform a simulation that consisted of the experimental data and showed the real topology of different conformations. Dynamic DNA structures are highly programmable, easy to modify, and are self-assembling, making them a feasible next-generation drug delivery platform. Modelling may be a useful tool to help predict the structures that are needed for specific drug delivery.

Chapter 1

Introduction

Nanotechnology is utilized in the medical field to overcome inherent difficulties within traditional medicine. Various nanoparticle drug delivery platforms [1] have been investigated, such as quantum dots, nanotubes, 2-D materials, polymers, liposomes, inorganic systems, hydrogels, and mesoporous, micelles, each having their own advantages. DNA is also recognized as a novel material in the field of nanotechnology. The specific bonding of base pairs can be used to direct the assembly of highly structured materials with specific nanoscale features such as periodic 2D arrays, 3D nanostructures, assembly of nanomaterials, and DNA nanomachines. In recent years, a variety of DNA nanomachines have been developed due to their potential applications in biosensing, diagnostics, and therapeutic applications. It is believed that these DNA-based nanomachines and hybrid motifs will become an integral point-of-care diagnostics and smart, site-specific therapeutic delivery. As such, this chapter will highlight and discuss pre-existing DNA dynamic structures, whose working mechanisms are inspired by or derived from natural phenomena and nanomachines. In each section, the mechanisms and the usage of the DNA structures in the biomedical field are described.

1.1   Background

Nanotechnology is an expanding field that encompasses a wide variety of technologies including energy, materials, sensor technology, and medicine.[1] Nanomaterials possess unique chemical and physical properties such as high surface area[2] and easy functionalization, making them ideal as static drug carriers.[3] On top of these characteristics, "smart" targeting abilities[3,4] and motion capabilities[5] can be synthesized on these static drug carriers to increase their delivery capabilities and limit off-target effects of therapeutics.[6] Examples of nanomaterials for drug delivery applications include catalytically fueled nanomotors,[7] pH-responsive polymer structures,[4,8,9] and DNA nanotechnology.[10,11] The smart carriers are aptly named nanomachines and are capable of conformational and positional action in response to environmental stimuli,[4] allowing them to be driven to specific regions or functionalized to deliver the cargo only where it is most needed.[12] The nanomachines can also be adapted to function detectors and amplifiers[13] for the diagnostics of hard-to-detect diseases[14] and the better understanding of nanomachine transportation on the nanoscale.[15]

As such, these "nanomachines" have the potential to completely revolutionize site-specific therapeutics by overcoming significant challenges in dosage, off-site effects, and microenvironment specific delivery. There are obstacles, however, to creating such machines because motion on the nanoscale is difficult,[16] the synthetic materials used in more conventional machines may include non-biocompatible fuels,[17,18] and many machines require additional treatment[19] in order to be functionalized with targeting ligands. A promising way to address these challenges is through a two-step mechanism: (1) drawing inspiration and design from biological nanomotors[20] and incorporating existing biological

modalities into our designs; and (2) working with a biological material such as DNA to create synthetic DNA structures, which does not require many of the same harmful organic chemistries. Biological nanomotors, such as actin/myosin,[21] kinesin,[22] and the adenosine triphosphate (ATP) Fo/F1 motor[23] can function to deliver cargo, move in biological environments, and discern specific targets. We can derive inspiration from their motion and how they interact with environmental stimuli to design our synthetic structures. It is also possible to draw inspiration from the asymmetric propulsion movement of prokaryotes such as Escherichia coli (*E. coli*), which move through the propulsion of flagella.[24] Additionally, the incorporation of existing biological molecules or structures such as enzymes,[25] proteins,[26] and aptamers [27] is another promising route to create motion or responsiveness with a bioinspired focus.

DNA nanotechnology is a branch of nanoengineering that takes advantage of the precise, elegant base-pairing nature, self-assembly, geometry, and structure of DNA to engineer synthetic structures for various applications including drug delivery, detection, and computing.[10] The field, which originated in the early 1980s from the lab of Seeman and co-workers,[28] has rap- idly expanded due to its versatility and adaptability. When certain design rules are obeyed, DNA nanostructures can be designed to have a wide variety of 2D and 3D geometries, including periodic arrays and lattices, nanoparticles, nanorods, and nanomachines.[29] DNA nanostructures can also be easily functionalized for cellular targeting,[10] while remaining biodegradable. Thus, DNA-based structures have great potential for drug delivery, disease diagnostics, and biological imaging. These structures can also be easily attached to other nanomodalities such as gold nanomotors,[30] polymers,[31] or carbon nanostructures[32] to create hybrid detection, diagnostic, or delivery structures. This flexibility allows engineers to

create hybrid nanostructures with both DNA and other materials, thus expanding the range of applications for DNA nanotechnology. We can also include within these synthetic DNA structures the potential for responsiveness to pH[33], light[34–37], or small molecule targets[31,38–40] by incorporating DNA secondary structures, such as DNA triplex structures[32,41] or the intercalated cytosine motif.[42–44] This allows us to create responsive nanostructures that can be classified as nanomachines. The responsiveness can also be derived from pre-existing motifs called "aptamers" which are artificially selected and can selectively bind proteins and small molecules.[45] Responsiveness to these cues facilitates selective delivery and can be triggered based on microenvironment cues, enabling researchers to begin to work on targeting specific disease modalities.[11] Consequently, DNA nanomachines can be both bioinspired and bioderived, allowing huge potential and variety in what can be achieved through creative design.[46]

In vivo stability is a main concern of using DNA as the drug delivery carrier. Inspired by natural viral structures, which are important for them to survive in serum and escape from immune system, Perrault and Shih developed an enveloped DNA nanostructure system.[47] They first synthesized DNA octahedrons with several lipid–DNA conjugate handles pointing outward. Surfactant was added to form micelles around the lipid conjugate. After adding polyethylene glycol-functionalized liposomes and dialyzing out the surfactant, the tail of the DNA–lipid conjugates fuse into and wrapped up by the liposome. The successful formation of enveloped DNA octahedron was witnessed under negative stain transmission electron microscopy (TEM). DNase I stability of DNA octahedron was significantly elevated by the protection membrane. *In vitro* immune response test over splenocytes revealed that the interferon production decreased by over two orders of magnitude. An *in vitro* test in mice

also indicated prolonged circulation lifetime and slower renal removal of enveloped DNA octahedron. Perrault and Shih's work provided a good option to increase serum stability when using DNA nano-structures to deliver drugs.[47] Within this review, we will begin by a brief introduction of two common nanomachines in nature, we will follow with discussion on DNA nanomachines that draw inspiration from four sources: (1) natural phenomena, (2) natural mechanisms to create motion, (3) natural nanomachines, and (4) systems that incorporate natural, existing DNA adaptive motifs. The machines will be characterized by their functioning mechanisms and comparisons will be drawn to natural nanomotors. Additionally, we will explain how the incorporation of natural DNA nanomotifs can create motion. We will then provide a summary and outlook to identify potential applications within the field of nano-drug delivery, diagnostics and biosensing, and therapeutics in relation to their primary operating mechanism.

Nanomachines are extremely significant in nature, from the intracellular pumps that maintain homeostasis [48] to the functioning of muscle fibers,[49] even to the kinesins and dyneins that carry molecular targets along tracks and perform functions during cell division.[50] Nanomachines are an integral part of natural functionality. Many biological motors, such as the actin–myosin complex require fuel such as ATP because the myosin head is an enzyme that hydrolyzes ATP and undergoes a conformational change, thus allowing it and actin to move past each other.[51] Other motors that utilize the interaction of ATP binding to cause conformational changes include transport proteins, such as kinesins and dyneins. Kinesins are motor proteins that also function through ATP hydrolysis which promotes binding that draws the kinesin heads forward in a stepwise fashion.[52] However, these proteins walk along a microtubule through a "highly processive" [52] mechanism, where its two heads binding sequentially, allowing it to move along the track. These concepts of fuel-mediated

motion and motor conformational changes are the inspiration for many of the DNA nanomachines that currently exist. Similarly, the processional motion of motor transport proteins, initiated by stimuli and conformational changes, is a concept that can be incorporated into the functioning of DNA nanodevices to advance the machines such that they can create motion and function on the nanoscale.

1.2 Strand-Mediated Displacement Motors

Like kinesin, some DNA nanomachines require external fuel for motion. Some even walk along a track, like kinesin, towing cargo for delivery or detection. Many of these nanomachines have provided the impetus in the development of DNA nanomachines to create fuel-free nanomachines. We open the discussion of DNA nanomachines with a brief introduction to nanomachines that function solely by a process known as fuel strand-mediated displacement. Fuel strand-mediated displacement is a process that takes advantage of the fact that a strand – one that is only partially hybridized to one strand – will preferentially bind to strands that allow the formation of a complete duplex. DNA designers can include sequences known as "toe-holds," which are single-stranded overhangs, in order to facilitate this reaction.[53] This process can be compared to the binding of ATP to kinesin, allowing the DNA to change conformation or perform a function based on the presence or absence of the fuel strand. Fuel strand-mediated displacement has been used to power DNA tweezers,[54] DNA rotator motors,[55] and DNA biodetection motifs.[56]
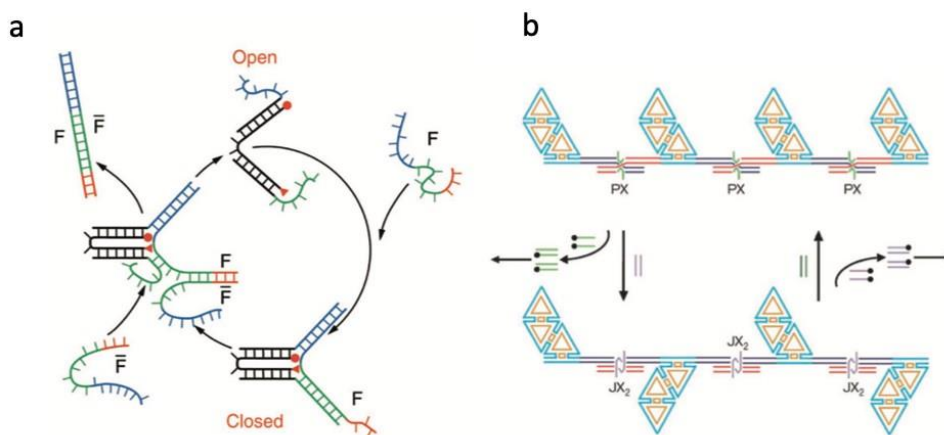
Figure 1.1: Strand-mediated displacement motors. (a) DNA nanotweezers functioning through fuel strand-mediated displacement. Reproduced with permission.[54] Copyright 2000, Nature Publishing Group. (b) DNA rotary motor utilizing fuel strands to controvert between PX and JX2 motifs. Reproduced with permission.[55] Copyright 2002, Nature Publishing Group.

In 2000, Neumann and co-workers[54] synthesized DNA tweezers – or machines that could reversibly open and close – that used fuel strand-mediated displacement. The design (Figure 1.1a) consisted of three strands in its open configuration, with two of the strands only partially hybridizing to the third. When exposed to the fuel strand, which was complementary to the two overhangs, the tweezer closed. However, the fuel strand itself also contained a toe-hold overhang which allowed the fuel strand to be removed when the complementary fuel strand was flowed into the system. The reaction was cyclic and repeatable, however it did require external input and creates waste.[54] This idea was extended by Seeman and co-workers[55] in 2002 where the authors created a DNA rotary nanomotor that also functioned through the use of fuel strand-mediated displacement (Figure 1.1 b). The fuel strands allowed the paranemic crossover motif PX to convert to its topoisomer, while the overhangs in the sets of fuel strands allowed the motif to be cycled between the two configurations in a robust manner. These motifs were included as linkages between DNA nanostructures and are shown to be able to vary their configuration in atomic force microscopy (AFM). Thus, this more robust motif allowed the possibility that larger scale structures could be manipulated and used to act upon environments external to the system.[55] One major challenge for this type of system was that fuel strand waste can have deleterious effects on the system. Unless added in a stoichiometric amount, single strands can remain between cycles and prematurely interact with one another, decreasing the efficacy of the device's cycling. Trying to correct for this error can lead to a massive quantity of waste and make it almost impossible to operate the device. This was not a concern for duplex waste of at least 20 base pairs because the duplex is more stable and will not interfere with the device.[57]

8

Shin and Pierce[58] achieved molecule transport by DNA nanowalkers using fuel strands. They mimicked the natural molecule motor system and replaced the ATP power by adding DNA strands and kinesins with DNA motors. A linear DNA duplex with several handles simulates a microtubule-like track and can guide DNA walkers across it. When triggered by fuel strands, the walker detaches from the track and moves from handle to handle. The design was demonstrated by gel electrophoresis and fluorescence experiments. The loading of molecules could potentially be achieved by covalent linkage or intercalation.[58] In 2010, Sleiman and co-workers[59] showed that DNA nanotubes are effective delivery vehicles, fueled by strand displacement, to load and release cargo. The basic building blocks of the nanotubes were triangular shapes with distinct sizes. The building blocks were linked together with spacers of triangles with varying sizes. They then synthesized the DNA nanotube with longitudinal variations of small and large capsules an alternating pattern. The authors showed that gold nanoparticles could be captured in the nanotube through scanning electron microscopy (SEM). The microscopy also showed that the gold nanoparticles displayed a periodical distribution. The rigid nanotube can be loosened by a single-strand DNA through strand displacement which released the gold nanoparticle. The authors took advantage of the high aspect ratio, high cargo loading capacity, and high programmability of the DNA nanotube to very precisely load and release the cargo at predesigned locations. As such, fuel strand-mediated DNA devices are potentially useful in the nanomanufacturing of periodical patterns, well controlled drug delivery, and biodetection.[59] Indeed, in 2016, Sleiman and co-workers[60] presented their studies trying on a DNA nanosuitcase for site-specific small interfering RNA or siRNA release. The DNA nanosuitcase is a cuboid consisting of 8 DNA strands, two of which are replaced for loading siRNA drug in the center of the cuboid. The

nanosuitcase changes its conformation with the existence of trigger microRNA (miRNA) or siRNAs, which were like the replaced strands in sequence, thus functioning through strand displacement. The siRNA was released from the original DNA nanosuitcase and enter the cell cytoplasm to downregulate target genes. Locked nucleic acids (LNA) components and hexaethylene glycol spacers were inserted in the DNA strands to increase stability. The system was tested *in vitro* on fixed HeLa cells with the prism designed to lose fluorescence signal with the release of the cargo. The novel system is capable of loading, protecting, and selectively releasing RNA drugs in specific environment, and it is potentially useful as an effective drug delivery machine.[60]

In 2017, the lab of Tan and co-workers[61] developed a DNA nanotweezer to detect tumor-related messenger RNA or mRNA inside living cells. They constructed a DNA tetrahedron and attached cy3 and cy5 dyes separately on the handles at two different vertices. The target tumor-related mRNA molecule was used as the fuel strands that bring two dyes together, which generated förster resonance energy transfer (FRET) emission. They have demonstrated the sensitivity and specificity of the nanotweezer by concentrating associated FRET signal change and FRET failure in negative controls. The system has been further applied in gene differential expression which can be used between different cell lines or same cell line with different treatments, proving the high potential of DNA nanotweezers in the biodetection field.[61]

One advantage of DNA nanomachines in biosensing is that they can be designed to function as molecular logic gates[62–64] and, as such, can be very sensitive diagnostic tools in very specific micro-environments. The usage of this technique was pioneered by Winfree and co-workers in 2006, who created nucleic acid circuits that functioned without the incorporation of enzymes.[65] Winfree and co-workers hypothesized DNA nanomachinese could be used for

biodetection where siRNA and miRNA would be system inputs. These logic gates can be used to "enhance the smartness"[46] of the system leading to the ability to distinguish certain environmental cues. In 2008, Qian and Winfree contributed to the practical application by using DNA catalytic gates to construct complex logic networks or circuits by involving thousands of different logic gates in the same system.[66] Song and co-workers[14] utilized a DNA origami nanostructure as the scaffold for the DNA-based logic gates system.[14] DNA origami is a technique, pioneered by Rothemund in 2006.[67] This technique is used to create DNA nanostructures by folding a bacterial scaffold and "stapling" it with multiple short-stranded oligonucleotides.[67] Since DNA origami contains DNA, the surface is easily functionalizable and, as such, DNA nanomachines can be placed on the surface. Meldrum and co-workers[68] also demonstrated in 2011 that DNA origami structures are the more stable in cellular lysate than both single- and double-stranded DNA. When incubated for 12 h at room temperature, with increasing concentration of lysate, the treated origami showed no appreciable difference in comparison to the untreated origami within a native gel. AFM showed that the origami structures, extracted from the gel, were unchanged by the lysate.[68] The work of Song and co-workers placed logic gates on the surface of the origami to function as microRNA sensors.[14] MicroRNA can be an excellent indicator for many diseases, including heart disease and can used to classify cancer with high degrees of sensitivity.[69] The logic gate indicators, microRNA-21 and microRNA-195, on the origami have the potential to detect signs of heart failure.[14] The system consisted of a single origami substrate that utilized two separate regions: the computation module for detection and output module for signal readout. The computation module could function as one of two possible logic gates: one to detect only the presence of miRNA-21 and one to detect if both miRNA-21 and miRNA-195 were

present. Through fuel strand-mediated displacement, the microRNA replaced a signal strand of DNA on the computation module. The biotinylated signal strand then flowed over to the output module and bound to a strand of DNA, called capture DNA. This occurs by another fuel strand-mediated displacement reaction as the capture DNA had to be blocked from binding to the gate strands themselves. Readout was generated by introducing avidin into the system and the changes were detected with AFM. This system potentially could be used for microenvironment-specific drug delivery and for microRNA-based disease detection.[14] Indeed, in 2017, Yuan and co-workers[70] also utilized DNA nanotechnology to create a DNA nanowalker with the potential to be used for sensitive detection of these biomarkers. This walker, which moves bidirectionally, allows the detection of multiple miRNA targets.[70] Another complex nanorobot that functioned, on an origami surface, by strand displacement was created by the lab of Winfree and co-workers in 2017.[56] This robot was able to walk on a surface, as well as pick up and sort two distinct cargos on the origami. In many circumstances, the target molecule can be used as fuel strands for the DNA motor. However, the amount of DNA or RNA might be below the detection threshold. To solve this problem, researchers have developed other DNA cascade nanomachines to amplify the signal while using fuel strands as catalyst to initiate the reaction. In 2015, Jia and co-workers[13] developed a cascade DNA nanomachine to detect tumor related genes *in vitro*. The authors adopted a dual-cyclical nucleic acid strand-displacement polymerization (dual-CNDP) strategy to amplify the signal. Target DNA (fuel strands) was used repeatedly like catalysts to involve more and more effectors to generate strong fluorescent signal in presence of target DNA. The DNA nanomachine was used to detect tumor suppressor gene p53, its mutants and measure p53 concentrations. The dual-CNDP exponential amplification was also proven to perform more sensitively than any

single CNDP process[13] Similar to the research of Jia and co-workers, Shen *et al.*[71] constructed the molecular beacon-padlock probe (MB-PP) system for the sensitive detection of the K-ras gene mutation. The padlock probe was ligated into a circular form with the target DNA, then rolling circle amplification (RCA) was applied to amplify the signals. Afterward, the molecule beacon turns on through a series of cutting and conformational changes. The authors demonstrated the increase of fluorescence density after being exposed in K-ras DNA. Further, they showed a differential fluorescence pattern between wild type K-ras gene and mutants. This new system sensitively detected cancer related genes and their point mutations, providing a promising tool for early clinical diagnostics.[71] Chen and co-workers[72] also published their studies using the RCA process to amplify signal for biodetection in 2017. They combined a DNA tetrahedron structure with an electro-chemiluminescence platform together to construct a biosensor. Subsequently, the DNA tetrahedron provided a scaffold for capturing glucose oxidase (GOD)-labeled DNA and $[Ru(bpy)_3]^{2+}$ and the electro-chemiluminescence platform used the captured GOD-labeled DNA and glucose to generate H_2O_2 and to quench $[Ru(bpy)_3]^{2+}$. The target DNA initiated and activated the toehold strand displacement reaction to release GOD-labeled DNA for tetrahedron capturing. This target DNA repeatedly enters the cyclic strand displacement reaction to release GOD-labeled DNA strands and amplify the signal. Toehold strand displacement took place in equilibrium without base pair gain or loss to increase specificity. The biosensor demonstrated a wide detection range from 100×10^{-18} to 10×10^{-12} M and a high detection limit of 40×10^{-18} M, which is extremely promising in DNA analysis. Overall, either dual-CNDP or RCA technique helps to amplify the signal with limited amounts of the target molecule, highlighting their potential application in future bio-detection.

1.3   DNAzyme Motors

It is possible to trace the origin of DNA nanomachines to the fuel stranded machines, however, as discussed earlier in the review, they require external manipulation and can create a buildup of fuel strand waste. Therefore, one of the methodologies that nanoengineers used to tackle this problem is the incorporation of natural, catalytic DNA sequences called DNAzymes.

DNAzymes are sequences of single-stranded DNA (ssDNA) that act as catalytic modalities. DNAzymes can cleave mRNA, siRNA, or microRNA molecules. They function similarly to siRNA in that, through their cleavage of very specific mRNA sequences, they can cause downregulation of undesirable proteins. Through modifications, DNAzymes are stable in solution for up to 2–3 days depending on the conditions. These tiny DNA nanomachines are used widely in biomedicine, including the inhibition of RNA viral replication, cancer therapeutics, tumor inhibition, other disease modalities relying on mRNA disruption. Further, DNAzymes have potential usages in sensing applications as well.[73] This work is well-reported in literature. For example, Mao and co-workers[74] designed a motor that incorporated and took advantage of the autonomous nature of a DNAzyme. Bishop and Klavins improved upon the motor of Mao *et al.* in 2007 by including ribonuclease H in the system to digest any waste strands, thus preventing loss of function in the motor.[75] In 2005, Mao and co-workers[15] advanced the field by incorporating a DNAzyme into a system to act as nanomachine walker along a track. Due to the specific cleavage nature of the DNAzyme, the machine was able to move autonomously along a track comprised of RNA substrate without the addition of strands to fuel its motion. The autonomous motion of this track – which did not require the creation of stoichiometric duplex waste within the system – combined with the many potential

DNAzyme applications discussed above suggests that this machine could be adapted for use as biosensor and signal amplifier in the case of mRNA diseases.[15]

1.4   Light- and Heat-Fueled Motor

We can also look at utilizing environmental triggers in place of fuel strand-mediated changes, for example the use of light. This can be achieved through the incorporation of a photo-sensitive modality like azobenzene into the DNA nanostructure. This will allow the machine to switch configurations, depending on the cis–trans isomerization of the azobenzene.[34] This was shown in 2008, when Asanuma and co-workers[36] created a DNA nanomotor that functioned reversibly through the use of a DNA strand modified with azobenzene. When the azobenzene was in its trans configuration, the tweezer was held closed. However, when exposed to UV light, the azobenzene strand dissociated as cis-azobenzene which destabilized base-pair stacking. Unlike fuel strand-mediated tweezers, this reaction produced no waste, allowing rapid cycling efficacy even after ten cycles.[36] The same group extended the usage of azobenzene in DNA nanomachines by using it to regulate the catalytic ability of DNAzymes.[37]

Heat can also be used as an an environmental trigger for DNA nanomachines. This was shown in 2013 by Ho and co-workers[76] where they demonstrated a temperature-responsive enzyme encapsulation and release by a DNA nanocage. The authors replaced one vertex with a 32-nucleotide long DNA strand which formed hairpin structures at lower temperatures. As the temperature increased, the hairpin structure change conformation. They used the nanocage to encapsulate and release horseradish peroxidase (HRP) protein. The authors showed that encapsulation occurred by decreasing the temperature from 37 to 4 °C and protein

release was achieved by returning to 37ºC. This was shown in gel electrophoresis studies which indicated the retention of the enzyme in the nanocage at 4 °C and the release in nanocage at 37 °C. The authors developed the temperature-responsive system for enzyme encapsulation and release while maintaining the enzyme functionality in the carrier. This has potential usefulness in drug delivery and single molecule detection.[76]

Consequently, there are many DNA nanomotors that derive inspiration from biological motors. These motors are the building blocks for nanoscale DNA-powered motion and contribute to the creation of highly sensitive diagnostic and delivery tools. Many of these tools will be incorporated into later motifs discussed during this review.

1.5 i-Motif-Powered Motors

Not only can we draw inspiration from nature to create functioning DNA nanomachines, but we can also incorporate natural DNA sequences within our synthetic designs. By doing so, we can create responsive functionalities and conformational changes that react to specific microenvironments, which allow eventual responsiveness for targeted action. There are DNA sequences, which are unique secondary structures, that respond to pH stimuli in the environment and DNA sequences whose unique structures allow them to bind with specific small molecules, proteins, and certain elements.[77] The initial inspiration for these types came from a motor synthesized in 1999 by Seeman and co-workers. The work showed that the motor underwent a conformational change from B DNA to Z DNA based on environmental conditions.[78] DNA sequences that are rich in cytosine can form two intercalated parallel duplexes under low pH through the hemiprotonation of a cytosine–cytosine pair.[43] This structure has a height proportional to the length of the ssDNA sequence.[44] Consequently, this structural formation change can be incorporated into DNA nanodevices for usage in biomapping and therapeutic delivery due to the acidification of late stage endosomes.[42] In 2009, Krishnan and co-workers[33] utilized this motif – known as an i-motif or intercalated motif – and created a DNA nanomotor that mapped pH change from an early to late stage endosome. This nanoswitch would close in response to low pH and displayed a fluorescent signal. The switch was cyclic, which demonstrates the ability of DNA nanodevices to be robust and work within functioning cells. Further, this work demonstrated the ability of DNA nanodevices to take advantage of cellular microenvironment changes.[33] The same lab extended this work to living organisms, specifically the nematode Caenorhabditis elegans[79] (Figure 1.2a). This work demonstrated that an i-motif-based nanomachine can maintain

function within a living organism.[79] In 2009, Zhou and co-workers[80] synthesized a nanotriangle nanomotor, similar to that of the nanomotor of Krishnan *et al.*,[33,79] that could open and close in response to environmental stimulation. However, Zhou *et al.* utilized an i-motif structure as the trigger strand, where another strand was able to bind to it under higher pH, thus allowing the motor to close under low pH and reopen when the pH is switched back. This device has potential for drug delivery under cellular or extracellular microenvironment conditions due to both endocytotic acidification and tumor acidification. The authors also posit that by combining multiple machines, a structure that functions similarly to muscle fiber could be created where the i-motif structure formation would simulate a contraction.[80] The lab of Willner and co-workers[81] also created a DNA tweezer that utilized the properties of the i-motif to change machine conformation with respect to pH. When the pH was lowered, the tweezers released a strand that was holding them in a closed position by forming two i-motif structures. This strand functioned in opposition to the second pair of tweezers as a closing strand, such that when the pH was lowered, the first set of tweezers opened and the second set of tweezers closed. This was found to be reversible because the fuel strand to close both tweezers was more favorable to hybridize with the pH-responsive tweezers than not, but was forced to release during the formation of the i-motif.[81] The i-motif was also utilized by Fan and co-workers, who created an adaptable DNA tetrahedron that could function as logic gates.[82] One edge of the tetrahedron functioned as a sensor that was responsive to microenvironment conditions. During the annealing process, the tetrahedron was flexible enough that the sensing strand was switched out for other potential sensing DNA sequences. Depending on the sequence(s) used in the responsive strand, various types of DNA logic gates were constructed. The i-motif sequence allowed for the construction of an INH gate. Gates such as an OR gate, XOR gate,

and an AND gate were constructed using various DNA sequences that are responsive. The flexibility of this system, and the fact that this work proved the functionality of the tetrahedral sensors *in vivo*, suggests that a wide range of smart biosensing and detection at the cellular level can be developed.[82] Recently, LaBean and co-workers[44] synthesized DNA origami that was able to actuate spatially through the incorporation of i-motif sequences (Figure 1.2b). The authors mentioned that the length of the actuation can be designed through the length of the i-motif sequence.[44] Thus, the incorporation of pH-responsive DNA i-motifs have many potential benefits to help understand and map cellular pH on a deeper level. These motifs also clearly have potential in targeted release due to tumor acidification and late-stage endosome acidification.
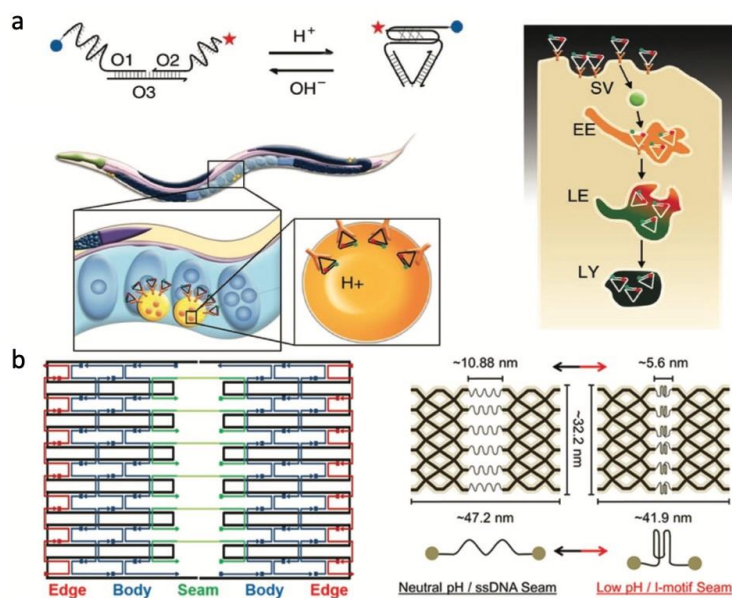
Figure 1.2: (a) i-Motif switched used to map pH inside a living organisms. Reproduced with permission.[79] Copyright 2011, Nature Publishing Group. (b) DNA origami actuated through the incorporation of the i-motif sequence. Reproduced with permission.[44] Copyright 2017, American Chemical Society.

In contrast to the usage of the i-motif, the lab of Lee and DeRosa[83] created a pH-responsive DNA nanostructure that took advantage of the unique nature of the adenine–guanine

(A–G) mismatch. The A–G mismatch becomes more stable under low pH, as confirmed by melting temperature data, and this property allowed Lee and DeRosa to create a simple motor that undergoes conformation changes based on pH changes. The A–G mismatch requires less space than i-motif within the DNA design and it could potentially decrease the limitations on other sequence designs since it does not require a repeating cytosine motif, making it a potentially more advantageous option to the i-motif[83].

1.6 DNA Triplex-Based Motors
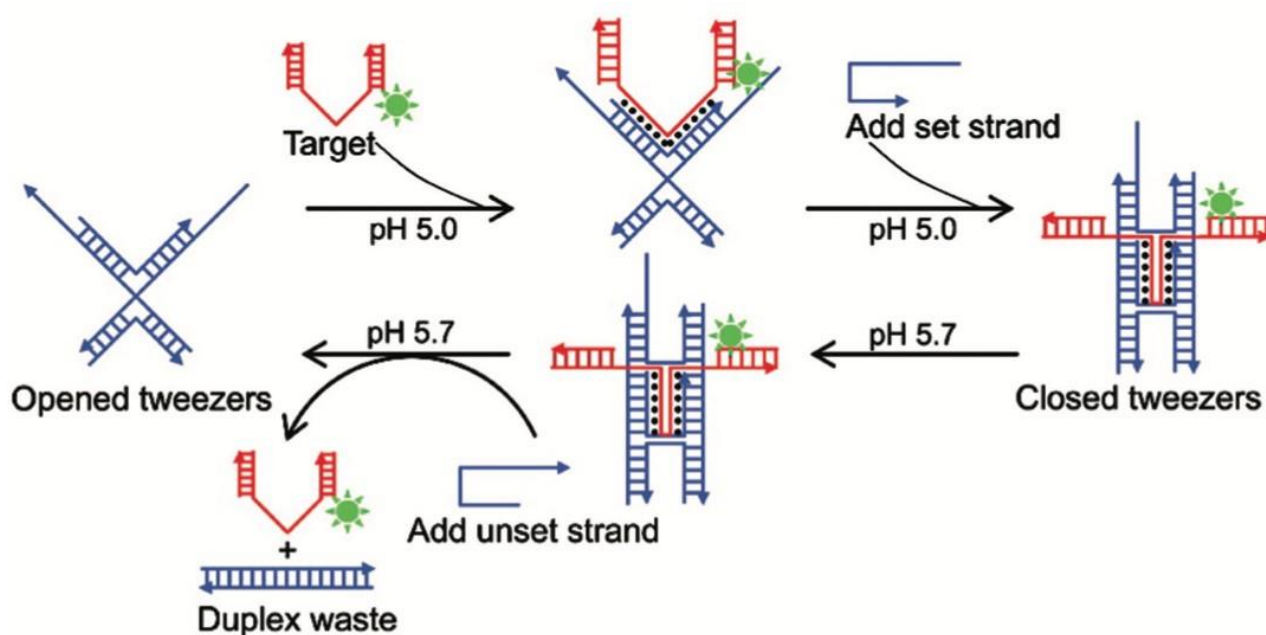
Figure 1.3: DNA tweezers powered through triplex binding and fuel strand-mediated displacement. Reproduced with permission.[86] Copyright 2008, American Chemical Society.

Another potential pH-responsive DNA structure, existing in nature, is that of the DNA triplex. Triplex DNA is stabilized through Hoogstein hydrogen bonding in the major groove of B DNA.[84] Depending on the type of triplex, purine or pyramidine, the structure can be designed to be responsive to low pH. This is because purine triplexes are stable at physiological pH where pyramidine triplexes form at low pH. Thus, with the incorporation of pyramidine triplexes, we can create pH-responsive DNA nanomachines.[85] The lab of Mao and co-workers[41] created a DNA nanomachine by utilizing the pH responsiveness of a C^+G-C DNA triplex sequence. The three-strand design formed a triplex under low pH, closing the machine, and reopened under higher pH. The machine did not require any external fuel strand DNA and thus did not create DNA waste within the system.[41] In 2008, Deng and co-workers[86] utilized the pH-responsive DNA triplex motif and fuel strand-mediated displacement to create

21

DNA tweezers that can actually capture and hold a target (Figure 1.3), like actual tweezers. The target DNA sequence contains a ssDNA region nestled between two duplexes that formed a triplex tweezer complex under low pH (5). The full tweezer complex structure was set through the addition of another strand which closes the tweezer motif, effectively trapping the target DNA. With an increase in pH, to 5.7, and the addition of a strand that was more fully complementary to the set strand, the target DNA sequence was released. This concept was tested through FRET quenching experiments.[86] Similar to the motor created by Krishnan and co-workers, Tan and co-workers[87] created a device to map intracellular pH by utilizing the DNA triplex motif and FRET. This work utilized polyethylenimine (PEI) to protect the DNA switch from enzymatic degradation and to aid in cellular internalization, although their motif was able to enter the cell without the PEI entirely.[87] In 2013, the lab of Mao and co-workers[88] created a DNA tetrahedron that can assemble into a 3D structure in response to pH, utilizing a combination of the CGC DNA triplex motif, which is pH responsive, and the TAT triplex motif, which is unresponsive. These three stranded motifs formed a DNA star under alkaline pH, however, as the pH decreased, the cytosine hemiprotonated and transformed the star motif into a tetrahedron. As with the other pH-responsive motifs discussed during the review, this motif could potentially be utilized for pH-triggered therapeutic release or pH related biodiagnostics. Recently, Ricci and co-workers[89] synthesized a DNA nanodevice that opened and closed in response to an antibody cue due to the attachment on an antigen. The machine functioned by binding to an antibody cue which forced dissociation of a triplex structure holding the device closed by destabilizing the Hoogstein bonding that was essential to triplex formation. This reaction allowed a DNA payload sequence to be rapidly released in direct, proportional response to that specific antibody key, such as an anti-human

22

immunodeficiency virus (HIV) antibody, an anti-Digoxigenin antibody, and an anti-dinitrophenol (DNP) antibody. The nanodevice would allow potential delivery of therapeutic nucleic acid sequences such as siRNA or microRNA.[89] Inspired by hemoglobin functionality, Ricci and co-workers[90] also developed a DNA-based nanodevice with multiple binding sites for cargo loading and release, which is a process that is well controlled by allosteric effectors or environmental conditions like pH and temperature. This machine utilized triplex interactions. The authors built an *in vitro* system with molecule beacons to characterize the cargo loading and release profile. The project successfully mimicked heterotropic allosteric effects, inverted Bohr effect, and temperature dependence in the artificial system. It was the first artificial DNA nanodevice which mimicked complex nature-inspired control mechanisms, which can be useful for diagnostics and drug delivery.[90]

1.7 G-Quadruplex-/Aptamer-Based Motors

It is also necessary to examine the DNA structure that has been used for DNA nanomachines known as the guanine quadruplex or G-quadruplex. A G-quadruplex (Figure 1.4a) is a DNA secondary structure that forms when two or more guanine tetrads stack in a planar fashion through π-stacking. The guanine tetrads themselves are held together through a combination of Hoogstein and Watson–Crick bonding. The quadruplex can be contained to a single strand or can be formed by multiple strands and there are many potential orientations of G-quadruplexes based on factors such as loop length and quantity of tetrads.[91] In the early 2000s, Li and Tan[92] created a simple motor based on the G-quadruplex and fuel strand-mediated displacement (Figure 1.4b). Similar to the i-motif motor created by Zhou and co-workers in 2006[93] (discussed later), this motor functioned through binding to another strand, forcing the G-quadruplex to straighten out. The G-quadruplex was allowed to reform when a third strand was flowed that is more complementary to the strand bound to the G-quadruplex.[92]

G-quadruplexes are often the functional component of DNA sequences known as aptamers, which are nucleic acid sequences that target and bind to small molecules, proteins, and certain elements.[94] Aptamer-based sensors are less expensive and more stable than antibodies, giving them distinct advantages in biosensing and diagnostics.[95] Similarly, aptamers also demonstrate high thermostability and have "similar target-binding specificities" to antibody–antigen interac- tions.[96] In 2004, the Lab of Simmel and co-workers[97] created a nanomachine based on the G-quadruplex thrombin binding aptamer. The machine could bind and release thrombin by utilizing fuel strand-mediated displacement. A fuel strand, called the opening

strand, with an overhang was introduced into the system and bound to much of the sequence that included the thrombin binding aptamer. The binding disrupted the guanine tetrads and forced the aptamer to release the protein. The aptamer structure was recovered when a second strand – one completely complementary to the opening strand – was introduced into the system. Like other fuel strand motifs, this system generated waste, however the aptamer motor experiment was the basis for other catch and release thrombin and protein motifs that can be used for sorting, biodiagnostics, and smart delivery.[97]
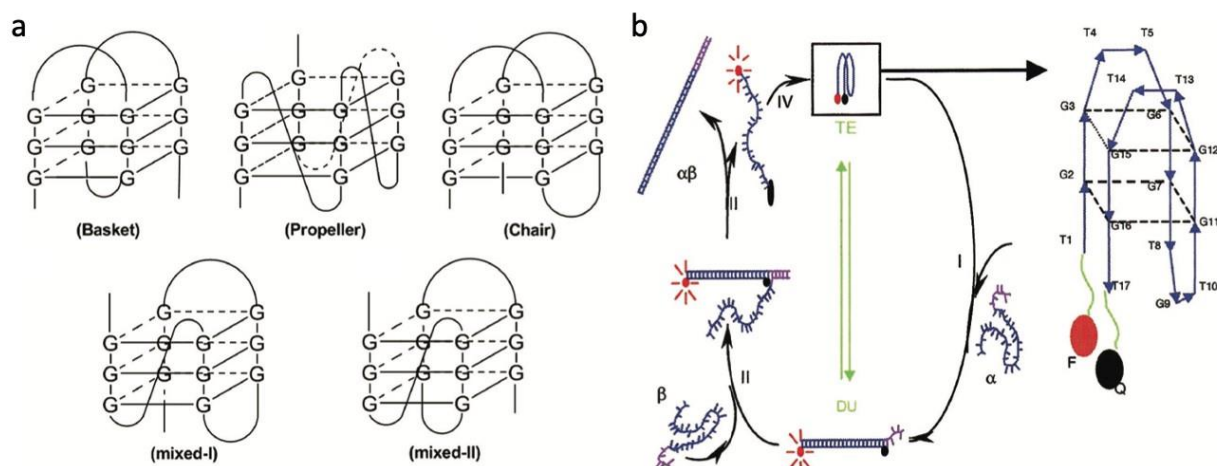
Figure 1.4: (a) Guanine quadruplex configurations. Reproduced with permission.[91] Copyright 2013, Oxford University Press. (b) Fuel strand-mediated powered Guanine quadruplex-powered motor. Reproduced with permission.[92] Copyright 2002, American Chemical Society.

Cancer cells often demonstrate changes in regulation and expression of cellular membrane receptors. We can use this knowledge and DNA nanodevices to target those cancer cells, whether they overexpress or underexpress certain signals.[63] Perhaps one of the most interesting nanorobots that takes advantage of this phenomenon would be the aptamer logic-gated nanorobot that was fabricated in 2012 by Church and co-workers.[11] As seen in Figure 1.5, DNA origami has been used in many different cases to construct DNA nanomachines, including DNA boxes and hatches used to encapsulate a payload.[98] The origami nanorobot, fabricated by Church and

co-workers, contained binding regions inside for cargo transport. The binding regions were locked by aptamer locks that only opened when both protein cues were available. This resulted in a nanorobot that functioned as an AND gate and removed the possibility for delivery under false positive conditions. The aptamer locks were specifically designed to be sensitive, but also to avoid spontaneous activation by tailoring the length of the binding duplex. The highly sensitive locks were tested against specific cell lines that expressed combinations of antigens
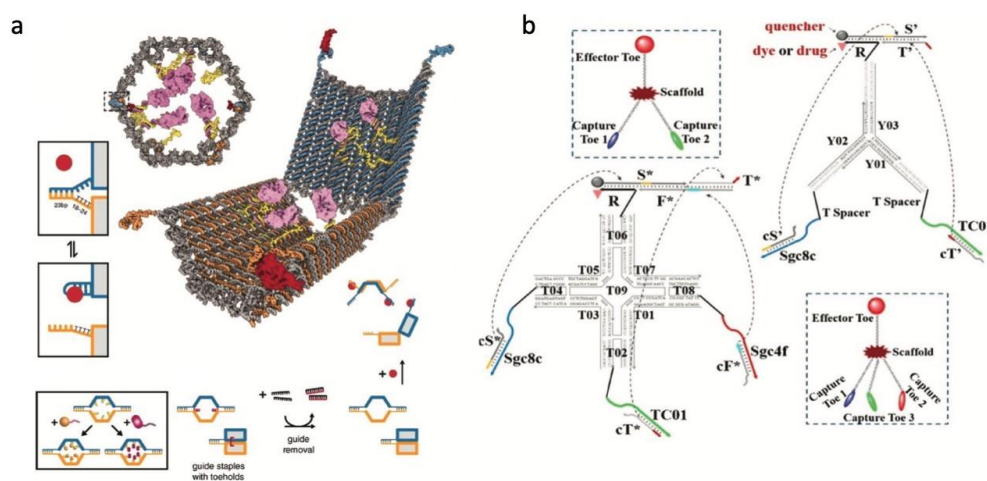
Figure 1.5: (a) Aptamer logic gate keyed nanorobot for drug delivery. Reproduced with permission.[11] Copyright 2012, The American Association for the Advancement of Science. (b) Logic-gated "Nano-Claw" for delivery and diagnostics. Reproduced with permission.[63] Copyright 2014, American Chemical Society.

that activated all aptamers in the locks. They found that the locks were highly specific and only activated in the presence of the cell population that expressed the precise combination of antigens. Further, the robot showed potential for targeted drug delivery because it was able to stop growth in leukemia cells. The robot could also induce T cell signaling pathways by collecting flagellin from solution. These characteristics suggest that the robots could also be used for scavenging applications.[11] Similar to the nanorobot demonstrated by Church and co-workers, the Lab of Tan and co-workers (Figure 1.5 (b))[63] created a "nano-claw" to interact with various levels of cellular membrane markers and perform therapeutic actions

autonomously. This functional DNA nanodevice was able to both generate diagnostic signals and release therapeutic modalities. Like the robot of Church and co-workers, this robot requires multiple inputs (i.e., AND gate or INH gate) to avoid false positives in reporting and release. The nano-claw was designed to require two or more binding inputs for aptamer-based "capture toes" – or aptamer sequences bound to complementary DNA. Once the target is available, the complementary DNA was released and bound to an "effector toe," which caused a diagnostic or therapeutic action to occur. This type of technology provided a level of specificity and prevented false negatives in theranostics.[63] In 2015, the Lab of Tan and co-workers[99] also created a highly specific, logic-gated aptamer-based Boolean cascade with "12 three-input conditions and 2 four-input conditions" for cancer diagnostics. The cascade allowed for incredibly selective delivery based on either the presence or absence of necessary cell markers.[99] Funabashi and co-workers[100] utilized the G-quadruplex motif and created a DNA nanosensor for nucleic acid sequences that could demonstrate a colorimetric readout. The three-stranded design contained two strands with sites that recognized the nucleic acid target and a third strand that contained a split G-quadruplex (half of the sequence on one end of the strand and the other half on the other end of the strand). When the desired target hybridized to the target recognition sequence, the device closed and allowed the split strand G-quadruplex to form its secondary structure. This allowed the device to function as an aptamer and bind to hemin. Further, this allowed 2,2$'$-azino-bis (3-ethylbenzothiazoline-6-sulfonic acid) (ABTS) to be oxidized in the presence of hydrogen peroxide, which produced a colorimetric signal. With this design, the authors were able to detect norovirus mRNA with a minimum concentration of 4×10^{-9} M. This device has the potential to act a sensor for many nucleic acid disease indicators because it could easily be modified to various desired target

sequences. However, there are some drawbacks relating to free hemin in solution which limits the device sensitivity.[100]

In 2017, Tanner and co-workers[39] demonstrated a colorimetric aptamer-based sensor to detect a malarial biomarker by incorporating a split version (similar to that of Funabashi and co-workers) of the Plasmodium falciparum lactate dehydrogenase aptamer within DNA tweezers. In the presence of the protein, the split aptamer bound the protein and forced a split G-quadruplex to form and bind to hemin, which, in the presence of hydrogen peroxide, oxidized ABTS and yielded a colorimetric readout.[39] As such, it is easy to visualize the massive advantage that natural aptamer sequence-incorporated smart DNA nanomachines have in site-specific, targeted therapeutic delivery and diagnostics.

Recently, in 2017, Li and co-workers[101] combined both aptamer DNA and G-quadruplex DNA to synthesize a DNA-based ATP nano-biosensor. This system consisted of a three-strand design that, without the presence of indicator Thioflavin T or ATP, formed a single strand triangle in the middle, surrounded by three pairs of duplexes. The single-stranded region of this three-way junction contained three ATP aptamers to capture the target molecule of ATP. Thioflavin, a ligand that was bound to the ATP aptamer, acted as a fluorescent indicator for the binding of ATP to the aptamer. This mechanism occurred by thioflavin competitively binding to the aptamer in the absence of ATP and releasing once ATP is present. Once a release strand that contained a G-quadruplex sequence hybridized to the ATP aptamer, the ATP was released and the Thioflavin was captured by the release strand. The system can be reset with the addition of another strand.[101] At the beginning of 2017, Qiu and co-workers[102] modified exosomes with an aptamer-based nanoarchitecture. Exosomes, which are extracellular vesicles, are biocompatible and carry many biomarkers, thus allowing for

potential usage in disease diagnostics and drug delivery. Exosomes presented challenges in modifying the surface, however, aptamers allowed researchers to overcome those challenges by binding to molecules expressed on the surface of the exosomes.[102] Therefore, the potential of incorporating natural motifs into our DNA nanomachines was easily visualized as they can function as detection modalities, delivery modalities, and as a surface modification technique.

1.8   Summary and Future Outlook

Bioinspired DNA nanomachines have revolutionized bio-diagnostics and have great future potential to revolutionize targeted, smart therapeutic delivery. By combining bioderived mechanisms and natural DNA motifs with special properties, researchers can create uniquely sensitive devices with the ability to smartly diagnose and treat specific diseases in a targeted fashion. DNA nanomachines have the capacity to greatly increase diagnostic sensitivity through amplification reactions that are triggered by small quantities of disease analyte. The incorporation of natural DNA motifs can also be used to create diagnostic readouts for the detection of often fatal diseases. Due to their unique flexibility and ease of functionalization, DNA nanostructures and machines can be made to target specific cellular populations due to irregularities in their microenvironments or on their cellular surface or carry very high loads of therapeutic or diagnostic motifs. The future of bioderived DNA nanomachines for biological applications is incredibly wide and varied and there are many motifs and machines that could be used eventually in a clinical aspect, however there is still a dearth of translational DNA nanomachines used clinically. Yet, we believe that through their ability to both derive inspiration for functionality from mimicking natural nanomachines and their ability to incorporate natural motifs, these DNA-based nanomachines and hybrid motifs will become an integral point-of-care diagnostics and smart, site-specific therapeutic delivery.

Chapter 1, in part, is a reprint of the paper published in Advanced Healthcare Materials, 2018. Chava Angel, Mingxuan Kai, Sibai Xie, Xiangyi Dong, Yi Chen. The dissertation author was co-author.

1.9 Reference

[1] G. Cao, Y. Wang, Nanostructures and Nanomaterials. World Scientific, Singapore 2011, pp. 1–17.

[2] F. Mensah, H. Seyoum, P. Misra, Applied Spectroscopy and the Science of Nanomaterials (Ed: P. Misra), Springer, Singapore 2015, pp. 253–277.

[3] Mout, R., Moyano, D.F., Rana, S. and Rotello, V.M., "Surface functionalization of nanoparticles for nanomedicine. " Chemical Society Reviews 41.7 (2012): 2539-2544.

[4] Mura, Simona, Julien Nicolas, and Patrick Couvreur. "Stimuli-responsive nanocarriers for drug delivery." Nature materials 12.11 (2013): 991-1003.

[5] Gao, Wei, and Joseph Wang. "Synthetic micro/nanomotors in drug delivery." Nanoscale 6.18 (2014): 10486-10494.

[6] Shi, Jinjun, Alexander R. Votruba, Omid C. Farokhzad, and Robert Langer. "Nanotechnology in drug delivery and tissue engineering: from discovery to applications." Nano letters 10.9 (2010): 3223-3230.

[7] Paxton, Walter F., Kevin C. Kistler, Christine C. Olmeda, Ayusman Sen, Sarah K. St. Angelo, Yanyan Cao, Thomas E. Mallouk, Paul E. Lammert, and Vincent H. Crespi. "Catalytic nanomotors: autonomous movement of striped nanorods." Journal of the American Chemical Society 126.41 (2004): 13424-13431.

[8] Schmaljohann, Dirk. "Thermo-and pH-responsive polymers in drug delivery." Advanced drug delivery reviews 58.15 (2006): 1655-1670.

[9] Soppimath, Kumaresh S., DC-W. Tan, and Y-Y. Yang. "pH-triggered thermally responsive polymer core–shell nanoparticles for drug delivery." Advanced materials 17.3 (2005): 318-323.

[10] Angell, Chava, Sibai Xie, Liangfang Zhang, and Yi Chen. "DNA nanotechnology for precise control over drug delivery and gene therapy." Small 12.9 (2016): 1117-1132.

[11] Douglas, Shawn M., Ido Bachelet, and George M. Church. "A logic-gated nanorobot for targeted transport of molecular payloads." Science 335.6070 (2012): 831-834.

[12] Li, Jinxing, Pavimol Angsantikul, Wenjuan Liu, Berta Esteban-Fernández de Ávila, Soracha Thamphiwatana, Mingli Xu, Elodie Sandraz, Xiaolei Wang, Jorge Delezuk, Weiwei Gao, Liangfang Zhang, and Joseph Wang. "Micromotors Spontaneously Neutralize Gastric Acid for pH-Responsive Payload Release." Angewandte Chemie International Edition 56.8 (2017): 2156-2161.

[13] Xu, Jianguo, Zai-Sheng Wu, Weiyu Shen, Huo Xu, Hongling Li, and Lee Jia. "Cascade DNA nanomachine and exponential amplification biosensing." Biosensors and Bioelectronics 73 (2015): 19-25.

[14] Wang, Dongfang, Yanming Fu, Juan Yan, Bin Zhao, Bin Dai, Jie Chao, Huajie Liu,

Dannong He, Yi Zhang, Chunhai Fan, and Shipping Song. "Molecular logic gates on DNA origami nanostructures for microRNA diagnostics." Analytical chemistry 86.4 (2014): 1932-1936.

[15] Tian, Ye, Yu He, Yi Chen, Peng Yin, and Chengde Mao. "A DNAzyme that walks processively and autonomously along a one-dimensional track." Angewandte Chemie 117.28 (2005): 4429-4432.

[16] Wang, Joseph. Nanomachines: fundamentals and applications. John Wiley & Sons, 2013.

[17] Liu, Ran, and Ayusman Sen. "Autonomous nanomotor based on copper–platinum segmented nanobattery." Journal of the American Chemical Society 133.50 (2011): 20064-20067.

[18] Abdelmohsen, Loai KEA, Fei Peng, Yingfeng Tu, and Daniela A. Wilson. "Micro-and nano-motors for biomedical applications." Journal of Materials Chemistry B 2.17 (2014): 2395-2408.

[19] Edmund Larenas, Tim Fowler, Samarth Kulkarni, Allan S. Hoffman, and Patrick S. Stayton." Photoresponsive polymer–enzyme switches." Proceedings of the National Academy of Sciences 99.26 (2002): 16592-16596.

[20] Guix, Maria, Carmen C. Mayorga-Martinez, and Arben Merkoçi. "Nano/micromotors in (bio) chemical science applications." Chemical reviews 114.12 (2014): 6285-6322.

[21] Manning, Gerald S. "An ionic–chemical–mechanical model for muscle contraction. " Biopolymers 105.12 (2016): 887-897.

[22] Marx, Alexander, Andreas Hoenger, and Eckhard Mandelkow. "Structures of kinesin motor proteins." Cell motility and the cytoskeleton 66.11 (2009): 958-966.

[23] Wada, Yoh, Yoshihiro Sambongi, and Masamitsu Futai. "Biological nano motor, ATP synthase FoF1: from catalysis to $\gamma\epsilon c10–12$ subunit assembly rotation." Biochimica et Biophysica Acta (BBA)-Bioenergetics 1459.2-3 (2000): 499-505.

[24] Maier, Alexander M., Cornelius Weig, Peter Oswald, Erwin Frey, Peer Fischer, and Tim Liedl." Magnetic propulsion of microswimmers with DNA-based flagellar bundles." Nano letters 16.2 (2016): 906-910.

[25] Qu, Xiangmeng, Dan Zhu, Guangbao Yao, Shao Su, Jie Chao, Huajie Liu, Xiaolei Zuo, Lihua Wang, Jiye Shi, Lianhui Wang, Wei Huang, and Hao Pei. "An exonuclease III-powered, on-particle stochastic DNA walker." Angewandte Chemie 129.7 (2017): 1881-1884.

[26] Hwang, Wonmuk, and Matthew J. Lang. "Mechanical design of translocating motor proteins." Cell biochemistry and biophysics 54.1 (2009): 11-22.

[27] R. Mo, T. Jiang, R. DiSanto, W. Tai, Z. Gu, Nat. Commun. 2014, 5, 3364.

[28] Kallenbach, Neville R., Rong-Ine Ma, and Nadrian C. Seeman. "An immobile nucleic acid junction constructed from oligonucleotides." Nature 305.5937 (1983): 829-831.

[29] Rosenthal, Sandra Jean, and David W. Wright, eds. Nanobiotechnology protocols. Vol.

303. Totowa: Humana Press, 2005.

[30] Esteban-Fernández de Ávila, Berta, Chava Angell, Fernando Soto, Miguel Angel Lopez-Ramirez, Daniela F. Báez, Sibai Xie, Joseph Wang, and Yi Chen. "Acoustically propelled nanomotors for intracellular siRNA delivery." Acs Nano 10.5 (2016): 4997-5005.

[31] Shastri, Ankita, Lynn M. McGregor, Ya Liu, Valerie Harris, Hanqing Nan, Maritza Mujica, Yolanda Vasquez, Amitabh Bhattacharya, Yongting Ma, Michael Aizenberg, Olga Kuksenok, Anna C. Balazs, Joanna Aizenberg and Ximin He. "An aptamer-functionalized chemomechanically modulated biomolecule catch-and-release system." Nature chemistry 7.5 (2015): 447-454.

[32] Li, Xue-Mei, Jian Song, Tao Cheng, and Pei-Yu Fu. "A duplex–triplex nucleic acid nanomachine that probes pH changes inside living cells during apoptosis." Analytical and bioanalytical chemistry 405.18 (2013): 5993-5999.

[33] Modi, Souvik, M. G. Swetha, Debanjan Goswami, Gagan D. Gupta, Satyajit Mayor, and Yamuna Krishnan. "A DNA nanomachine that maps spatial and temporal pH changes inside living cells." Nature nanotechnology 4.5 (2009): 325-330.

[34] Kamiya, Yukiko, and Hiroyuki Asanuma. "Light-driven DNA nanomachine with a photoresponsive molecular engine." Accounts of chemical research 47.6 (2014): 1663-1672.

[35] Kohman, Richie E., and Xue Han. "Light sensitization of DNA nanostructures via incorporation of photo-cleavable spacers." Chemical Communications 51.26 (2015): 5747-5750.

[36] Liang, Xingguo, Hidenori Nishioka, Nobutaka Takenaka, and Hiroyuki Asanuma. "A DNA nanomachine powered by light irradiation." ChemBioChem 9.5 (2008): 702-705.

[37] Zhou, Mengguang, Xingguo Liang, Toshio Mochizuki, and Hiroyuki Asanuma. "A light-driven DNA nanomachine for the efficient photoswitching of RNA digestion." Angewandte Chemie International Edition 49.12 (2010): 2167-2170.

[38] Chang, M., C. S. Yang, and D. M. Huang. "ACS Nano 2011, 5, 6156; b) D." Bhatia, S. Surana, S. Chakraborty, SP Koushika, Y. Krishnan, Nat. Commun 2 (2011): 339.

[39] Fraser, Lewis A., Andrew B. Kinghorn, Roderick M. Dirkzwager, Shaolin Liang, Yee-Wai Cheung, Bryce Lim, Simon Chi-Chin Shiu, Macro S. L. Tang, Dean Andrew, Joseph Manitta, Jack Richards, and Julian Tanner. "A portable microfluidic Aptamer-Tethered Enzyme Capture (APTEC) biosensor for malaria diagnosis." Biosensors and Bioelectronics 100 (2018): 591-596.

[40] Zhang, Huimin, Yanli Ma, Yi Xie, Yuan An, Yishun Huang, Zhi Zhu, and Chaoyong James Yang. "A controllable aptamer-based self-assembled DNA dendrimer for high affinity targeting, bioimaging and drug delivery." Scientific reports 5.1 (2015): 1-8.

[41] Chen, Yi, Seung-Hyun Lee, and Chengde Mao. "A DNA nanomachine based on a duplex–triplex transition." Angewandte Chemie International Edition 43.40 (2004): 5335-5338.

[42] Liu, D., and E. Cheng. "NPG. Asia Mater. 2011, 3, 109-114; d) Y. Dong, Z. Yang, D. Liu." Acc. Chem. Res 47 (2014): 1853-1860.

[43] Leroy, J. L. "M. Guéron, JL Mergny, C. Hélène." Nucleic Acids Res 22 (1994): 1600-1606.

[44] Majikes, Jacob M., Lucas CC Ferraz, and Thomas H. LaBean. "pH-driven actuation of DNA origami via parallel I-motif sequences in solution and on surfaces." Bioconjugate chemistry 28.7 (2017): 1821-1825.

[45] Hermann, Thomas, and Dinshaw J. Patel. "Adaptive recognition by nucleic acid aptamers." Science 287.5454 (2000): 820-825.

[46] Song, Chen, Zhen-Gang Wang, and Baoquan Ding. "Smart nanomachines based on DNA self-assembly." Small 9.14 (2013): 2382-2392.

[47] Perrault, Steven D., and William M. Shih. "Virus-inspired membrane encapsulation of DNA nanostructures to achieve in vivo stability." ACS nano 8.5 (2014): 5132-5140.

[48] J. C. Skou, Membrane Transport (Ed: D. C. Tosteson), Springer, New York, NY, USA 1989, pp. 155–185.

[49] Winder, S. J., B. G. Allen, O. W. M. P. CLÉMENT-CHOMIENNE, and M. P. Walsh. "Regulation of smooth muscle actin—myosin interaction and force by calponin." Acta Physiologica Scandinavica 164.4 (1998): 415-426.

[50] Zhu, Changjun, Jian Zhao, Marina Bibikova, Joel D. Leverson, Ella Bossy-Wetzel, Jian-Bing Fan, Robert T. Abraham, and Wei Jiang. "Functional analysis of human microtubule-based motor proteins, the kinesins and dyneins, in mitosis/cytokinesis using RNA interference." Molecular biology of the cell 16.7 (2005): 3187-3199.

[51] Rayment, Ivan, Hazel M. Holden, Michael Whittaker, Christopher B. Yohn, Michael Lorenz, Kenneth C. Holmes, and Ronald A. Milligan. "Structure of the actin-myosin complex and its implications for muscle contraction." Science 261.5117 (1993): 58-65.

[52] Berg, Jeremy M., John L. Tymoczko, and Lubert Stryer. "Biochemistry." (2002).

[53] Baker, Bryan A., Gita Mahmoudabadi, and Valeria Tohver Milam. "Strand displacement in DNA-based materials systems." Soft Matter 9.47 (2013): 11160-11172.

[54] Yurke, Bernard, Andrew J. Turberfield, Allen P. Mills, Friedrich C. Simmel, and Jennifer L. Neumann. "A DNA-fuelled molecular machine made of DNA." Nature 406.6796 (2000): 605-608.

[55] Yan, Hao, Xiaoping Zhang, Zhiyong Shen, and Nadrian C. Seeman. "A robust DNA mechanical device controlled by hybridization topology." Nature 415.6867 (2002): 62-65.

[56] Thubagere, Anupama J., Wei Li, Robert F. Johnson, Zibo Chen, Shayan Doroudi, Yae Lim Lee, Gregory Izatt, Sarah Wittman, Niranjan Srinivas, Damien Woods, Erik Winfree, and Lulu Qian. "A cargo-sorting DNA robot." Science 357.6356 (2017).

[57] F. C. Simmel, W. U. Dittmer, Small 2005, 1, 284.

[58] Shin, Jong-Shik, and Niles A. Pierce. "A synthetic DNA walker for molecular transport." Journal of the American Chemical Society 126.35 (2004): 10834-10835.

[59] Lo, Pik Kwan, Pierre Karam, Faisal A. Aldaye, Christopher K. McLaughlin, Graham D. Hamblin, Gonzalo Cosa, and Hanadi F. Sleiman. "Loading and selective release of cargo in DNA nanotubes with longitudinal variation." Nature chemistry 2.4 (2010): 319-328.

[60] Bujold, Katherine E., John CC Hsu, and Hanadi F. Sleiman. "Optimized DNA "nano-suitcases" for encapsulation and conditional release of siRNA." Journal of the American Chemical Society 138.42 (2016): 14030-14038.

[61] He, Lei, Dan-Qing Lu, Hao Liang, Sitao Xie, Can Luo, Miaomiao Hu, Liujun Xu, Xiaobing Zhang, and Weihong Tan. "Fluorescence resonance energy transfer-based DNA tetrahedron nanotweezer for highly reliable detection of tumor-related mRNA in living cells." ACS nano 11.4 (2017): 4060-4066.

[62] Okamoto, Akimitsu, Kazuo Tanaka, and Isao Saito. "DNA logic gates." Journal of the American Chemical Society 126.30 (2004): 9458-9463.

[63] You, Mingxu, Lu Peng, Na Shao, Liqin Zhang, Liping Qiu, Cheng Cui, and Weihong Tan. "DNA "nano-claw": logic-based autonomous cancer targeting and therapy." Journal of the American Chemical Society 136.4 (2014): 1256-1259.

[64] Ma, Dik-Lung, Hong-Zhang He, Daniel Shiu-Hin Chan, and Chung-Hang Leung. "Simple DNA-based logic gates responding to biomolecules and metal ions." Chemical Science 4.9 (2013): 3366-3380.

[65] Seelig, Georg, David Soloveichik, David Yu Zhang, and Erik Winfree. "Enzyme-free nucleic acid logic circuits." science 314.5805 (2006): 1585-1588.

[66] L. Qian, E. Winfree, DNA Computing (Eds: A. Goel, F. C. Simmel, P. Sosík), Springer, Berlin 2008, pp. 70–89.

[67] Rothemund, Paul WK. "Folding DNA to create nanoscale shapes and patterns." Nature 440.7082 (2006): 297-302.

[68] Mei, Qian, Xixi Wei, Fengyu Su, Yan Liu, Cody Youngbull, Roger Johnson, Stuart Lindsay, Hao Yan, and Deirdre Meldrum. "Stability of DNA origami nanoarrays in cell lysate." Nano letters 11.4 (2011): 1477-1482.

[69] Jiang, Qinghua, Yadong Wang, Yangyang Hao, Liran Juan, Mingxiang Teng, Xinjun Zhang, Meimei Li, Guohua Wang, and Yunlong Liu. "miR2Disease: a manually curated database for microRNA deregulation in human disease." Nucleic acids research 37.1 (2009): D98-D104.

[70] Peng, Lichun, Pu Zhang, Yaqin Chai, and Ruo Yuan. "Bi-directional DNA walking machine and its application in an enzyme-free electrochemiluminescence biosensor for sensitive detection of microRNAs." Analytical chemistry 89.9 (2017): 5036-5042.

[71] Wang, Zheng-Yong, Feng Li, Yan Zhang, Hui Zhao, Huo Xu, Zai-Sheng Wu, Jian-Xin Lyu, and Zhi-Fa Shen. "Sensitive detection of cancer gene based on a nicking-mediated RCA

of circular DNA nanomachine." Sensors and Actuators B: Chemical 251 (2017): 692-698.

[72] Feng, Qiu-Mei, Yue-Hua Guo, Jing-Juan Xu, and Hong-Yuan Chen. "Self-assembled DNA tetrahedral scaffolds for the construction of electrochemiluminescence biosensor with programmable DNA cyclic amplification." ACS applied materials & interfaces 9.20 (2017): 17637-17644.

[73] Kumar, Binod, Kumari Asha, and S. P. S. Chauhan. "DNAzyme mediated post-transcriptional gene silencing: A novel therapeutic approach." (2013).

[74] Chen, Yi, Mingsheng Wang, and Chengde Mao. "An autonomous DNA nanomotor powered by a DNA enzyme." Angewandte Chemie 116.27 (2004): 3638-3641.

[75] Bishop, Joshua D., and Eric Klavins. "An improved autonomous DNA nanomotor." Nano letters 7.9 (2007): 2574-2577.

[76] Juul, Sissel, Federico Iacovelli, Mattia Falconi, Sofie L. Kragh, Brian Christensen, Rikke Frøhlich, Oskar Franch, Emil Kristoffersen, Magnus Stougaard, Kam Leong, Yi-Ping Ho, Esben Sørensen, Victoria Birkedal, Alessandro Desideri and Birgitta Knudsen. "Temperature-controlled encapsulation and release of an active enzyme in the cavity of a self-assembled DNA nanocage." ACS nano 7.11 (2013): 9724-9734.

[77] Ruscito, Annamaria, and Maria C. DeRosa. "Small-molecule binding aptamers: Selection strategies, characterization, and applications." Frontiers in chemistry 4 (2016): 14.

[78] Mao, Chengde, Weiqiong Sun, Zhiyong Shen, and Nadrian C. Seeman. "A nanomechanical device based on the B–Z transition of DNA." Nature 397.6715 (1999): 144-146.

[79] Surana, Sunaina, Jaffar M. Bhat, Sandhya P. Koushika, and Yamuna Krishnan. "An autonomous DNA nanomachine maps spatiotemporal pH changes in a multicellular living organism." Nature communications 2.1 (2011): 1-7.

[80] Wang, Wenxing, Yang Yang, Enjun Cheng, Manchun Zhao, Haifeng Meng, Dongsheng Liu, and Dejian Zhou. "A pH-driven, reconfigurable DNA nanotriangle." Chemical Communications 7 (2009): 824-826.

[81] Elbaz, Johann, Zhen-Gang Wang, Ron Orbach, and Itamar Willner. "pH-stimulated concurrent mechanical activation of two DNA "tweezers". A "SET− RESET" logic gate system." Nano letters 9.12 (2009): 4510-4514.

[82] Pei, Hao, Le Liang, Guangbao Yao, Jiang Li, Qing Huang, and Chunhai Fan. "Inside Back Cover: Reconfigurable Three-Dimensional DNA Nanostructures for the Construction of Intracellular Logic Sensors (Angew. Chem. Int. Ed. 36/2012)." Angewandte Chemie International Edition 51.36 (2012): 9185-9185.

[83] Lee, Jennifer A., and Maria C. DeRosa. "A pH-driven DNA switch based on the $A^+ \cdot G$ mispair." Chemical communications 46.3 (2010): 418-420.

[84] Rich, Alexander. "DNA comes in many forms." Gene 135.1-2 (1993): 99-109.

[85] Mills, Martin, Paola B. Arimondo, Laurent Lacroix, Thérèse Garestier, Claude Hélène, Horst Klump, and Jean-Louis Mergny. "Energetics of strand-displacement reactions in triple helices: a spectroscopic study." Journal of molecular biology 291.5 (1999): 1035-1054.

[86] Han, Xiaogang, Zihao Zhou, Fan Yang, and Zhaoxiang Deng. "Catch and release: DNA tweezers that can capture, hold, and release an object under control." Journal of the American Chemical Society 130.44 (2008): 14414-14415.

[87] Yang, Mengqi, Xiaoling Zhang, Haipeng Liu, Huaizhi Kang, Zhi Zhu, Wen Yang, and Weihong Tan. "Stable DNA nanomachine based on duplex–triplex transition for ratiometric imaging instantaneous pH changes in living cells." Analytical chemistry 87.12 (2015): 5854-5859.

[88] Liu, Zhiyu, Yingmei Li, Cheng Tian, and Chengde Mao. "A smart DNA tetrahedron that isothermally assembles or dissociates in response to the solution pH value changes." Biomacromolecules 14.6 (2013): 1711-1714.

[89] Ranallo, Simona, Carl Prévost-Tremblay, Andrea Idili, Alexis Vallée-Bélisle, and Francesco Ricci. "Antibody-powered nucleic acid release using a DNA-based nanomachine." Nature communications 8.1 (2017): 1-9.

[90] Ranallo, Simona, Carl Prévost-Tremblay, Andrea Idili, Alexis Vallée-Bélisle, and Francesco Ricci. "Antibody-powered nucleic acid release using a DNA-based nanomachine." Nature communications 8.1 (2017): 1-9.

[91] H.-Z. He, D. S.-H. Chan, C.-H. Leung, D.-L. Ma, Nucleic Acids Res. 2013, 41, 4345.

[92] Li, Jianwei J., and Weihong Tan. "A single DNA molecule nanomotor." Nano Letters 2.4 (2002): 315-318.

[93] Liu, Dongsheng, Andreas Bruckbauer, Chris Abell, Shankar Balasubramanian, Dae-Joon Kang, David Klenerman, and Dejian Zhou. "A reversible pH-driven DNA nanoswitch array." Journal of the American Chemical Society 128.6 (2006): 2067-2071.

[94] O Tucker, W., K. T Shum, and J. A Tanner. "G-quadruplex DNA aptamers and their ligands: structure, function and application." Current pharmaceutical design 18.14 (2012): 2014-2026.

[95] Wu, Yongmei, Lina Zou, Sheng Lei, Qian Yu, and Baoxian Ye. "Highly sensitive electrochemi-cal thrombin aptasensor based on peptide-enhanced electrocatalysis of hemin/G-quadruplex and nanocomposite as nanocarrier." Biosensors and Bioelectronics 97 (2017): 317-324.

[96] Wei, Bryan, Immensee Cheng, Kathy Q. Luo, and Yongli Mi. "Capture and release of protein by a reversible DNA-induced sol–gel transition system." Angewandte Chemie International Edition 47.2 (2008): 331-333.

[97] Dittmer, Wendy U., Andreas Reuter, and Friedrich C. Simmel. "A DNA-based machine that can cyclically bind and release thrombin." Angewandte Chemie International Edition 43.27 (2004): 3550-3553.

[98] Kuzuya, Akinori, and Yuichi Ohya. "Nanomechanical molecular devices made of DNA origami." Accounts of chemical research 47.6 (2014): 1742-1749.

[99] You, Mingxu, Guizhi Zhu, Tao Chen, Michael J. Donovan, and Weihong Tan. "Programmable and multiparameter DNA-based logic platform for cancer recognition and targeted therapy." Journal of the American Chemical Society 137.2 (2015): 667-674.

[100] Nakatsuka, Keisuke, Hajime Shigeto, Akio Kuroda, and Hisakage Funabashi. "A split G-quadruplex-based DNA nano-tweezers structure as a signal-transducing molecule for the homogeneous detection of specific nucleic acids." Biosensors and Bioelectronics 74 (2015): 222-226.

[101] Peng, Pai, Lili Shi, Huihui Wang, and Tao Li. "A DNA nanoswitch-controlled reversible nanosensor." Nucleic acids research 45.2 (2017): 541-546.

[102] Wan, Shuo, Liqin Zhang, Sai Wang, Yuan Liu, Cuichen Wu, Cheng Cui, Hao Sun, Muling Shi, Ying Jiang, Long Li, Liping Qiu, and Weihong Tan. "Molecular recognition-based DNA nanoassemblies on the surfaces of nanosized exosomes." Journal of the American Chemical Society 139.15 (2017): 5289-5292.

Chapter 2

Dissociable DNA Nanogel

ABSTRACT. DNA nanotechnology has great potential for smart therapeutic delivery. We propose a new drug delivery platform that consists of pure DNA strands inspired by viruses' pH-responsive properties. This platform adopted a G-quadruplex structural configuration and induced a pH-responsive unit called intercalated motif (i-motif) as a pH-responsive unit for dynamic conformation change. The system was then modified with folic acid on the surface to enhance receptor-mediated cancer cell uptake. During endocytosis, the drug release procedure was initiated by i-motif-related nanogel dissociation, which responded to the local environmental switch from neutral to acidic. To demonstrate this concept, doxorubicin (Dox) was loaded onto DNA. Drug release was tested by Dox fluorescence recovery. The results showed that 56% of the cargo was released immediately after pH change. Cytotoxicity was then tested on folate receptor–enriched MCF-7, MDA-MB-231, and KB cells. The pH-responsive DNA nanogel decreased the IC50 from 1.3 to 0.5 µM and was 40% more cytotoxic to targeted cancer cell lines in a 1 µM drug dose compared to free Dox. Compared with a pH-insensitive DNA nanogel, the dissociable nanogel decreased the IC50 more than threefold.

2.1 Introduction

The enhanced permeability and retention effect [1, 2] allows nanoscale particles to accumulate in tumor tissues because of these tissues' higher nutrition demands and looser blood vessel junctions. Various drug delivery systems [3-11] have been developed in the past decades, including polymer nanoparticles [5,8], liposomes [10, 11], and some inorganic materials [3, 9]. Several nanoscale delivery systems have already been approved[12-23] for clinical therapy and have significantly improved the efficiency of drug delivery compared with traditional delivery methods. Polymer-based nanoparticles (Polyethylene glycol (PEG)-conjugation[12,13], micelles[14], and dendrimers[15]) are used to prolong the circulation time and improve the targeting effect. Liposomes[16-19] have been widely used in small-molecule drugs and vaccine delivery (i. e., Covid-19 mRNA vaccines[19]). Hydrogels[20-21] provide a tunable platform with a high water content and improved sustained release. Inorganic particles[22], such as silica nanoparticles[22], can be used for external stimulus-response (i.e., thermal heating[22]). However, the existing drug delivery systems still pose challenges. To increase their biocompatibility, circulation time, targeting effect, and controllable release, drug delivery systems must be multifunctional[14, 16]. However, multifunctional designs are complex and less programmable and may cause issues such as impurity and wide size distribution[23]. As discussed in Chapter 1, DNA-based platforms can perform diverse functions using different DNA motifs or sequence designs for base pairing, which are characterized by highly programmable self-assembly procedures and nano-size precision. Previous research has revealed two major DNA dynamic interactions, the Watson-Crick[24-29] and Hoogsteen base pairs[30-33], both of which follow clear rules and enable programming for artificial DNA structures. DNA nanotechnology provides state-of-the-art platforms in nanomedicine because of their

biodegradable and programmability [34].

Hydrogels [20-21, 35, 36] are excellent candidates for drug delivery because of their large pore sizes and loading capacity in the water phase. DNA hydrogels[35-37] are made of multiple building tiles that are cross-linked by stacking hydrogen bonds to assemble into the porous structure. An enzyme-catalyzed assembly method for the synthesis of DNA hydrogels was first reported in 2006 [35]. Different DNA nanogels could be produced by designing different building tiles. Li et al. reported the self-assembly of a DNA nanohydrogel for targeted gene regulation therapy [37]. However, DNA building tiles require long annealing times under exact temperature gradient conditions.

In this study, we employed a guanine quadruplex (G-quadruplex) structure to build a nanogel. G-quadruplex [30, 38, 39] is a specific DNA motif different from the Watson-Crick interaction, in which four guanine bases form a square planar arrangement square by Hoogsteen binding. Compared to the existing DNA nanostructure synthesis procedures, G-quadruplex is instantaneously formed and remains stable in the circulation system[40]. In 1910, Bang et al. reported the formation of a gel using a high concentration of guanylic acid[41]. Gellert et al.[42] found that four guanine molecules formed a square planar structure in which each guanine interacted with two adjacent guanines through Hoogsteen binding. When a monovalent cation is introduced into the structure, the ion occupies the central position between the stacks, thus enhancing the structure. Monovalent cations, especially potassium, are required to maintain the stability of the G-quadruplex structure. An instantaneous potassium-triggered G-quadruplex structure formation was reported in 2017 [43]. The G-quadruplex structure shows higher biostability, which improves heat and denaturation resistance, both in vitro and in vivo[44].

As previously discussed, controlled release is an essential step for drug delivery systems

41

[45,46]. Various triggering mechanisms, both internal and external, have been developed [47, 48]. As external triggering mechanisms require devices or extra procedures, the direct use of internal physiological conditions is preferred. Among internal triggering mechanisms, pH-based triggering [49] is a promising method. During endocytosis, the pH of the endosome decreases from 7.4 to approximately 5. In human influenza [50, 51], the virus travels along the endocytic system toward late endosomes, where the environment becomes acidic (pH 4–6). The pH change causes a conformation change in the glycoprotein hemagglutinin (HA) to enhance envelope fusion, followed by viral core disassembly in the cytosol and viral ribonucleoproteins (RNPs) entering the nucleus. Inspired by the pH-responsive dissociable properties of viruses, we propose a dissociable DNA nanogel.

Various DNA motifs are used to achieve pH-responsive behaviors. The intercalation cytosine motif (i-motif), first characterized in 1993 [52], is a DNA motif with the ability to change its conformation at different pH levels. Poly-cytosine sequences form the i-motif structure under a pH of less than 7 because protonation induces Hoogsteen bonding with cytosine (C:C+). Cheng et al. [53] integrated the i-motif into cross-linking to create a fast-responsive pH triggered DNA hydrogel.

In this Chapter, we used this technology to create nanoparticles for pH-based drug delivery. Drugs can be loaded onto the proposed DNA nanogel under physiological conditions and released during endocytosis. To test our platform, we chose doxorubicin (Dox) as a model drug. When DNA carriers travel in the circulation system, DNA can be easily degraded[54]. PEG has been reported to prolong the circulation time[12]. We designed the DNA nanogel to have non-hybridized 20A single strands hanging from its surface for easy binding to PEG-modified 20T single-stranded DNA.
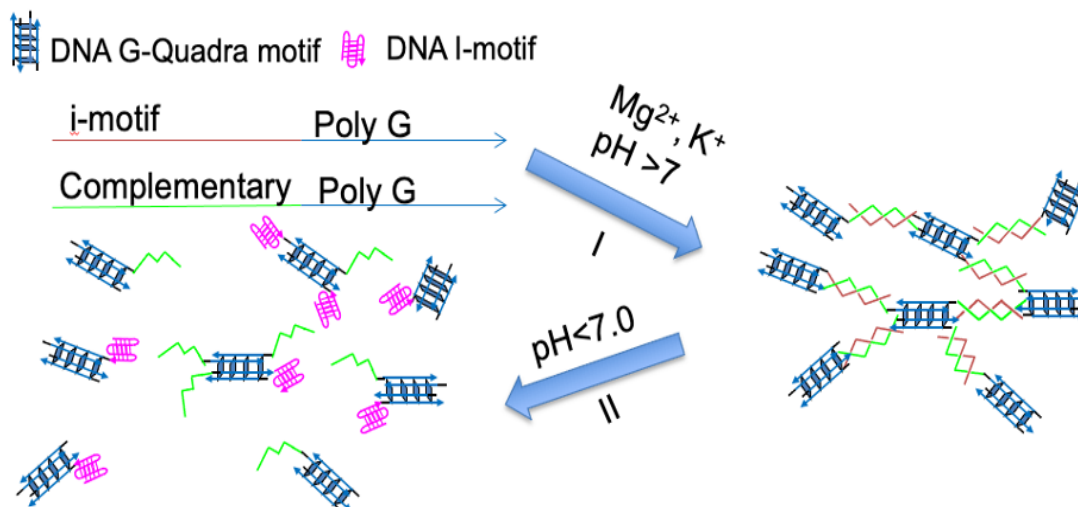
Figure 2.1: Schematic drawing of DNA nanogel formation and acid dissociation. Stage I: Nanogel formation by single-stranded DNA contains poly-G (forming a G-quadruplex) and an i-motif region (hybridized with its complementary strands) in the presence of Mg^{2+} and K^+ to form the nanogel. Stage II: When pH decreases to acidic levels, the DNA duplex dissociates, followed by i-motif structure formation.

As previously reported [55], DNA structures are difficult to deliver to cells, and folic acid is a widely used targeting agent for DNA carrier delivery. Cell membranes consist of a phospholipid bilayer embedded with various lipids and membrane proteins. Negatively charged nucleic acids are not easily taken up by cells without transfection agents. Although some DNA nanostructures can be taken up through caveolin-dependent receptor-mediated endocytosis, strategies to improve the targeting effect are needed. Conjugation with cell ligands [55, 56] is a widely used method for the uptake of DNA structures through receptor-mediated endocytosis. Because folate receptors are overexpressed on cancer cell membranes [55], folic acid is conjugated to DNA structures to produce a targeting effect. Mao et al.[57] conjugated folic acid to DNA nanotubes to improve uptake by HeLa cells. Similarly, Lee et al[58]. transfected a folate-modified DNA tetrahedron to KB cells. In this study, we modified the surface of the DNA nanogel with PEG–folic acid to prolong its lifetime and enhance cancer cell targeting. We conjugated PEG-modified 20T single-stranded DNA with a thiol group using folic acid–

maleimide to form single-stranded DNA modified with PEG–folic acid for easy binding to 20A overhanging the DNA nanogel.

2.2 Design
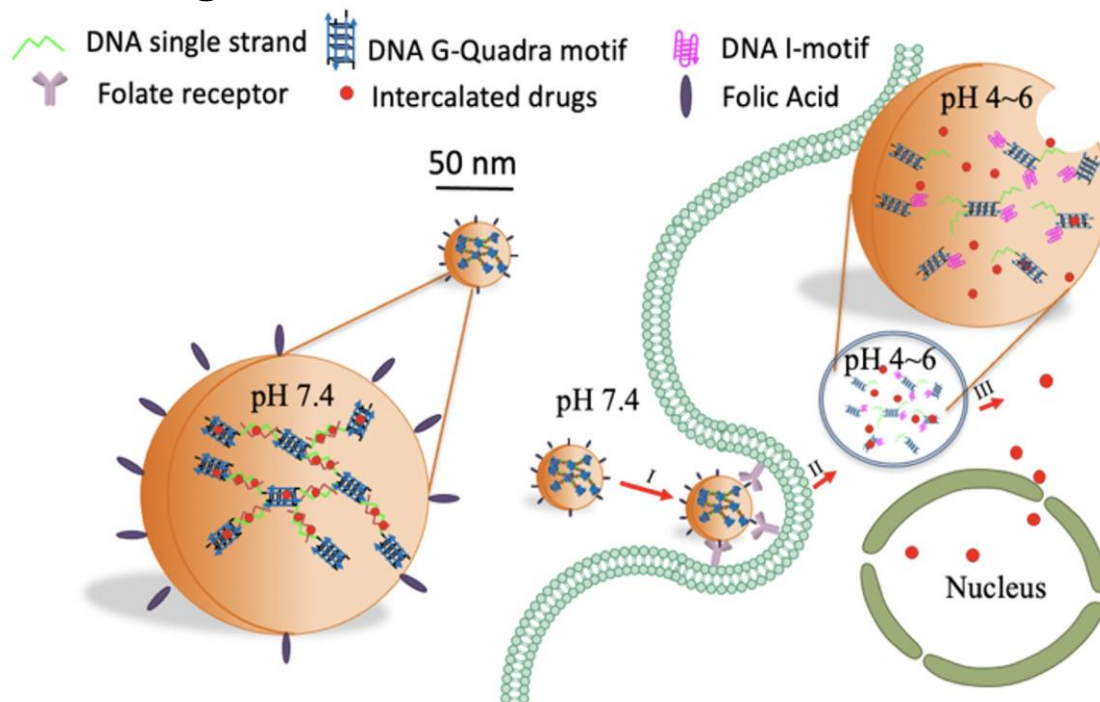
Figure 2.2: Schematic design of dissociable DNA nanogel drug release system. I, specific binding of nanogel to the over-expressing receptors on the tumor cells triggers receptor-mediated endocytosis; II, pH decreases and DNA nanogel dissociates followed by small molecule drugs release; III, diffusion of the released drug.

The proposed G-quadruplex-based DNA nanogel is illustrated in Figure 2.1. Stage I shows the nanogel formation. Under physiological pH, in the presence of Mg^{2+}, the i-motif sequence (green) and its complementary sequence (brown) hybridize and form double-stranded DNA. Both the i-motif strand and its complementary strand have poly-G bases at the 3' end. Thus, four poly-G bases form a G-quadruplex unit, which connects four strands and forms a cross-linking three-dimensional structure, which is called a nanogel system. Stage II shows nanogel dissociation under an acidic pH. C-rich i-motif strands designed to have C bases become pronated due to the low pH and form an intramolecular quadruplex i-motif structure. At the 5'

44

end of the i-motif/complementary strands, a sticky end (20A) was designed for further modification. Different functional elements, including antisense oligonucleotides for gene silencing, aptamers for targeting, and surface modification, can be designed for various applications.
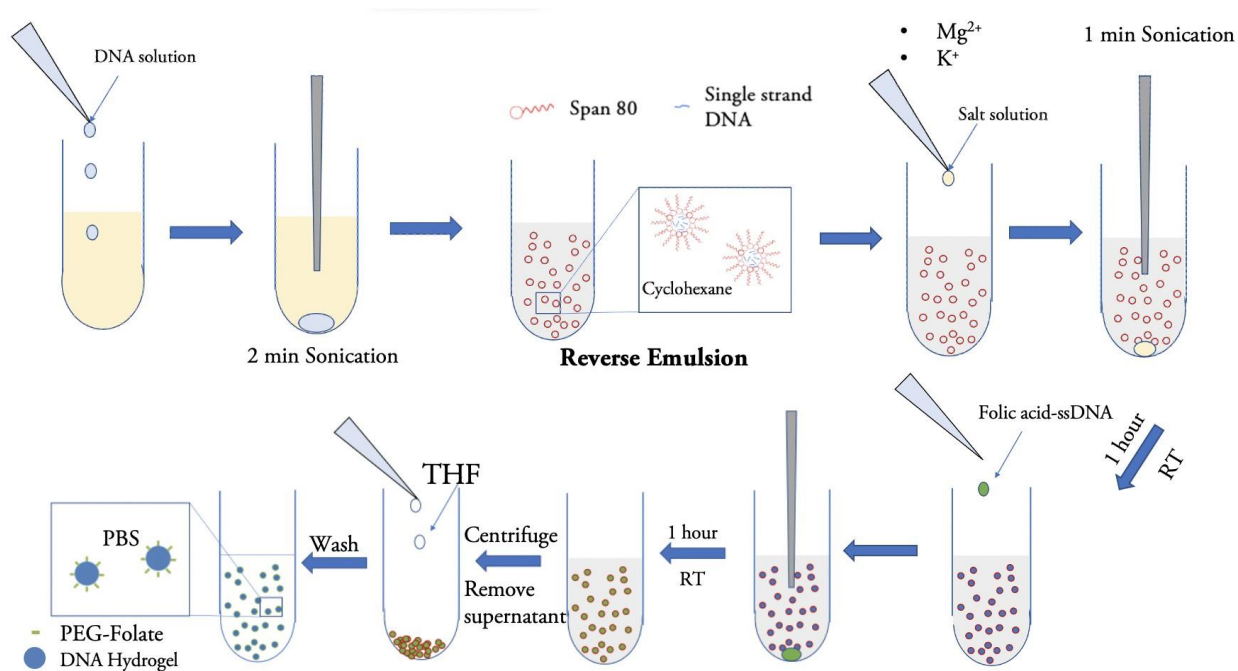
Figure 2.3: Synthesis of the DNA nanogel system by reverse emulsion.

Figure 2.2 shows an application of our dynamic dissociable DNA nanogel for cancer therapy. We chose Dox [56] to test the pH-responsive nanogel platform not only because it is widely used as an anticancer drug but also because its fluorescence property can be used to assess its loading onto the DNA duplex. When pH decreases during endocytosis, Dox loaded between base pairs is released because of the dissociation of the double helix. We modified folic acid on the surface of the nanogel for overexpressed folic acid receptor cancer cell targeting. In Stage I, the Dox-loaded DNA nanogel is taken up by cells via receptor-mediated endocytosis, during which the pH decreases from physiological levels to ~5. The i-motif is an energy-preferred structure compared to the double helix under acidic pH condition. It releases the complementary

45

strands to form an intramolecular i-motif structure, causing DNA nanogel dissociation. Drugs loaded onto the DNA nanogel are released and diffused into cytoplasm, finally accumulating in the nucleus and inducing cancer cell death. We used a DNA nanogel without the i-motif design as a control. This nanogel underwent no conformation change in an acidic microenvironment.

We employed a reverse emulsion system to synthesize the DNA nanogel (Figure 2.3; detailed description in Section 2.6) and ultrasonication to form the emulsion system. We used cyclohexane as the oil phase and Span 80 as a surfactant. We formed the DNA nanogel in the inner water phase in the presence of K^+ and Mg^{2+}, followed by the addition of DNA strands modified with folic acid to conjugate it. Then, we obtained the final product by washing away the surfactant after centrifugation using tetrahydrofuran (THF) and dispersed it in a phosphate-buffered saline (PBS) buffer.

The 20A overhang on the DNA nanogel are able to hybridize with a modified 20T strands. The modified 20T strand will be using a thiol maleimide click reaction. That is to say 20T DNA strands will be produced with a thiol group at the 3' end, which is prepared for conjugate with functional targeting structures[55,59,60] like arginylglycylaspartic acid (RGD), ligand of numb protein (LNX) or folic acid.

2.3   Characterization
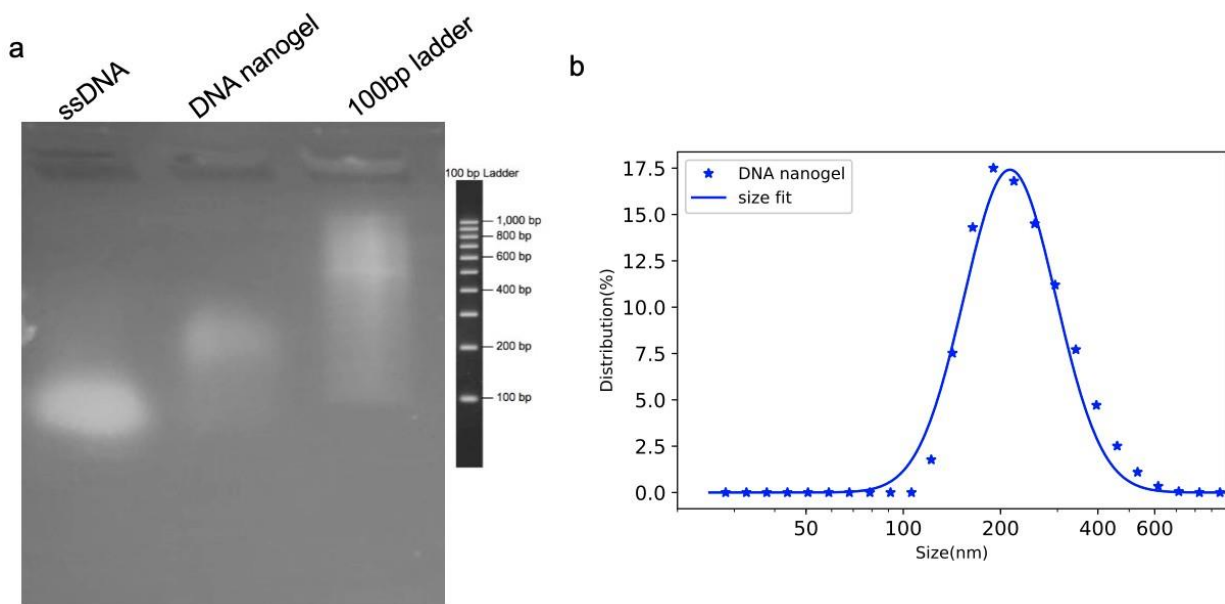
Figure 2.4: Formation of the DNA nanogel. (a) 1% agarose gel. Left: single-stranded DNA; middle: DNA nanogel; right: 100-bp ladder. (b) Measurement of DNA nanogel size using DLS.

We confirmed the formation of the G-quadruplex-based nanogel by electrophoresis (Figure 2.4 (a)) and dynamic light scattering (DLS) (Figure 2.4 (b)). Figure 2.4 (a) shows a 1% native agarose gel. The first lane is single-stranded DNA, the second lane is the DNA nanogel, and the third lane is the 100-bp DNA ladder. The mobility of the DNA nanogel was considerably lower than that of single-stranded DNA, suggesting the formation of a larger structure. Moreover, the DLS data (Figure 2.4 (b)) showed a ~200 nm structure in PBS, further confirming the formation of nanogel particles.

The 20A overhangs on the nanogel surface is supposed to further modification with functional agents. The advantage of DNA modification is that the conjugation doesn't require reaction with the whole DNA nanogel structure, which may cause the complexity of the self-assembly procedure of DNA nanogel. Instead, the covalent bonds with 20T-SH strands could be

formed first and then self-assemble with the DNA nanogel that has surface overhangs to the system. The 20T DNA strand was purchased with S-S group, which should be reduced to -SH group by reducing agent. The other advantage of this modification is the flexibility, we can expand similar procedure to conjugates different ligands to target different cells. In this study, we try conjugate 20T-SH group to RGD, LNX1, and folic acid, and the successful conjugation makes our design possible to be a general application.
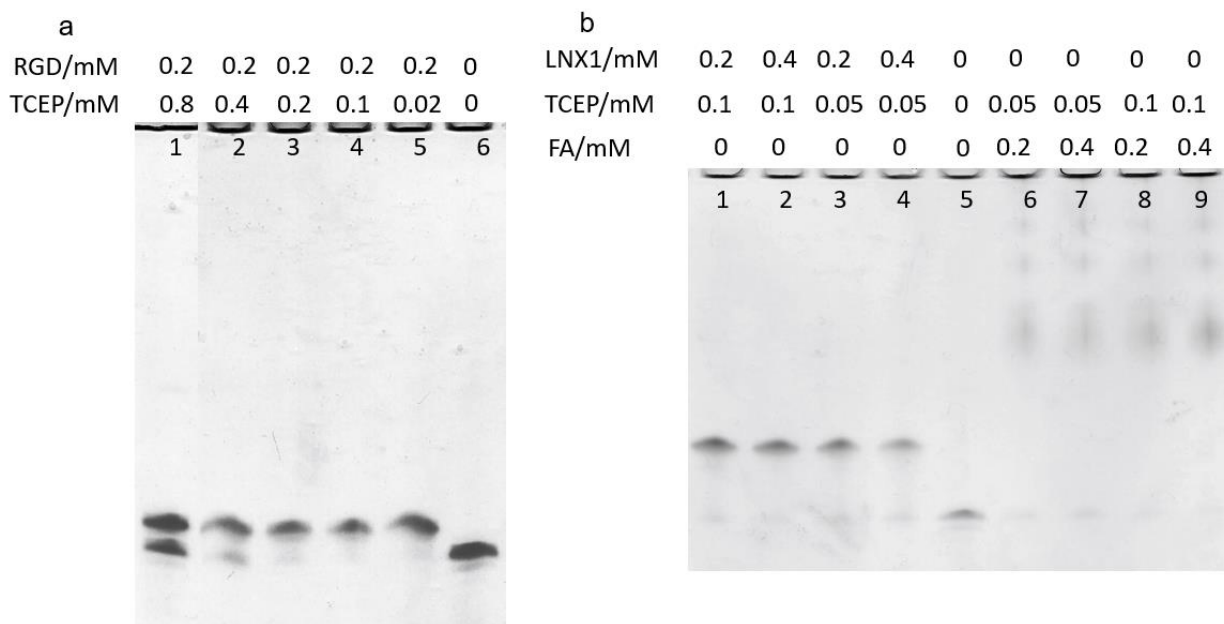
Figure 2.5: High yield ligand modification on 20T DNA single strands by click reaction. (a) RGD conjugation. Lane 1-5 RGD concentrations are fixed at 0.2 mM, which the TCEP concentration was 0.8, 0.4, 0.2, 0.1, and 0.02 respectively. The single strand DNA concentration was fixed at 10 μM. (b) LNX1 and PEG-Folic acid conjugation. Lane 1-4 showed the conjugation of single strand DNA-LNX1, lane 6-9 showed the conjugation of single strand DNA-folic acid.

Tris (2-carboxyethyl) phosphine (TCEP) and dithiothreitol (DTT) are widely used reducing agents, while TCEP is reported to be more stable and effective compared to DTT. In this study, we optimized the ratio of reducing agent to reactant and got an almost full conjugation yield. Figure 2.5 showed the high yield conjugation of RGD, LNX1, and PEG-folic acid with 20T single strand DNA. The lane 6 in figure 2.5 (a) and lane 5 in figure 2.5 (b) were the control that only contained unmodified single strand DNA. All the single strand DNA concentration was

fixed as 10 µM. Compared to other TCEP concentration, 0.1 mM showed the largest yield according to the electrophoresis, because the same position as single strand DNA was almost fully disappeared, and a higher mobility structure formed which is supposed to be the modified DNA single strand.
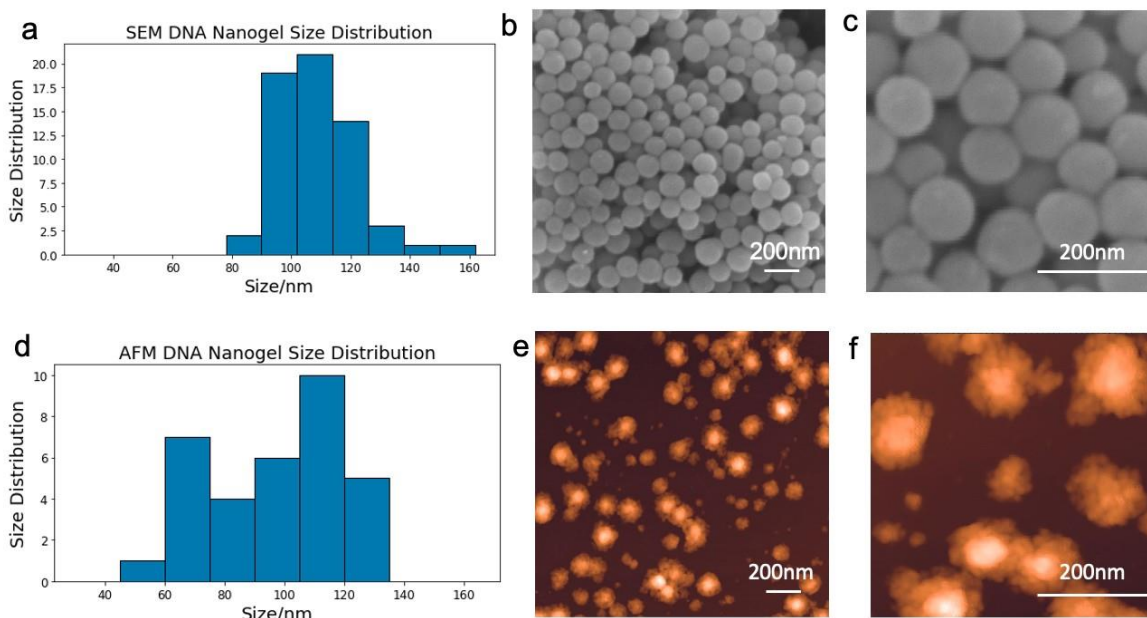
Figure 2.6: Characterization of G-quadruplex DNA nanogel. (a), size distribution of DNA nanogel under SEM; (b, c) SEM images of DNA nanogel; (d), size distribution of DNA nanogel under AFM; (e, f) AFM images of DNA nanogel.

To characterize the morphology of the DNA nanogel, we used scanning electron microscopy (SEM) and atomic force microscopy (AFM), as shown in Figure 2.6. The average diameter of the dry DNA nanogel was around 100 nm. The AFM images showed all the distributions as well as small particles, while the SEM images showed aggregation during the drying procedure. We also performed iridium sputtering to increase the conductivity of the DNA nanogel. SEM showed larger particle diameters (109 nm) than AFM (97 nm). As the nanogel tended to aggregate, we optimized the reverse emulsion parameters (such as ultrasonication and Span 80 concentration). After optimization of the synthesis conditions and conjugation with PEG–folic acid, aggregation was prevented, and the diameter decreased (Figure 2.7) to around 50

49

nm (46 nm as measured using AFM and 68 nm as measured using SEM). This was possibly because PEG-folate was positively charged and compressed the DNA nanogel. Furthermore, PEG-folate conjugation prevented the DNA nanogel from aggregating, resulting in smaller particles in the system. Moreover, ultrasonication made the reverse emulsion system more stable, also resulting in a smaller size.
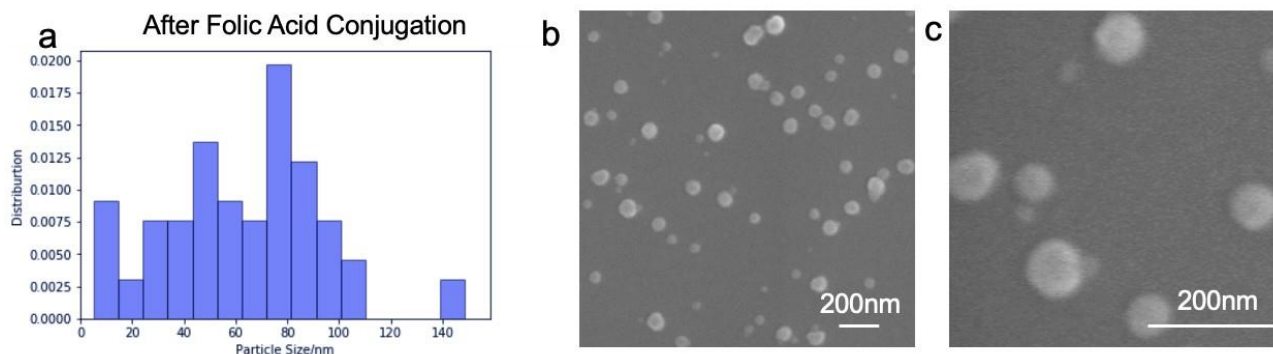
Figure 2.7: Folic acid conjugation. (a) Size distribution of DNA nanogel after PEG-folic acid modification. (b, c) SEM images of PEG-folic acid modified DNA nanogel, (c) is a magnification of (b). Scale bar: 200 nm.

After confirming the formation of the G-quadruplex DNA nanogel, we proceeded to apply the i-motif design. Since our platform is meant to be used under physiological conditions, we tested the size at pH 7.4 and 5.5. We confirmed the formation of the dissociable DNA nanogel at physiological pH by both polyacrylamide gel electrophoresis (PAGE) and agarose gel electrophoresis (Figure 2.8 (a, c)). The control lane consisted of a single-stranded DNA marker, which had the same molecular weight and bases as the single-stranded DNA that we used to create the nanogel. When the nanogel formed, its mobility decreased because of the formation of larger structures. The mobility difference between the sample and the control in agarose gel indicated the successful formation of the DNA nanogel.
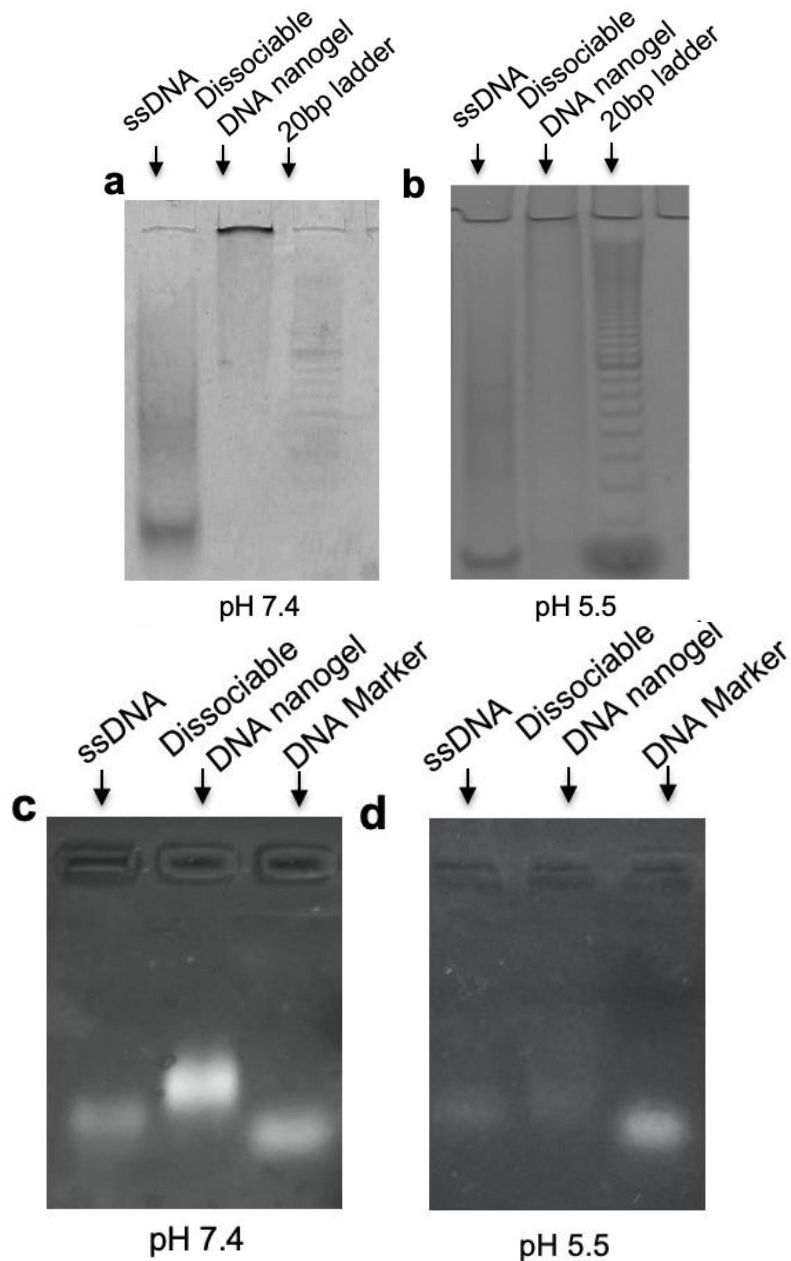
Figure 2.8: Behavior of the pH-responsive dissociable DNA nanogel. (a, b) 5% PAGE gel. (a) TAE/Mg buffer, pH 7.4; (b) MES buffer, pH 5.5. (c, d) 1% agarose gel. (c) TAE/Mg buffer, pH 7.4; (d) MES buffer, pH 5.5. (e, f) AFM images of dissociable DNA nanogel.

To characterize the conformation change of the pH-responsive dissociable DNA nanogel, we performed electrophoresis in buffers at pH 7.4 (Figure 2.8 (a, c)) and 5.5 (Figure 2.8 (b, d)). In Figure 2.8 (a–d), the first lanes are single-stranded DNA, the second lanes are dissociable DNA,

51

and the third lanes are the DNA ladder (PAGE) or DNA marker (agarose gel). The pH-responsive

DNA nanogel could not run into the 5% PAGE gel (Figure 2.8 (a, b)), suggesting that a new

DNA product with a greater molecular weight was formed. Although most of the DNA nanogels

were in the sample loading zone and could not run into the gel, differences in gel bands could still

be observed. Notably, at pH 5.5, more DNA strands dissociated and ran into the PAGE gel

because the intensity of that lane was higher. Moreover, at pH 7.4, the DNA nanogel did not have

a band at the single-stranded DNA position, while there was a faint band in the DNA nanogel

with mobility similar to that of single-stranded DNA, which indicated its dissociation at pH 5.5.
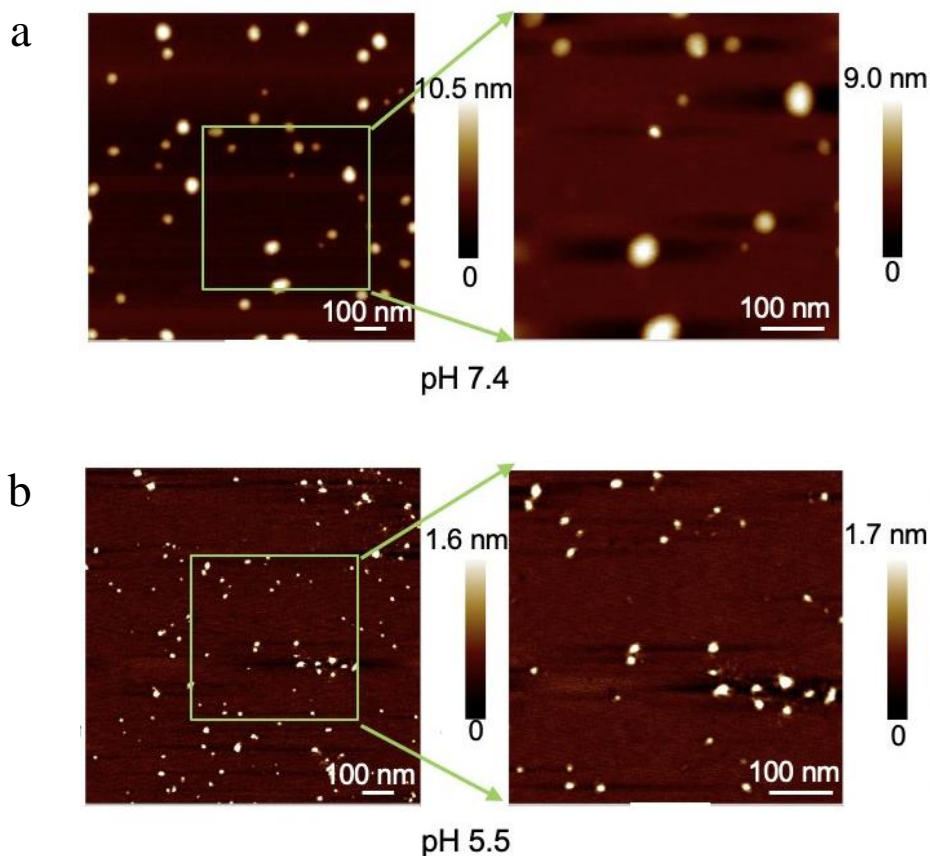
Figure 2.9 AFM images of dissociable DNA nanogel. (a) pH 7.4. (b) pH 5.5. The right-hand
AFM image shows a magnified area of the left-hand one. All scale bars: 100 nm.

Although more DNA strands dissociated and migrated into the PAGE gel under the lower

pH condition, the major bands were stuck in the well because most DNA structures were still

intact, held together by the G-quadruplex structure. This is because G-quadruplex has a wider pH
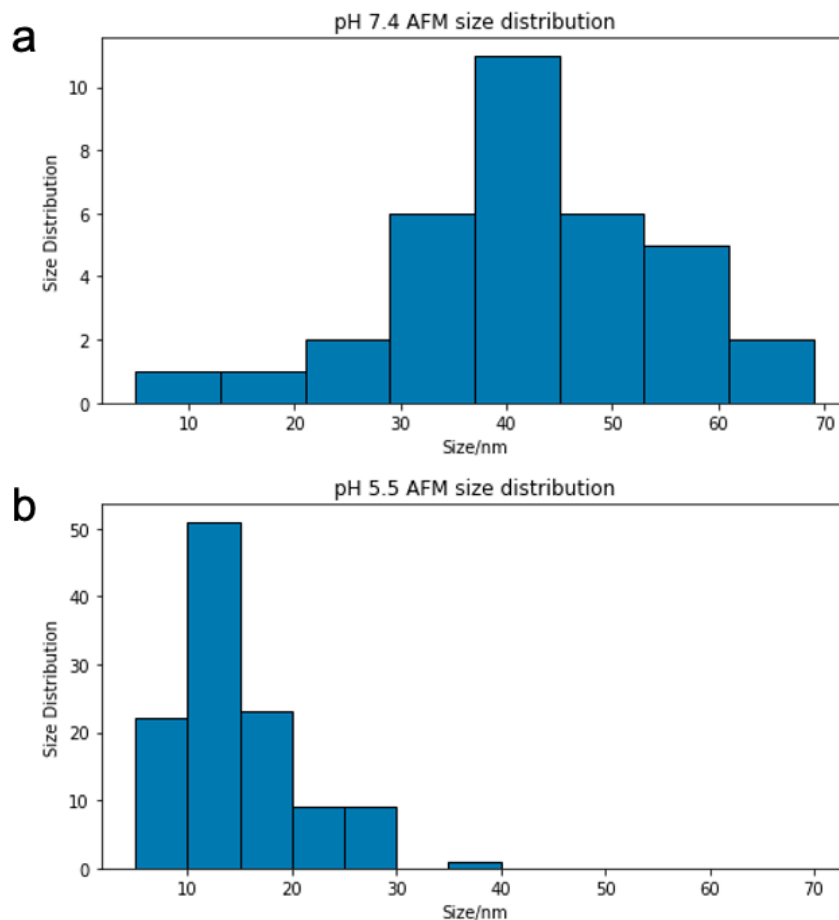
Figure 2.10: Size distribution of the dissociable DNA nanogel obtained from AFM images (analyzed using ImageJ). (a) pH 7.4. (b) pH 5.5.

tolerance range, which makes it less vulnerable to pH changes.

To compare the sizes of the larger DNA structures, we chose 1% agarose gel (Figure 2.8

(c, d)) to compare the conformation changes under the different pH conditions, as it permits

larger structures. The comparison showed that the pH-responsive DNA nanogel had higher

mobility in the acidic condition (pH 5.5) than in the physiological condition (pH 7.4).

Moreover, whereas the distances between single-stranded DNA and the marker at pH 7.4 and

5.5 were the same, the distance between the DNA nanogel and the marker at pH 5.5 was half of that at pH 7.4, confirming the dissociation of the pH-responsive DNA nanogel under acidic conditions.

AFM air-mode images (Figure 2.9) further confirmed the dissociation of the pH-responsive nanogel under acidic conditions. The nanogel had a smaller size and an irregular shape at pH 5.5 compared to pH 7.4 in terms of both diameter and height profiles. The diameter was 43 nm at pH 7.4, while the size changed to less than 15 nm at pH 5.5, as measured using ImageJ (Figure 2.10). Notably, the height was around 1.5 nm at pH 5.5 and around 9 nm at pH 7.4, further confirming that the nanogel dissociated under acidic conditions.
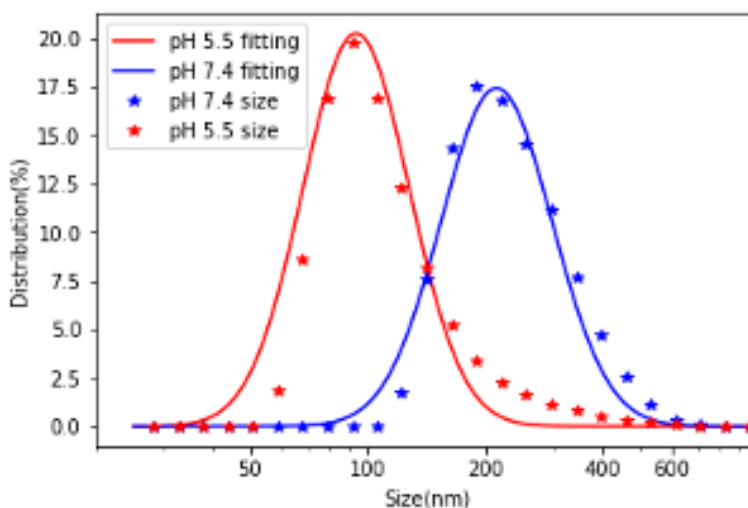
Figure 2.11: Size distribution of the dissociable DNA nanogel measured by DLS. Blue: size distribution at pH 7.4. Red: size distribution at pH 5.5.

DLS (Figure 2.11) also confirmed the size difference under the different pH conditions. The DNA nanogel dissociated under acidic pH, which resulted in an irregular shape, as revealed by AFM. The DLS data lacked this information. Although DLS is not an ideal method for nanogel characterization, it still showed the nanogel's tendency to dissociate. The

hydration size of the nanogel at pH 7.4 was 208.9 nm with a polydisperse index (PDI) of 0.155, while at pH 5.5, the size changed to 93.3 (mean peak) with a PDI of 0.233. The results confirmed the formation of the pH-responsive DNA nanogel and its dissociation under acidic conditions, indicating that our design was successful.

2.4   Enhanced Drug Release and Cytotoxicity

After validating the basic transformation mechanism of the system, we tested its drug loading and release profiles. For this purpose, we chose Dox. The advantage of Dox as a testing drug is that it can be loaded onto the DNA double helix through intercalation [27,31]. Moreover, it has a fluorescence peak at 590 nm, which is quenched once intercalated into the DNA double helix [27,31] due to the initiation of Forster resonance energy transfer between Dox molecules. Hence, its fluorescence signal can be used to assess drug loading and release.

We used a Dox-loaded DNA nanogel under native conformation as a control pH-insensitive nanogel, designed using a random duplex sequence with the same length as the i-motif sequence to ensure that no conformation change would occur during pH change. The release profile mimicking a delivery system releasing Dox from a membrane system was obtained by a dialysis assay, is shown in Figure 2.12. The solid lines indicate the pH 7.4 condition, and the dashed lines indicate the pH 5.5 condition. Black indicates free Dox, blue indicates the Dox-loaded pH-insensitive DNA nanogel, and red indicates the Dox-loaded dissociable DNA nanogel. Dox in both systems was the same concentration, while free Dox had similar absorbance under both physiological and acidic conditions. Within 20 h, the pH-responsive DNA nanogel released ~65% at pH 5.5. Compared to the pH 7.4 condition, the released Dox increased by 22%, suggesting that the acidic condition enhanced the release of

Dox because of the conformation change. This indicates that the i-motif structure is essential for the conformation change of the dissociable DNA nanogel and induces a fast release of intercalated Dox in a low pH environment. Conversely, in a physiological environment, Dox remains intercalated in the inner position of the DNA nanogel. Notably, the pH-insensitive DNA nanogel also released Dox under the acidic condition (from 42.42% to 53.79%), probably because Dox was protonated and was easier to diffuse. A comparison between the pH-insensitive and pH-sensitive DNA nanogels showed that at pH 7.4, the amounts of Dox released were at the same level, whereas at pH 5.5, the pH-sensitive nanogel showed more than 10% release after 20 h. Moreover, the i-motif conformation change was rapid, suggesting that Dox release was immediate. Figure 2.12 shows the Dox releasing against the dialysis membrane instead of dynamic release, which mimics the drug's penetration from the membrane system to the cell plasm. To further investigate the immediate dynamic dissociation of the DNA duplex and the release of Dox, we conducted a Dox fluorescence quenching experiment.
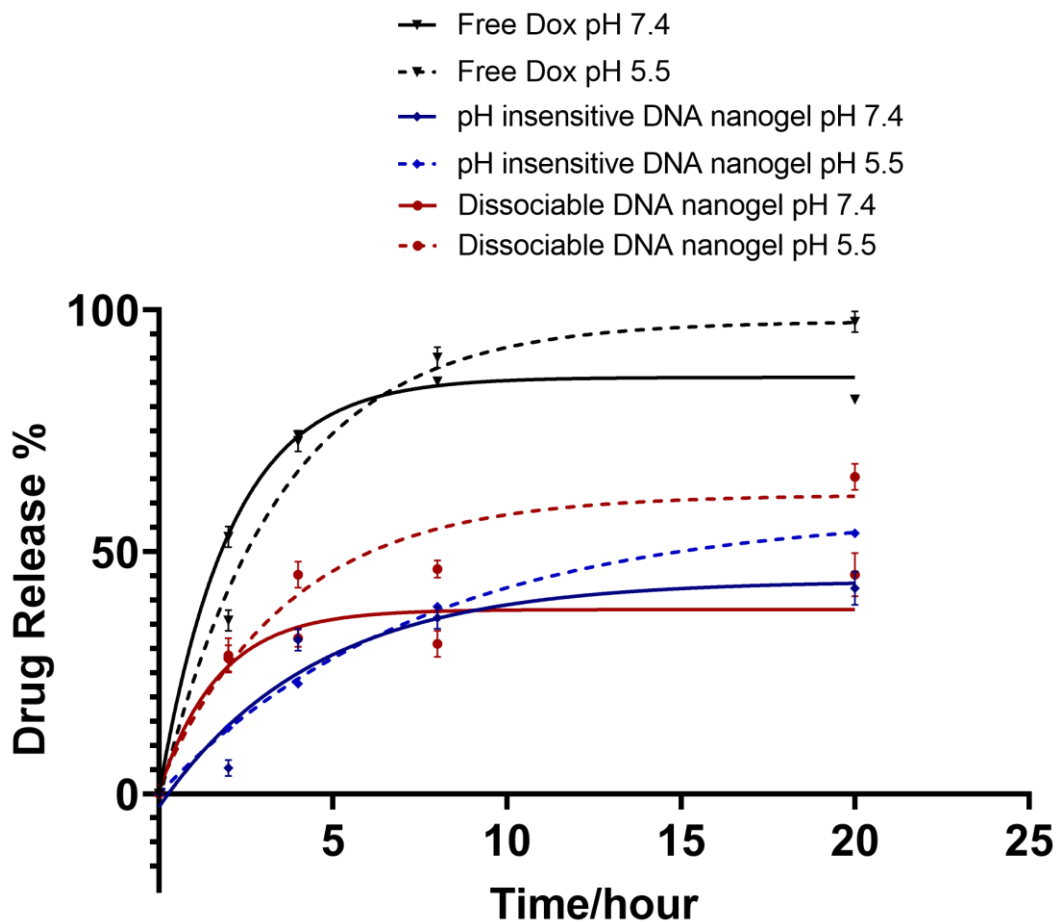
Figure 2.12: Release profile of the dissociable DNA nanogel. The solid lines are the release profiles at pH 7.4, and the dashed lines are the release profiles at pH 5.5. The red curves indicate the Dox-loaded dissociable DNA nanogel. Free Dox (black) and Dox-loaded pH-insensitive DNA nanogel (blue) were used as controls.

It has been reported that when Dox is incubated with the DNA duplex, its fluorescence decreases due to the initiation of Forster resonance energy transfer between Dox molecules when intercalated into the DNA duplex, whereas the dissociation of a Dox-loaded duplex causes the release of Dox, which is indicated by the recovery of its fluorescence signal [27]. We exploited this property of Dox to test its instantaneous release. Figures 2.13 and 2.14 show the observed fluorescence recovery. Free Dox was used as a control (Figure 2.13, left-hand set), to which we added a PBS buffer instead of DNA nanogel (in the same amount) to

57

avoid the effect of dilution on fluorescence signal quenching. Free Dox was inserted into the

DNA double helix immediately after the addition of the DNA nanogel to the system, and the

fluorescent signal of Dox was subsequently quenched. After pH decreased to acidic levels,

Dox was released during double helix dissociation and i-motif formation, leading to

fluorescent signal recovery. In Figure 2.13, the black columns show the fluorescence intensity

of Dox, the gray columns show the fluorescence intensity after adding samples at pH 7.4, the

orange columns show the fluorescence intensity of Dox-loaded samples after decreasing the

pH to 5.5, and the red columns show the fluorescence intensity after adjusting the pH to 5. The

gray, orange, and red columns in the control set show the fluorescence intensity of Dox after
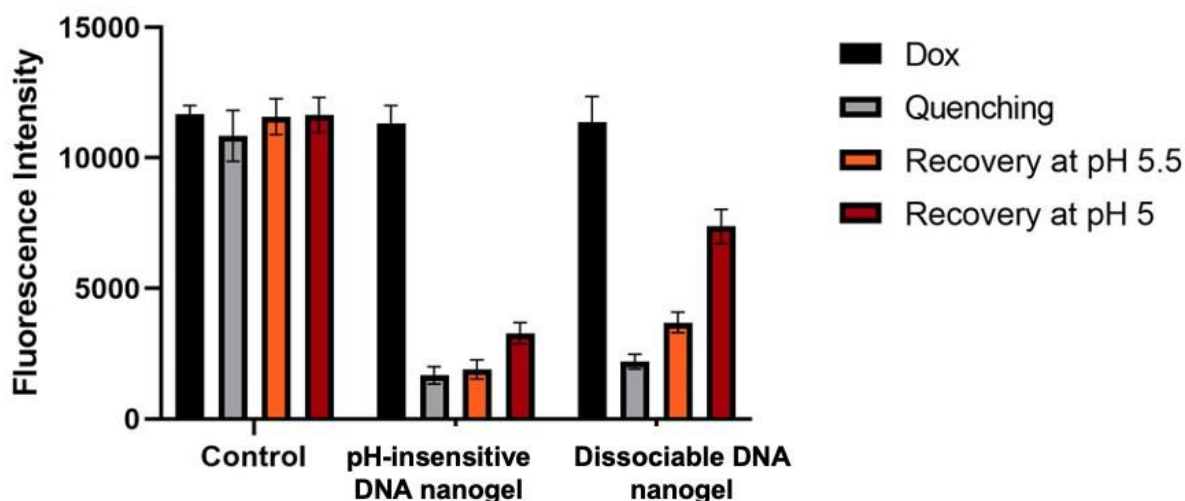
Figure 2.13: Dox loading onto and instantaneous release from the dissociable DNA nanogel. Black: Dox fluorescence; gray: Dox fluorescence after quenching by the DNA nanogel; orange: recovered Dox fluorescence after the pH decreased to 5.5; red: recovered Dox fluorescence after the pH was adjusted to 5. The left-hand set is the control with a PBS buffer instead of DNA nanogel (in the same volume), the middle set is the pH-insensitive DNA nanogel, and the right-hand set is the dissociable nanogel.

adding a PBS buffer in the same volume as that of the DNA nanogels. Both the pH-insensitive

and dissociable DNA nanogels quenched the Dox fluorescence signal by loading Dox into the

duplex. Dox in the dissociable DNA nanogel showed higher fluorescence recovery under

acidic conditions.
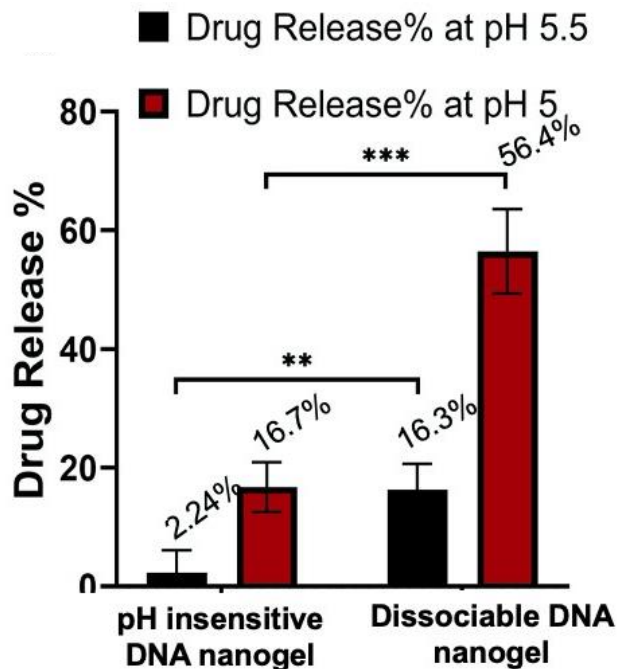
Figure 2.14: Dynamic drug release triggered under acidic conditions. Black: drug release percentage at pH 5.5, red: drug release at pH 5. The error bars indicate standard deviations (n = 3). **p < 0.01, ***p < 0.005 (two-tailed Student's t-test).

We calculated fluorescence recovery as $(F_{recover} - F_{quench})/(F_0 - F_{quench})$, where F_0 indicates the fluorescence intensity of free Dox, Fquench indicates the fluorescence intensity of Dox in the DNA nanogel at pH 7.4 at the same concentration as F_0, and Frecover indicates its fluorescence intensity in the nanogel at pH 5.5 at the same concentration as F_0. The results showed that Dox release from the DNA duplex was pH dependent. Figure 2.14 shows drug release under different pH conditions. The pH-responsive nanogel had a 56% fluorescence signal recovery after the pH decreased to 5 by hydrochloric acid (HCl). After the addition of the nanogel to the system, fluorescence was quenched 80.83. Quenched fluorescence recovered 16.5% at pH 5.5 and 56.53% at pH 5. By contrast, the pH-insensitive nanogel had only 16% of recovery, which indicated that our pH-responsive nanogel released 3-4 fold more

drug under acidic conditions compared to the nanogel without a pH-sensitive design.

Encouraged by its drug release performance, we tested our platform on breast cancer cell lines. Confocal microscopy (Figures 2.15 and 2.16) revealed that the pH-responsive DNA nanogel had a co-localized fluorescence signal of nuclei and Dox. We used the MDA-MB-231 cell line to investigate the intracellular Dox distribution in cancer cells incubated with free Dox, Dox-loaded pH-insensitive DNA nanogel, and Dox-loaded pH-sensitive nanogel. The blue fluorescence signal represents (diamidino-2-phenylindole) DAPI-stained nuclei and the red signal represents Dox. Dox accumulated at the nucleus with a co-localization of red and blue signals, indicating that it was delivered to the nucleus as expected. To further test the efficacy of drug delivery, we performed a cytotoxicity assay.
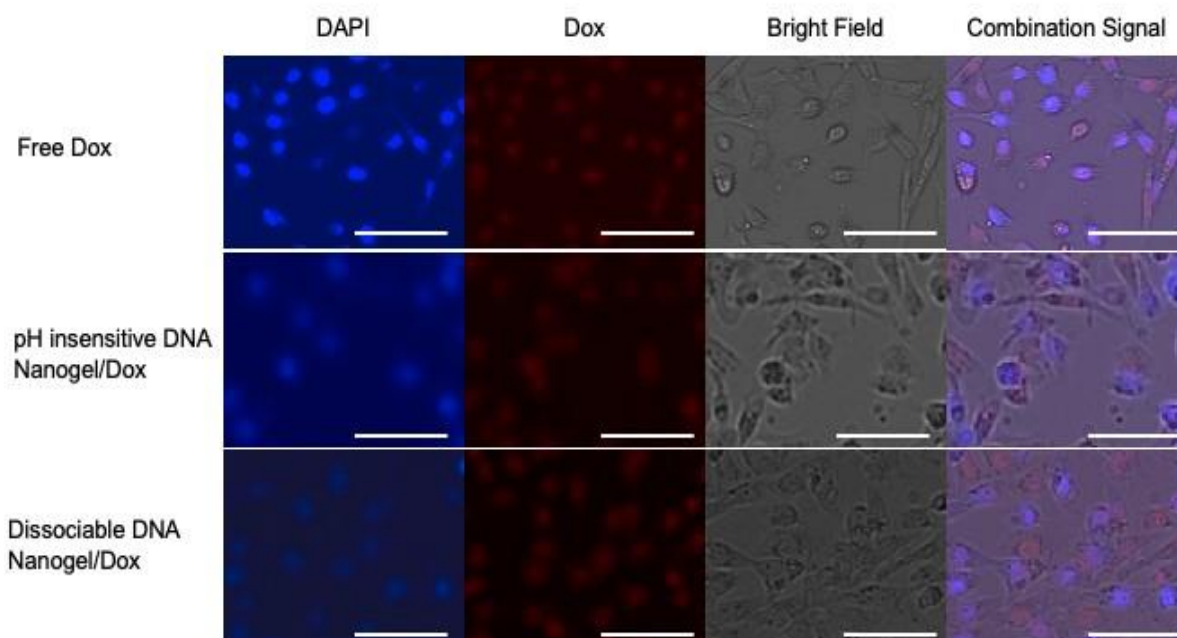
Figure 2.15: Confocal microscopy images of Dox aggregation at nuclei. Blue: DAPI-stained nucleus; red: Dox signal; purple: co-localized DAPI and Dox signals. All scale bars represent 100 µm. Cell line: MDA-MB-231.
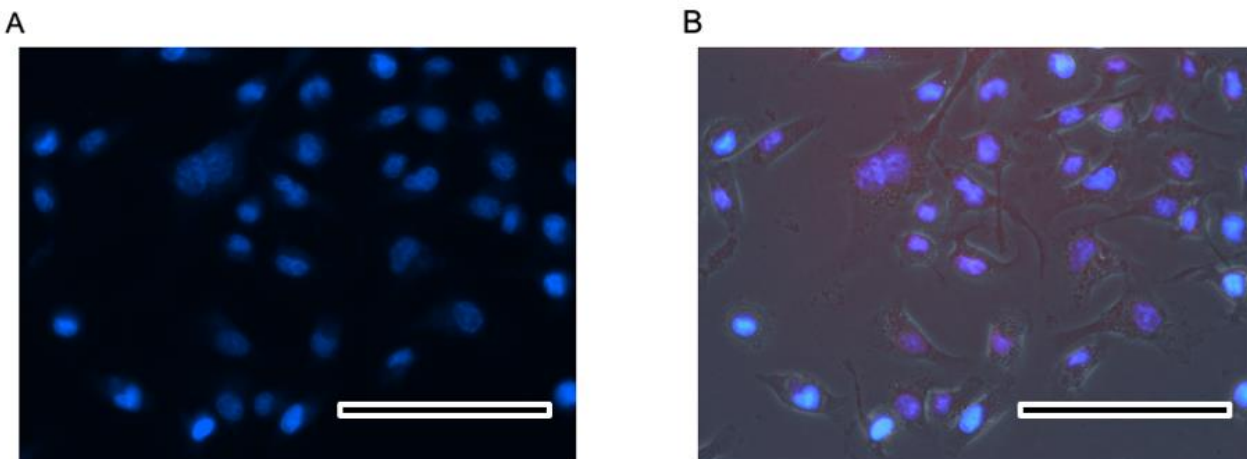
Figure 2.16: Co-localization of Dox and nucleus. (a) DAPI staining. (b) Merged signal of DAPI, Dox, and Bright field. Blue: DAPI-stained nucleus; purple: co-localized DAPI and Dox signal. Cell line: MDA-MB-231. All scale bars represent 100 µm.

To investigate the in vitro cytotoxicity of the Dox-loaded nanogel against folate receptor–rich MDA-MB-231 and MCF-7 cells, we performed a 3-(4,5-dimethylthiazol-2-yl)-2,5-diphenyltetrazolium bromide (MTT) assay. Figure 2.17 shows Dox loaded onto the pH-insensitive and pH-responsive nanogels in the same amounts as that of free Dox (1 µM). Black represents MCF-7 cells treated with PBS as controls, orange indicates the pH-insensitive nanogel, and gray indicates the pH-responsive nanogel. Notably, the cell viability of the controls indicated that the DNA nanogels were nontoxic to cells.

In the MCF-7 and MDA-MB-231 cell lines, the blue and red columns show the cell viability of Dox-loaded pH-insensitive and pH-responsive nanogels, respectively. The Dox concentration was the same as that in the control (1 µM). After 12-h treatment, the pH-responsive nanogel was more cytotoxic to both MDA-MB-231 and MCF-7 cells than free Dox and the pH-insensitive nanogel. Especially in the MCF-7 cell line, the pH-sensitive nanogel had only 37% cell viability, which showed 2-fold and 15% higher cytotoxicity than free Dox

and the pH-insensitive nanogel, respectively, suggesting that the dissociable design enhanced the delivery of Dox.
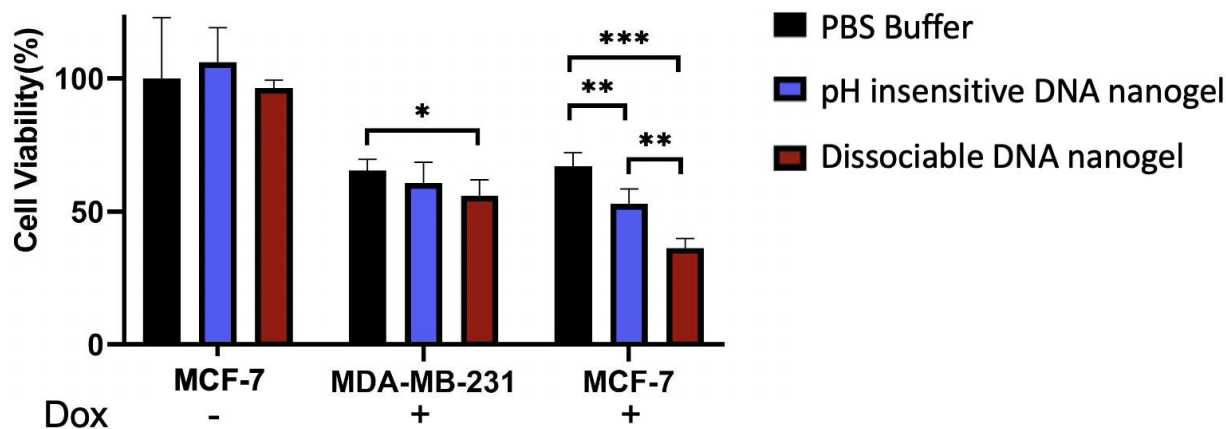
Figure 2.17: Cytotoxicity after 12-h treatment with Dox (1 µM) loaded onto the pH-insensitive and dissociable DNA nanogels. Black: cells treated with free Dox; blue: cells treated with the Dox-loaded pH-insensitive nanogel; red: cells treated with the Dox-loaded dissociable nanogel. Two cell lines were tested. The left-hand sets show control experiments without Dox treatment. The error bars indicate standard deviations (n = 3). *$p < 0.05$, **$p < 0.01$, ***$p < 0.005$ (two-tailed Student's t-test).
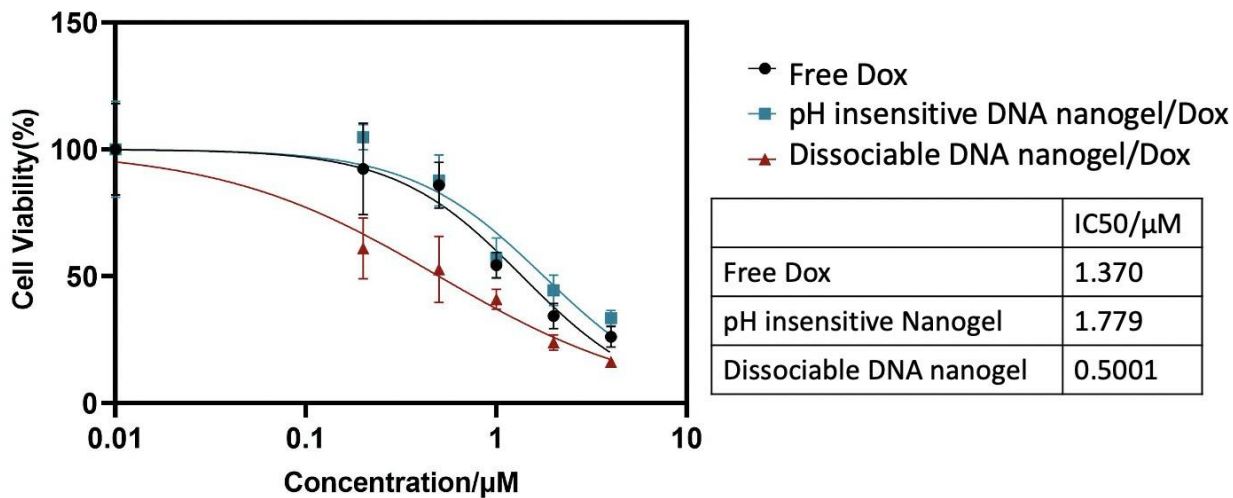
Figure 2.18: Dose-response cell viability of the Dox-loaded dissociable DNA nanogel. Black: free Dox; blue: Dox-loaded pH-insensitive nanogel; red: Dox-loaded dissociable nanogel. Cell line: KB cells.

To further investigate the effectiveness of our DNA nanogel in killing cancer cells, we created Dox dose-response curves using the KB cell line, shown in Figure 2.18. Half-maximal inhibitory concentration (IC50) is the concentration of an inhibitor at which the response is reduced by half, which is a good indicator of cell cytotoxicity. Cytotoxicity induced after 24-h treatment with the Dox-loaded pH-responsive DNA nanogel decreased the IC50 from 1.37 μM (free Dox cytotoxicity) to 0.5001 µM. Moreover, compared to the pH-insensitive nanogel (IC50 of 1.779 µM), the dissociable nanogel showed more than 3-fold higher cytotoxicity. These results showed that our pH-responsive dissociable DNA nanogel improved the efficacy of drug delivery to targeted cancer cell lines.

2.5   Conclusion

In this study, we developed a novel drug delivery platform based on a G-quadruplex-formulated DNA nanogel. To make the nanogel pH-responsive, we modified it by introducing an i-motif structure to achieve acid dissociation, thus enhancing drug release under acidic conditions. We confirmed the conformation changes from physiological to acidic conditions by performing electrophoresis, AFM, and Dox fluorescence quenching experiments. The pH-responsive nanogel showed higher cytotoxicity than the non-pH-responsive nanogel, and its conformation changed immediately. These properties make our dissociable DNA nanogel a promising platform for drug delivery. In this study, we used Dox intercalated into DNA strands. However, we speculate that other small molecule drugs, oligonucleotides, or peptides, could also be loaded onto the DNA nanogel using different interactions. Moreover, we believe that the nanogel platform has potential for larger molecular drugs as well because of the pore structure between the gel cross-links.

2.6   Methods

Materials. All DNA strands were purchased from Integrated DNA Technologies. Cyclohexane was purchased from Spectrum (CAS 110-82-7). Span 80 was purchased from Tokyo Chemical Industry Co. (CAS 1338-43-8). Water was made using MicroPure ST (Thermo Fisher Scientific). THF was purchased from EMD (TX0280-6). PAGE gels were made using a 40% acrylamide/bis-acrylamide solution (19:1) purchased from BIO-RAD (cat. No. 161-044) with the respective buffers. Agarose gels were made using Agarose LE purchased from Culgene (cat. No. C8740) with the respective buffers. Magnesium and potassium were made from magnesium acetate tetrahydrate (lot No. D26Y034; Alfa Aesar) and potassium chloride (M-12445; Thermo Fisher Scientific), respectively. Folic acid–PEG-maleimide was purchased from NANOCS (lot No. 110511). Tris (2-carboxyethyl) phosphine (TCEP) was purchased from MP Biomedicals. Dox was purchased from Thermo Fisher Scientific (lot No. 154656). Hydrochloric acid was purchased from J. T. Baker.

Buffers. The TBE buffer was made from $10\times$ TBE purchased from Apex (cat No. 20-195). TAE was made from a $50\times$ TAE buffer (2 M tris base, 1 M acetic acid, and 0.1 M H_2EDTA). The MES buffer was diluted 10 times from a 1 M MES buffer solution purchased from Alfa Aesar. TAE/Mg was made from 12 mM magnesium acetate in a TAE buffer.

Conjugation with PEG–folic acid. DNA 20T-SH strands were treated with TCEP for 4 h and then with maleimide modified PEG–folic acid overnight. They were then purified using a G-50 Micro Column (29-9034-08; GE Healthcare).

Nanogel synthesis. First, reverse emulsion was performed by 2-min sonication (pulse mode, 70% amplitude, 2-s sonication every 3 s) of 15 µl of DNA (20 µg of DNA in total) in 2 ml of cyclohexane (with 120 mg of Span 80) using a Dismembrator 150 (Thermo Fisher

Scientific). Then, 5 µl of salt solution was added to the reverse emulsion, followed by 1-min sonication. After a 1-h reaction, 20T-PEG–folic acid was added to the emulsion, followed by 1-min sonication. After a 1-h reaction, Span 80 and cyclohexane were removed by centrifugation and THF washing. The nanogel was then dispersed in PBS (with 10 mM magnesium and 1 mM potassium). The nanogel size was determined using DLS (Zetasizer Nano ZS90; Malvern Panalytical).

Atomic force microscopy. Nanogels were dispersed in PBS, and 5-µl samples were dropped on mica. Then, 40 µl of 2 mM magnesium acetate was dropped to remove the salt and keep the structure. The liquid was gently blown away. The samples were then scanned using a Veeco NanoScope IV scanning probe microscope (Digital Instruments) in tapping mode.

Scanning electron microscopy. Nanogels were dispersed in PBS, and 5-µl samples were dropped on mica. Then, 40 µl of 2 mM magnesium acetate was dropped to remove the salt and keep the structure. The liquid was gently blown away. Then, iridium was sputtered under 80 mV for 5 s to increase the conductivity of the samples. The samples were scanned under 5 kV using a Phillips XL 30 ESEM and an FEI SFEG UHR SEM.

Dox loading. Free Dox was mixed with nanogels and incubated overnight. Unbound Dox was removed using a 100K filter (lot No. R5BA49624; Microcon). Standard absorbance curves were acquired by fitting the different concentrations and absorbances (measured on a Nanodrop 2000C in UV-Vis mode; Malvern Panalytical).

Dox release. Free Dox, Dox with pH-insensitive nanogel, and Dox with pH-responsive nanogel were placed in dialysis tubes (100K MW) against PBS/Mg or MES/Mg buffer, and the buffers were gently stirred at room temperature. The total buffer solutions were renewed at predetermined intervals. The absorbance intensity of Dox remaining in the dialysis tubes was

measured using a Nanodrop.

Cell culture. MDA-MB-231 and MCF-7 cells were donated by Dr. Zhang's lab and cultured in Dulbecco's modified eagle medium (DMEM) with 10% (v:v) fetal bovine serum (FBS; HyClone) and 1% Pen Strep (Thermo Fisher Scientific) in an incubator (Thermo Fisher Scientific) at 37°C in a 5% CO2 atmosphere. The cells were subcultured approximately every two days at 80% confluence using 0.25% (w:v) trypsin at a split ratio of 1:3.

Fluorescence recovery. Amounts of 50 µl 3.4 µM free Dox were placed into wells in a 96-well plate, and the Dox fluorescence signals were measured using a plate reader (Synergy MX; BioTek). The fluorescence signals were measured again after adding 2 µg of DNA nanogels into the wells. An HCl solution was then added to reduce the pH to 5.5, and the fluorescence signals were measured again.

In vitro imaging study. MDA-MB-231 and MCF-7 cells (1.5 million per well) were seeded on a 12-well plate and cultured for 12 h. Dox-loaded (500 ng) nanogels were then added to the cells. After 1-h incubation at 37°C, Dox was removed, and a fresh medium was added into the wells. After 2-h incubation, the cells were fixed, and nuclei were stained with DAPI. Bright field and fluorescence images were obtained using a fluorescence microscope (EVOS FL). The images were collected using a GPF cube (Ex: 470/22; Em: 525/50).

Cytotoxicity. MDA-231-MA cells (7,000 per well) were seeded on a 96-well plate and cultured for 24 h. Dox-loaded nanogels (0.05–2 µmol per well) were then added to the cells and incubated for specific hours, followed by medium change with an MTT solution (5 mg/ml). After 4-h incubation, the liquid was removed using a small needle, and the cells were mixed with 100 µl of dimethyl sulfoxide (batch No. 0000082524; Macron). Absorbance was measured at a wavelength of 540 nm using a plate reader.

Chapter 2, in its entirety, is a reprint of a paper submitted for publication in 2021. Xiangyi Dong, Sibai Xie, Mingxuan Kai, Yi Chen. The dissertation author was the investigator and primary author of this study.

2.7   Reference

[1] Maeda, Hiroshi. "Macromolecular therapeutics in cancer treatment: the EPR effect and beyond." Journal of Controlled Release 164.2 (2012): 138-144.

[2] Park, Jooho, Yongwhan Choi, Hyeyoun Chang, Wooram Um, Ju Hee Ryu, and Ick Chan Kwon. "Alliance with EPR effect: Combined strategies to improve the EPR effect in the tumor microenvironment." Theranostics 9.26 (2019): 8073.

[3] Barbe, Christophe, John Bartlett, Linggen Kong, Kim Finnie, Hui Qiang Lin, Michael Larkin, Sandrine Calleja, Alexandra Bush, and Gerard Calleja. "Silica particles: a novel drug-delivery system." Advanced materials 16.21 (2004): 1959-1966.

[4] Mansuri, Shakir, Prashant Kesharwani, Keerti Jain, Rakesh K. Tekade, and N. K. Jain. "Muco-adhesion: A promising approach in drug delivery system." Reactive and functional polymers 100 (2016): 151-172.

[5] Cheng, Ru, Fenghua Meng, Chao Deng, Harm-Anton Klok, and Zhiyuan Zhong. "Dual and multi-stimuli responsive polymeric nanoparticles for programmed site-specific drug delivery." Biomaterials 34.14 (2013): 3647-3657.

[6] Pan, Yuan-Jia, Yuan-Yuan Chen, Dong-Rui Wang, Chuan Wei, Jia Guo, Da-Ru Lu, Chih-Chang Chu, and Chang-Chun Wang. "Redox/pH dual stimuli-responsive biodegradable nanohydrogels with varying responses to dithiothreitol and glutathione for controlled drug release." Biomaterials 33.27 (2012): 6570-6579.

[7] Huang, Gangliang, and Hualiang Huang. "Hyaluronic acid-based biopharmaceutical delivery and tumor-targeted drug delivery system." Journal of Controlled Release 278 (2018): 122-126.

[8] Zhang, Xudong, Yichen Dong, Xiaowei Zeng, Xin Liang, Xiaoming Li, Wei Tao, Hongbo Chen, Yuyang Jiang, Lin Mei, and Si-Shen Feng. "The effect of autophagy inhibitors on drug delivery using biodegradable polymer nanoparticles in cancer treatment." Biomaterials 35.6 (2014): 1932-1943.

[9] Zhu, Houjuan, Jingchao Li, Xiaoying Qi, Peng Chen, and Kanyi Pu. "Oxygenic hybrid semiconducting nanoparticles for enhanced photodynamic therapy." Nano letters, 2018, 18(1): 586-594.

[10] Mengoni, Tamara, Manuela Adrian, Susana Pereira, Beatriz Santos-Carballal, Mathias Kaiser, and Francisco M. Goycoolea. "A Chitosan—Based liposome formulation enhances the in vitro wound healing efficacy of substance P neuropeptide." Pharmaceutics, 2017, 9(4): 56.

[11] Di Zhang, Paige Baldwin, Ana S. Leal, Sarah Carapellucci, Srinivas Sridhar, and Karen T. Liby. "A nano-liposome formulation of the PARP inhibitor Talazoparib enhances treatment efficacy and modulates immune cell populations in mammary tumors of BRCA-deficient mice." Theranostics, 2019, 9(21): 6224.

[12Nucci, Mary L., Robert Shorr, and Abraham Abuchowski. "The therapeutic value of poly (ethylene glycol)-modified proteins." Advanced drug delivery reviews, 1991, 6(2): 133-151.

[13] Alconcel, Steevens NS, Arnold S. Baas, and Heather D. Maynard. "FDA-approved poly (ethylene glycol)–protein conjugate drugs." Polymer Chemistry, 2011, 2(7): 1442-1448.

[14] Locatelli, Erica, Francesca Broggi, Jessica Ponti, Patrick Marmorato, Fabio Franchini, Stefano Lena, and Mauro Comes Franchini. "Lipophilic Silver Nanoparticles and Their Polymeric Entrapment into Targeted-PEG-Based Micelles for the Treatment of Glioblastoma." Advanced healthcare materials, 2012, 1(3): 342-347.

[15] Chauhan, Abhay, Chaitrali Patil, Poonam Jain, and Hitesh Kulhari. "Dendrimer-based marketed formulations and miscellaneous applications in cosmetics, veterinary, and agriculture." Pharmaceutical Applications of Dendrimers. Elsevier, 2020: 325-334.

[16] Bulbake, Upendra, Sindhu Doppalapudi, Nagavendra Kommineni, and Wahid Khan. "Liposomal formulations in clinical use: an updated review." Pharmaceutics, 2017, 9(2): 12.

[17] Russell, Luisa M., Margot Hultz, and Peter C. Searson. "Leakage kinetics of the liposomal chemotherapeutic agent Doxil: The role of dissolution, protonation, and passive transport, and implications for mechanism of action." Journal of Controlled Release, 2018, 269: 171-176.

[18] Krauss, Aviva C., Xin Gao, Liang Li, Michael L. Manning, Paresma Patel, Wentao Fu, Kumar G. Janoria et al. "FDA approval summary:(daunorubicin and cytarabine) liposome for injection for the treatment of adults with high-risk acute myeloid leukemia." Clinical Cancer Research, 2019, 25(9): 2685-2690.

[19] Liu, Tiancai, Yongjun Liang, and Liping Huang. "Development and delivery systems of mRNA vaccines." Frontiers in Bioengineering and Biotechnology, 2021, 9.

[20] Mandal, Abhirup, John R. Clegg, Aaron C. Anselmo, and Samir Mitragotri. "Hydrogels in the clinic." Bioengineering & Translational Medicine, 2020, 5(2): e10158.

[21] Overstreet, Derek J., Dipankar Dutta, Sarah E. Stabenfeldt, and Brent L. Vernon. "Injectable hydrogels." Journal of Polymer Science Part B: Polymer Physics, 2012, 50(13): 881-903

[22] Ding, Yi, Yingmei Zhu, Shaohua Wei, Jiahong Zhou, and Jian Shen. "Cancer cell membrane as gate keeper of mesoporous silica nanoparticles and photothermal-triggered membrane fusion to release the encapsulated anticancer drug." Journal of Materials Science, 2019, 54(19): 12794-12805.

[23] Lagassé, HA Daniel, Aikaterini Alexaki, Vijaya L. Simhadri, Nobuko H. Katagiri, Wojciech Jankowski, Zuben E. Sauna, and Chava Kimchi-Sarfaty. "Recent advances in (therapeutic protein) drug development." F1000Research, 2017, 6.

[24] Hazarika, Pompi, Bülent Ceyhan, and Christof M. Niemeyer. "Reversible switching of DNA–gold nanoparticle aggregation." Angewandte Chemie, 2004, 116(47): 6631-6633.

[25] Andersen, Ebbe S., Mingdong Dong, Morten M. Nielsen, Kasper Jahn, Ramesh Subramani, Wael Mamdouh, Monika M. Golas et al. "Self-assembly of a nanoscale DNA box with a controllable lid." Nature, 2009, 459(7243): 73-76.

[26] Yurke, Bernard, Andrew J. Turberfield, Allen P. Mills, Friedrich C. Simmel, and Jennifer

L. Neumann. "A DNA-fuelled molecular machine made of DNA." Nature, 2000, 406(6796): 605-608.

[27] Zhou, Lin, Mingxuan Gao, Weiling Fu, Yunxia Wang, Dan Luo, Kai Chang, and Ming Chen. "Three-dimensional DNA tweezers serve as modular DNA intelligent machines for detection and regulation of intracellular microRNA." Science advances, 2020, 6(22): eabb0695.

[28] Thubagere, Anupama J., Wei Li, Robert F. Johnson, Zibo Chen, Shayan Doroudi, Yae Lim Lee, Gregory Izatt, Sarah Wittman, Niranjan Srinivas, Damien Woods, Erik Winfree, and Lulu Qian. "A cargo-sorting DNA robot." Science, 2017, 357(6356).

[29] Wang, Dongfang, Yanming Fu, Juan Yan, Bin Zhao, Bin Dai, Jie Chao, Huajie Liu et al. "Molecular logic gates on DNA origami nanostructures for microRNA diagnostics." Analytical chemistry, 2014, 86(4): 1932-1936.

[30] Ambrus, Attila, Ding Chen, Jixun Dai, Tiffanie Bialis, Roger A. Jones, and Danzhou Yang. "Human telomeric sequence forms a hybrid-type intramolecular G-quadruplex structure with mixed parallel/ antiparallel strands in potassium solution." Nucleic acids research, 2006, 34(9): 2723-2735.

[31] Chen, Xiaoxia, Tianshu Chen, Lingjie Ren, Guifang Chen, Xiaohu Gao, Genxi Li, and Xiaoli Zhu. "Triplex DNA nanoswitch for pH-sensitive release of multiple cancer drugs." ACS nano, 2019, 13(6): 7333-7344.

[32] Abrescia, Nicola GA, Andrew Thompson, Tam Huynh-Dinh, and Juan A. Subirana. "Crystal structure of an antiparallel DNA fragment with Hoogsteen base pairing." Proceedings of the National Academy of Sciences, 2002, 99(5): 2806-2811.

[33] Nikolova, Evgenia N., Eunae Kim, Abigail A. Wise, Patrick J. O'Brien, Ioan Andricioaei, and Hashim M. Al-Hashimi. "Transient Hoogsteen base pairs in canonical duplex DNA." Nature, 2011, 470(7335): 498-502.

[34] Gangrade, Ankit, Nicholas Stephanopoulos, and Dhiraj Bhatia. "Programmable, self-assembled DNA nanodevices for cellular programming and tissue engineering." Nanoscale, 2021, 13(40): 16834-16846.

[35] Um, Soong Ho, Jong Bum Lee, Nokyoung Park, Sang Yeon Kwon, Christopher C. Umbach, and Dan Luo. "Enzyme-catalysed assembly of DNA hydrogel." Nature materials, 2006, 5(10): 797-801.

[36] Cheng, Enjun, Yongzheng Xing, Ping Chen, Yang Yang, Yawei Sun, Dejian Zhou, Lijin Xu, Qinghua Fan, and Dongsheng Liu. "A pH-triggered, fast-responding DNA hydrogel." Angewandte Chemie International Edition, 2009, 48(41): 7660-7663.

[37] Li, Juan, Cheng Zheng, Sena Cansiz, Cuichen Wu, Jiehua Xu, Cheng Cui, Yuan Liu, Weijia Hou, Yanyue Wang, Liqin Zhang, I-ting Teng, Huang-hao Yang, and Weihong Tan. "Self-assembly of DNA nanohydrogels with controllable size and stimuli-responsive property for targeted gene regulation therapy." Journal of the American Chemical Society, 2015, 137(4): 1412-1415.

[38] Endo, Masayuki, Xiwen Xing, Xiang Zhou, Tomoko Emura, Kumi Hidaka, Bodin Tuesuwan, and Hiroshi Sugiyama. "Single-molecule manipulation of the duplex formation and dissociation at the G-quadruplex/i-motif site in the DNA nanostructure." ACS nano, 2015, 9(10): 9922-9929.

[39] Burge, Sarah, Gary N. Parkinson, Pascale Hazel, Alan K. Todd, and Stephen Neidle. "Quadruplex DNA: sequence, topology and structure." Nucleic acids research, 2006, 34(19): 5402-5415.

[40] Jin, Cheng, Xiaojing Liu, Huarong Bai, Ruowen Wang, Jie Tan, Xuehui Peng, and Weihong Tan. "Engineering stability-tunable DNA micelles using photocontrollable dissociation of an intermolecular G-quadruplex." ACS nano, 2017, 11(12): 12087-12093.

[41] Bang, I. "Examination or the guanyle acid." Biochemische Zeitschrift, 1910, 26: 293-311.

[42] Gellert, Martin, Marie N. Lipsett, and David R. Davies. "Helix formation by guanylic acid." Proc. Natl. Acad. Sci. U. S. A., 48 (1962), pp. 2013-2018

[43] Shrestha, Prakash, Sagun Jonchhe, Tomoko Emura, Kumi Hidaka, Masayuki Endo, Hiroshi Sugiyama, and Hanbin Mao. "Confined space facilitates G-quadruplex formation." Nature nanotechnology, 2017, 12(6): 582-588.

[44] Balasubramanian, Shankar, and Stephen Neidle. "G-quadruplex nucleic acids as therapeutic targets." Curr. Opin. Chem. Biol. 2009, 13 (3), 345–353.

[45] Liu, Chenyu, Kai K. Ewert, Ning Wang, Youli Li, Cyrus R. Safinya, and Weihong Qiao. "A multifunctional lipid that forms contrast-agent liposomes with dual-control release capabilities for precise MRI-guided drug delivery." Biomaterials, 2019, 221: 119412.

[46] Chen, Quan, Siheng Li, Zixiong Feng, Meng Wang, Chengzhi Cai, Jufang Wang, and Lijuan Zhang. "Poly (2-(diethylamino) ethyl methacrylate)-based, pH-responsive, copolymeric mixed micelles for targeting anticancer drug control release." International journal of nanomedicine, 2017, 12: 6857.

[47] Bayer, Ilker S. "A Review of Sustained Drug Release Studies from Nanofiber Hydrogels." Biomedicines, 2021, 9(11): 1612.

[48] Balaure, Paul C., Dragos Gudovan, and Iulia Alexandra Gudovan. "Smart triggered release in controlled drug delivery." Current drug targets, 2018, 19(4): 318-327

[49] Surana, Sunaina, Jaffar M. Bhat, Sandhya P. Koushika, and Yamuna Krishnan. "An autonomous DNA nanomachine maps spatiotemporal pH changes in a multicellular living organism." Nature communications 2.1 (2011): 1-7.

[50] Yoshimura, Akihiko, Kazumichi Kuroda, Kazunori Kawasaki, Shohei Yamashina, Toyozo Maeda, and Shun-Ichi Ohnishi. "Infectious cell entry mechanism of influenza virus." Journal of Virology 43.1 (1982): 284-293.

[51] Martin, K. E. L. S. E. Y., and A. Helenius. "Transport of incoming influenza virus nucleocapsids into the nucleus." Journal of virology 65.1 (1991): 232-244.

[52] Gehring, Kalle, Jean-Louis Leroy, and Maurice Gueron. "A tetrameric DNA structure with protonated cytosine-cytosine base pairs." Nature, 1993, 363(6429): 561-565.

[53] Cheng, Enjun, Yongzheng Xing, Ping Chen, Yang Yang, Yawei Sun, Dejian Zhou, Lijin Xu, Qinghua Fan, and Dongsheng Liu. "A pH-triggered, fast-responding DNA hydrogel." Angewandte Chemie International Edition, 2009, 48(41): 7660-7663.

[54] Steele, Christopher D., and David J. Balding. "Statistical evaluation of forensic DNA profile evidence." Annual Review of Statistics and Its Application, 2014, 1: 361-384.

[55 Zwicke, Grant L., G. Ali Mansoori, and Constance J. Jeffery. "Utilizing the folate receptor for active targeting of cancer nanotherapeutics." Nano reviews, 2012, 3(1): 18496.

[56] Mo, Ran, Tianyue Jiang, Rocco DiSanto, Wanyi Tai, and Zhen Gu. "ATP-triggered anticancer drug delivery." 2014, 5(1): 1-10.

[57] Ko, SeungHyeon, Haipeng Liu, Yi Chen, and Chengde Mao. "DNA nanotubes as combinatorial vehicles for cellular delivery." Biomacromolecules, 2008, 9(11): 3039-3043.

[58] Lee, Hyukjin, Abigail KR Lytton-Jean, Yi Chen, Kevin T. Love, Angela I. Park, Emmanouil D. Karagiannis, Alfica Sehgal, William Querbes, Christopher Zurenko, Muthusamy Jayaraman, Chang Peng, Klaus Charisse, Anna Borodovsky, Muthiah Manoharan, Jessica Donahoe, Jessica Truelove, Matthias Nahrendorf, Robert Langer, and Daniel Anderson. "Molecularly self-assembled nucleic acid nanoparticles for targeted in vivo siRNA delivery." Nature nanotechnology, 2012, 7(6): 389-393.

[59] Kapp, Tobias G., Florian Rechenmacher, Stefanie Neubauer, Oleg V. Maltsev, Elisabetta A. Cavalcanti-Adam, Revital Zarka, Ute Reuning, Johannes Hotni, Hans-Jurgen Wester, Carlos Mas-Moruno, Joachim Spatz, Benjamin Geiger, and Horst Kessler. "A comprehensive evaluation of the activity and selectivity profile of ligands for RGD-binding integrins." Scientific reports, 2017, 7(1): 1-13.

Chapter 3

Protein Encapsulation

ABSTRACT. Here, we demonstrated a new protein encapsulation method utilizing our DNA nanogel system. Self-assembly mechanisms between the DNA and the proteins allowed the proteins to be embedded. Like Chapter 2, the DNA nanogel was composed of single stranded DNAs, which formed a 3-dimensional nanogel structure by using the G-quadruplex structure as the crosslinker. The DNA nanogel had multiple overhanging 20 adenosine, which, through simple Watson-Crick base pairing, could be used to further modify the nanogel surface. In this chapter, we demonstrated that the DNA nanogel has embedded the unmodified proteins while still preserving their structure and function. As a proof of concept, we confirmed the embedding with a mobility shift assay using native agarose gel electrophoresis. The morphology of protein-loaded DNA nanogel was observed under Atomic Force Microscopy (AFM), and the size and the zeta potential were characterized by Dynamic Light Scattering (DLS). In addition, we discovered that the nanogel/IgG system could interact with the surface proteins of *E. coli* under both signal-colocalization and scanning electron microscope. This result demonstrated the self-assembled DNA nanogel system could embed functional proteins onto the DNA nanogel while preserving the protein function. To show the application of embedded protein nanogels as a drug delivery vehicle, Doxorubicin (Dox) was loaded into the nanogel and cancer cell cytotoxicity was investigated on KB cells. The protein embedded DNA nanogel showed higher cytotoxicity to KB cells than the physical mixture of random DNA strand, IgG, and Dox because of the targeting ability of the IgG.

3.1   Introduction

Functional proteins and peptides have been increasingly used for therapeutic purposes.[1] This is because protein therapy being safer than gene therapy due to its transient action of proteins in the targeted site. Protein therapy is non-random and does not cause permanent disruption of the site during the process.[2] However, the main challenges for protein delivery include the large size, fragile tertiary structure, and varying surface charge of proteins.[3] Native proteins suffer from serum instability, which results in degradation and inactivation. In addition, most native proteins are electrostatically unfavorable to the membrane. [4] Therefore, proper methods are necessary to deliver functional proteins to the cytosol – which should include endolysosomal escape to function in the cytosol or subcellular compartments and targeting the expect sites – while the function of protein should be perserved.[5] Improved protein stability, activity, immunogenicity, and delivery are also expected for the potential methods. [6]

Protein drugs have played more and more important role in the drug development and therapy[7-9]. They are widely used in oncology, genetic disease, immunology, infectious disease, etc[7]. For example, in 2011-2016, the US food and drug Administration Center for Drug Evaluation and Review and the Center for Biologics Evaluation and Review have approved 62 recombinant therapeutic proteins for various applications[8]. In 2020, 24.5% drugs approved by CDER in FDA are protein drugs[7]. The 5-year average for antibody approvals 2020 was more than ten per year when compared to 2006-2010 (where the FDA only approved two new antibodies per year). Among the protein drugs, more than 90% were monoclonal antibodies (mAb) and antibody-drug conjugates (ADC)[7]. However, the manufacturing of therapeutic proteins is complex[10]. A typical protein drug production may include up to 20

more steps than small molecule fabrication. In addition, the complex secondary and tertiary structures of the therapeutic proteins must be maintained during the whole procedure. During the processing steps, there are multiple parameters that could affect the final protein production, including manufacturing in live cells or bacterial, culture condition, chemical conjugation environment, purification processes, and possible damages caused by modification. In all, there is an opportunity for new protein delivery strategies that could have the ability to be biodegradable, biocompatible *in vivo*, have high encapsulation efficiency, sustained release, targeting capabilities, retain protein structure and bioactivity, and transportation to the cytosol. However, protein modification is necessary to achieve the specificity targeting, endosomal escape, and cargo release. Modification by chemical-conjugation recombinant modification often results in the ill-preserved the activity of protein because the conjugation environment, the conformation after modification, and parameter changes during genetic modification can significantly affect the protein stability.

Recently, protein nano-carriers have been reported to be a promising technology for optimized protein delivery. Nano-carriers can protect proteins from degradation and various denaturing conditions in the biological environment. [11] This is because nano-carriers can increase the stealth of the delivered proteins by covering antigenic and immunogenic epitopes, lessening the uptake of the reticuloendothelial system (RES)[12], and protecting from protein proteolysis. [13] From a pharmacokinetic perspective, the high surface area to volume ratio of nanoparticles can increase the effectiveness. Another important property of nano-carrier-based delivery systems is the ability to tailor the chemical and physical properties of the vehicles. [14] Size, surface charge, and displayed ligands can be controlled to increase cell penetration, endolysosomal escape, targeting specificity, and cargo release kinetics. [15]

However, it is still a major challenge for using conventional nano-carriers to deliver the unmodified, functional proteins with their active conformation and functions to the necessary site. [16] Methods to deliver proteins via nano-carrier include covalent bonding of the proteins to the vehicle or conjugation via chemical reaction, which may limit delivery to specific proteins and will apply irreversible modification on the structural conformation and function of the proteins, respectively. [2,3] Therefore, different approaches[17-20] have explored to deliver functional proteins via nano-carriers. These approaches include physical adsorption and non-covalent encapsulation. Noncovalent encapsulation strategies can preserve protein conformation and function. However, the stability in serum remains challenge. [21] One example of non-covalent binding is self-assembly between the proteins and nanocarrier, which allows us to preserve the function and structure of the protein.[3]

As is mentioned in the previous chapters, DNA nanotechnology has been used to design and construct DNA nanostructures, because the technology has well-controlled size, shape, and surface chemistry properties, by self-assembly. [22-25] These properties can overcome the challenges that are inherent to conventional protein delivery nanoparticles. Thus, DNA nanostructures are powerful vehicles that include unique size, control abilities, uniform size, loading delivery, and biocompatibility, non-covalent bond interaction. Among the advantages, self-assembly nature of the DNA nanostructure makes it more promising for a next-generation protein delivery vehicle. However, some DNA nanostructures are based on Watson-Crick base pairing which have intrinsic limitations such as low resistance to heating, denaturing reagents, susceptibility to DNase, flexibility, and deformability.[26] In addition, functionalization by the chemical stimuli is insufficient. [31] Instead of a DNA nanostructure that contains only Watson-Crick bonding, DNA structures such as G-Quadruplexes, triplexes,

76

and DNA junctions could be incorporated into drug delivery platforms to overcome these limitations. [26-32]

As we discussed in previous chapters, G-Quadruplexes have a tetrameric structure containing four guanine molecules that are arranged to make the square planar conformation.[26-29] Each guanine is bonded with the two adjacent guanines through hydrogen bonding making it form a G-quartet stack. When monovalent cations are introduced into the structure, they occupy the central core between the stacks to neutralize the electrostatic repulsion between them.[29] The stacking G-quartets comprise of the four Guanines structure and the single-strand loop is formed by the intervening DNA sequence.[27] Because of the G4 structure stability, it demonstrates improved resistance to thermal heating (over conventional Watson-Crick structures) and denaturing conditions.

In Chapter 2 we tested our G-quadruplexes DNA nanogel for small molecule drug delivery. Here, we expand to the application of protein drugs. In this chapter, we tried protein encapsulation utilizing our DNA nanogel. As discussed at Chapter 2, our nanogel system used pure DNA strands which has large pore size which made the system promising for large molecule encapsulation. The pH-responsive designs were integrated to get controlled release when necessary. Meanwhile, once the protein was encapsulated, the overhangs on DNA nanogel enabled modification by 20A-20T base-paring but did not interact with the embedded protein drugs. Even the DNA modification formed hydrogen bonds under physiological condition, which was found to not affect the environment of the embedded proteins. This was because DNA strands were modified and purified before it was added into the system. As such, G-quadraplexes DNA gels are proposed to be an excellent candidate for protein delivery given that the DNA nanostructures can encapsulate the

proteins with the proteins still functional.

Several reports[33-39] showed attempts to form DNA-protein complex. Yan and coworkers[36] used the biotin-streptavidin interaction to embed the protein in a DNA nanogrid by DNA origami. However, only specific proteins could be applied. Aptamers[37, 38] were also used for specific protein binding to from nano arrays. The Mao[39] group used antigen-modified DNA array to attract protein to form self-assembled 2D DNA-protein array. Hetero bifunctional crosslinkers[40] conjugation of DNA-protein/peptides by covalent bonding was also reported. However, these methods have limitations like protein categories or possible damage by covalent bonding. The DNA nanogel system presented here does not face the above limitations and is a promising candidate.

The synthesis procedure (Figure 3.1) was like that of chapter 2. The only differences were that we added proteins together with DNA. Noticeably, the potassium salt used was potassium Glutamate (KGlu) because Glutamate[41] can highly enhance the interaction between the DNA and the protein.
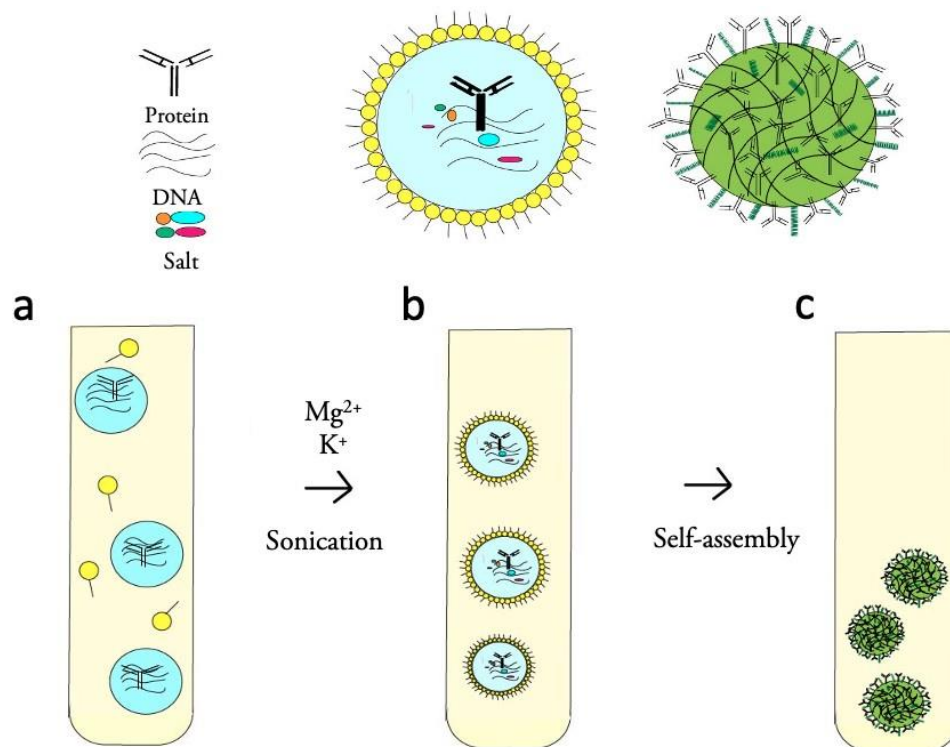
Figure 3.1: Schematic drawing of protein encapsulation. (a) A mixture of proteins and single-strand DNAs, in the solution of surfactant (Span 80) and cyclohexane before sonication. (b) After the addition of salt and sonication, a reverse emulsion formed, and proteins are embedded in the G4-Quadruplex cross-linkers by self-assembling. (c) After 1hr at room temperature, samples were centrifuged down and washed with tetrahydrofuran (THF). Lastly, pellets were re-suspended with PBS buffer.

3.2   Protein Loading in DNA nanogel

One of the greatest challenges of protein delivery is that different proteins have different charges under same condition. This makes it difficult to develop a perfect drug delivery system that is able to load various kinds of proteins. Here, we chose two proteins with different charges under the same condition. To validate the protein encapsulation, we performed a 1% native agarose gel electrophoresis to assay for mobility shift. The native agarose gel electrophoresis can preserve the DNA nanogel structure and the protein conformation. The electrophoresis highly depends on the particle size and surface charge. Therefore, the isoelectric point (pI) of the protein in the buffer should be considered. Avidin had a pI value of 10[47] – which indicated that it was positively charged – in the Tris/Borate/EDTA (TBE buffer), whereas goat-Immunoglobulin G (IgG)s[48] had a pI value of 6.1 – 8.5, which suggested that it can be variably charged in TBE buffer. During the electrophoresis, we found that the IgG was negatively charged in our running buffer.

We first tried the exact same conditions as chapter 2 for protein-loaded DNA and potassium chloride was used. Figure 3.2 shows the 1% agarose electrophoresis of DNA nanogel with IgG formed using potassium chloride. The protein could be stained by Coomassie Blue and not by ethidium bromide (EB), while DNA could be stained by EB and not Coomassie Blue. In the 1% native agarose gel, pure avidin did not run into the gel because the surface charge was positive in the running buffer (Figure 3.2b). However, pure DNA nanogel could run into the gel because DNA was negatively charged in the running buffer. Self-assembled protein-loaded DNA nanogel (lane 4) ran into the gel and the position was higher than pure DNA nanogel, which meant a higher mobility structure was formed. This suggested that the avidin-loaded DNA nanogel was successfully formed. Meanwhile, the same synthesis method did not work well for the IgG-loaded DNA nanogel (Figure 3.2a). The 4th lane, which contained the IgG loaded DNA nanogel, was similar to the physical

mixture of IgG and DNA nanogel, which were separated bands (where IgG was stained by Coomassie Blue, and DNA was stained by EB at the same position as the pure IgG and DNA nanogel). This result shows that there was no IgG loaded in DNA nanogel and Avidin was much easier to load in DNA nanogel. That was likely due to their different charges. Avidin showed a positive charge, and DNA had a negative charge due to the phosphate backbone. Because of the electrostatic force, Avidin and DNA should be easily self-assembled together. On the other hand, IgG and DNA both showed negative charges which would make assembling together during synthesis difficult.

There have been different reported strategies to improve DNA and protein interaction[]. One method is to use Glutamate[41]. In 1987, Sigrid *et al.* reported that replacement of potassium chloride by potassium glutamate dramatically enhanced the DNA-protein interaction. As such, we used potassium glutamate and the IgG loaded into the DNA nanogel successfully (figure 4.3).

The optimized protein capsulation electrophoresis is shown in Figure 3.3, where IgG was encapsulated in potassium glutamate. Lane 1 was Avidin, lane 2 was the IgG, lane 3 was the DNA nanogel, lane 4 was the mixture of Avidin and DNA nanogel, lane 5 was the Avidin encapsulated DNA nanogel, lane 6 was the mixture of IgG and DNA nanogel, and lane 7 was IgG encapsulated DNA nanogel. In Figure 3.2 a, the DNA was stained with EB (Figure 3.3a) in order to view DNA nanogel in lane 3, while there were no bands in lane 1 and 2 which contained proteins. The protein was stained with Coomassie Blue stained in Figure 3.3 (b) but no bands in lane 3 which contents DNA nanogel, and the merged signal is shown in Figure 3.3 (c). Lane 5 is our Avidin encapsulated DNA nanogel with lane 4 (mixture of Avidin and DNA nanogel) as the negative control. Lane 7 is our IgG encapsulated DNA

nanogel with lane 6 (physical mixture of IgG and DNA nanogel) as the negative control.
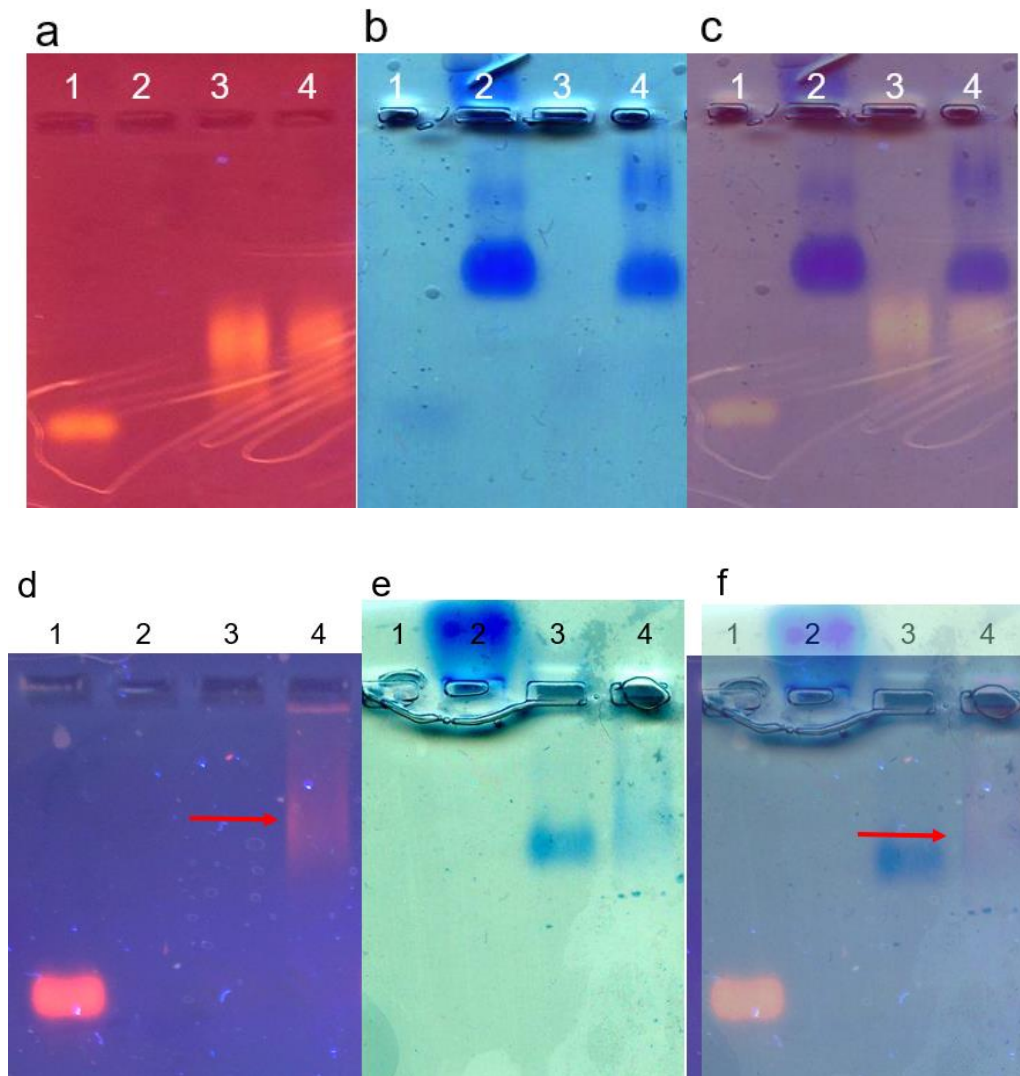
Figure 3.2: Electrophoresis of protein encapsulation using potassium chloride. 1% native agarose gel. (a-c) IgG encapsulation. Lane 1, IgG; Lane 2, DNA nanogel; Lane 3, the mixture of DNA nanogel and IgG; Lane 4, IgG encapsulated DNA nanogel; (a) EB stained (DNA), (b) Coomassie Blue stained (proteins), (c) Merged image of EB stained agarose gel (a) and Coomassie Blue stained agarose gel (b). (d-f) Avidin encapsulation. Lane 1, ssDNA marker; Lane 2, Avidin; Lane3, IgG; Lane 4, Avidin embedded DNA nanogel. (d) EB stained (DNA), (e) Coomassie Blue stained (proteins), (f) Merged image of EB stained agarose gel.
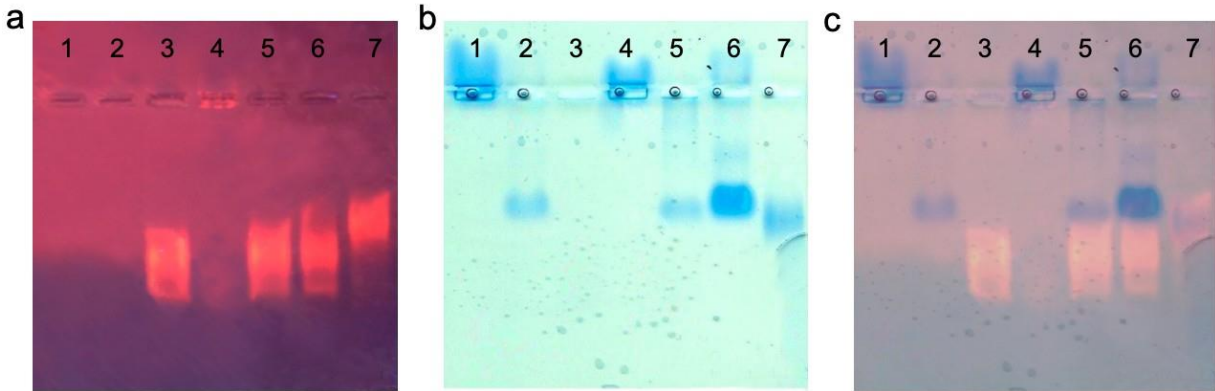
Figure 3.3: Electrophoresis of protein encapsulation. 1% native agarose gel. Lane 1, Avidin; Lane 2, IgG; Lane 3, DNA nanogel; Lane 4, the mixture of DNA nanogel and Avidin; Lane 5, Avidin encapsulated DNA nanogel; Lane 6, the mixture of DNA nanogels and IgG; Lane 7, IgG encapsulated DNA nanogels. (a) EB stained (DNA), (b) Coomassie Blue stained (proteins), (c) Merged image of EB stained agarose gel (a) and Coomassie Blue stained agarose gel (b). Avidin was embedded with potassium chloride, while IgG was embedded with potassium glutamate.

To compare the Avidin capsulation, band 1 (pure Avidin), 3 (DNA nanogel), 4 (Avidin mixed with DNA nanogel), and 5 (Avidin encapsulated DNA nanogel) were analyzed. Because the Avidin was positively charged in the running buffer, the Avidin band was running towards the top. When comparing with the Avidin mixed with DNA nanogel and avidin encapsulated DNA nanogel (lanes 4 and 5), we can see the mixture aggregated at the well. It was noticeable that in lane 5, the Avidin ran into the gel to a similar position with DNA nanogel, which indicated the Avidin is successfully embedded to DNA nanogel.

Similar to Avidin, we can compare the bands 2, 3, 6, and 7 to observe the mobility of IgG encapsulated protein. Because the IgG was negatively charged in the running buffer, the IgG (lane 2) ran into the gel and the mobility was slower than DNA nanogel (lane 3). When comparing the mixture of IgG and DNA nanogel (lane 6) and the IgG embedded DNA nanogel (lane 7), the mixture (lane 6) the IgG and DNA nanogel (lane 3) kept the same mobility as

compared to the pure IgG (lane2) and pure DNA nanogel (lane 3). While in our IgG embedded DNA nanogel (lane 7), we can see colocalization of DNA EB signal and IgG Coomassie Blue signal, which indicated the IgG was successfully captured in the DNA nanogel system.

The colocalization of EB-stained DNA bands and Coomassie Blue-stained proteins showed a successful protein encapsulation of both a negatively charged protein and positively charged protein. Overall, we conclude that our platform can incorporate proteins onto the DNA nanogels.

The Atomic Force Microscopy (AFM) images of samples showed different heights of the DNA nanogel and the DNA nanogel/IgG. In figure 3.4, we visualized the morphology of the physical mixture of DNA nanogel and IgG (a), DNA nanogel (b), and IgG encapsulated DNA nanogel (c). The DNA nanogel/IgGs (figure 3.4 c) have a globular shape with IgG embedded around the edge. The AFM height profile (Figure 3.4 d) clearly shows that the DNA nanogel/IgG was taller than the DNA nanogel with a 1-2 nm height difference. This evidence supports our hypothesis that proteins are embedded in the DNA nanogel. Compared to the mixture of DNA nanogels and IgGs, the DNA nanogel/IgG had an average 3 nm height increase. Overall, we can conclude that the proteins embedded onto the DNA nanogels according to both the gel analysis and the AFM height analysis.
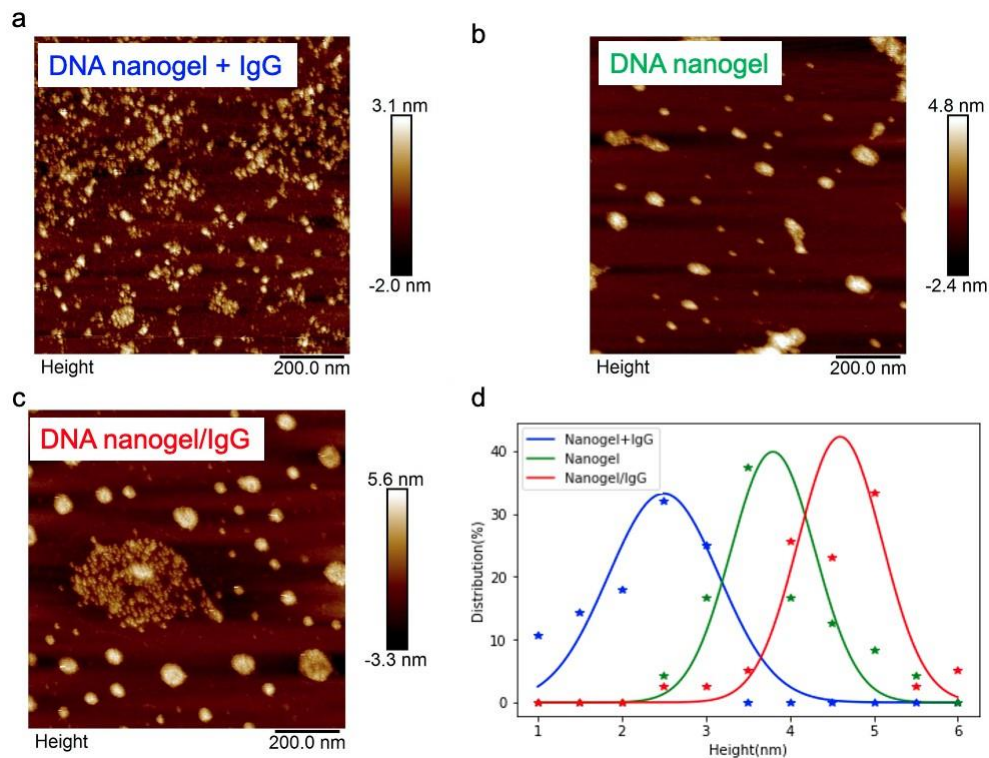
Figure 3.4: Atomic force microscopy (AFM) observation of protein encapsulation. (a) Physical mixture of DNA nanogel and IgG; (b) DNA nanogel; (c) IgG embedded DNA nanogel; (d) Height analysis of a (blue), b (green), c (red). Scale bars: 200 nm.

The zeta potential results also support our hypothesis that the proteins embedded onto the DNA Nanogel. Figure 3.5a shows that the DNA nanogel has a mean peak value of -51.4mV. The DNA nanogel/IgG were more negatively charged on their surface due to the negatively charged IgG with a first peak mean value of -78mV and a second peak mean value of -57.8 mV. We compared the DNA nanogel/IgG peaks with the DNA Nanogel peak and found that the first peak of DNA nanogel/IgG indicated that the proteins embedded onto the DNA nanogel which showed an overall distribution shift towards more negatively charged. However, the DNA nanogel/IgG second peak (-57.8 mV) remained similar to the DNA nanogel peak (-51.4 mV). This represents the fact that not all the DNA nanogels have embedded proteins. In addition, we added a control of the mixture of single stranded DNAs that could not form the nanogel with the

IgGs.
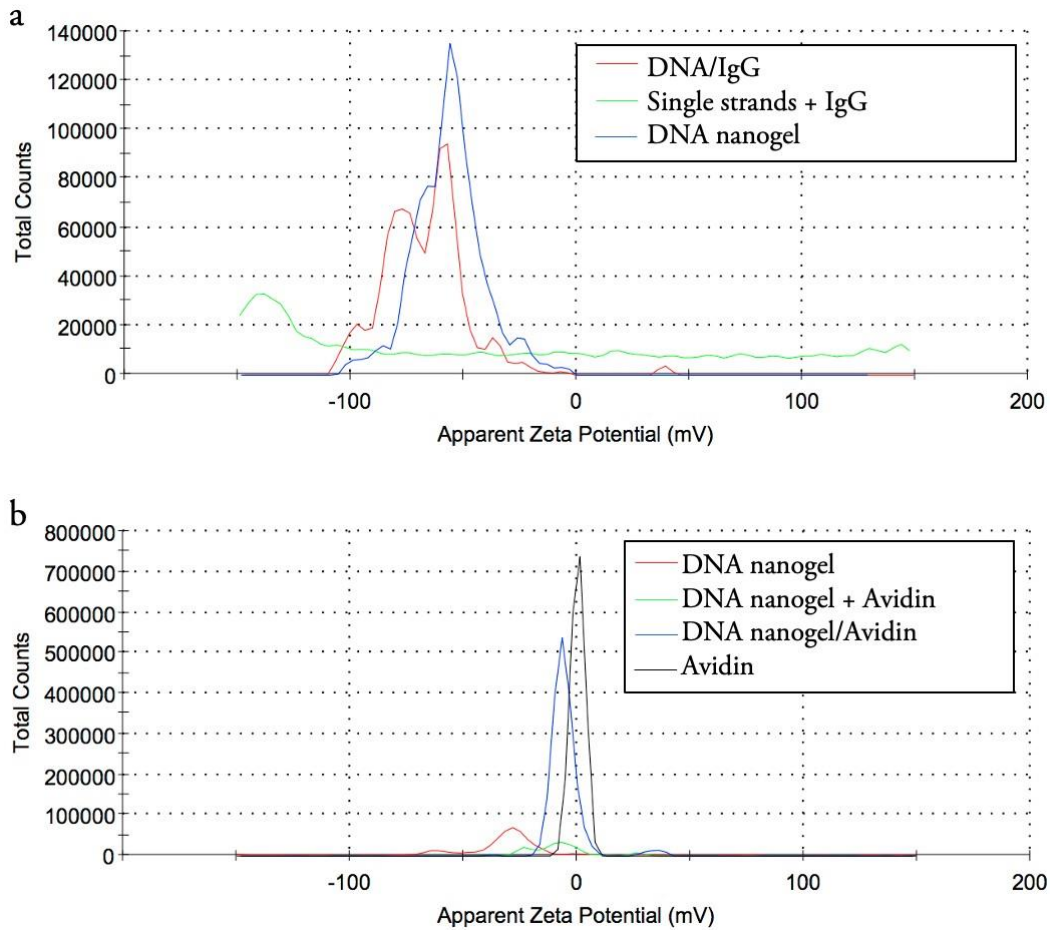
Figure 3.5: Zeta potential distribution of protein encapsulated DNA nanogel (a) Zeta potential distribution for the IgG encapsulation; Red, IgG encapsulated DNA nanogel. Green, single-strand DNA mixed with IgG. Blue, the DNA nanogel. (b) Zeta potential distribution for Avidin encapsulation; Red, DNA nanogel. Green, the mixture of Avidin and the DNA nanogel. Blue, Avidin encapsulated DNA nanogel. Black, Avidin.

Figure 3.5b shows the zeta potential distribution of the avidin embedded onto the DNA nanogel (DNA nanogel/Avidin). The blue-colored distribution represented DNA nanogel/Avidin which had a mean peak value of -5.98 mV. Compared to the DNA nanogel (mean value -51.4 mV), it shifted to be more positively charged. Also, as a control, we added a mixture of unembedded avidins with the DNA nanogels (Green distribution), which

had two mean peaks of zeta potential data, 23mV, and -6.03 mV. By comparing the controls, DNA nanogel/Avidin showed a different zeta potential distribution curve and a slightly positive shift of zeta potential (-5.98 mV), which indicated avidins embedded onto the DNA nanogels. Overall, the zeta potential results also supported our hypothesis, though indirectly, that proteins are embedded onto the DNA nanogels.

Both the electrophoresis result and AFM images confirmed proteins were successfully embedded in the DNA nanogel. Meanwhile, zeta potential indicates the embedded protein changed the DNA nanogel's surface charge, which makes it possible that the protein still active function. To test if the protein embedded on the DNA nanogel have the biding ability, we demonstrated some function tests.

3.3 Function Test
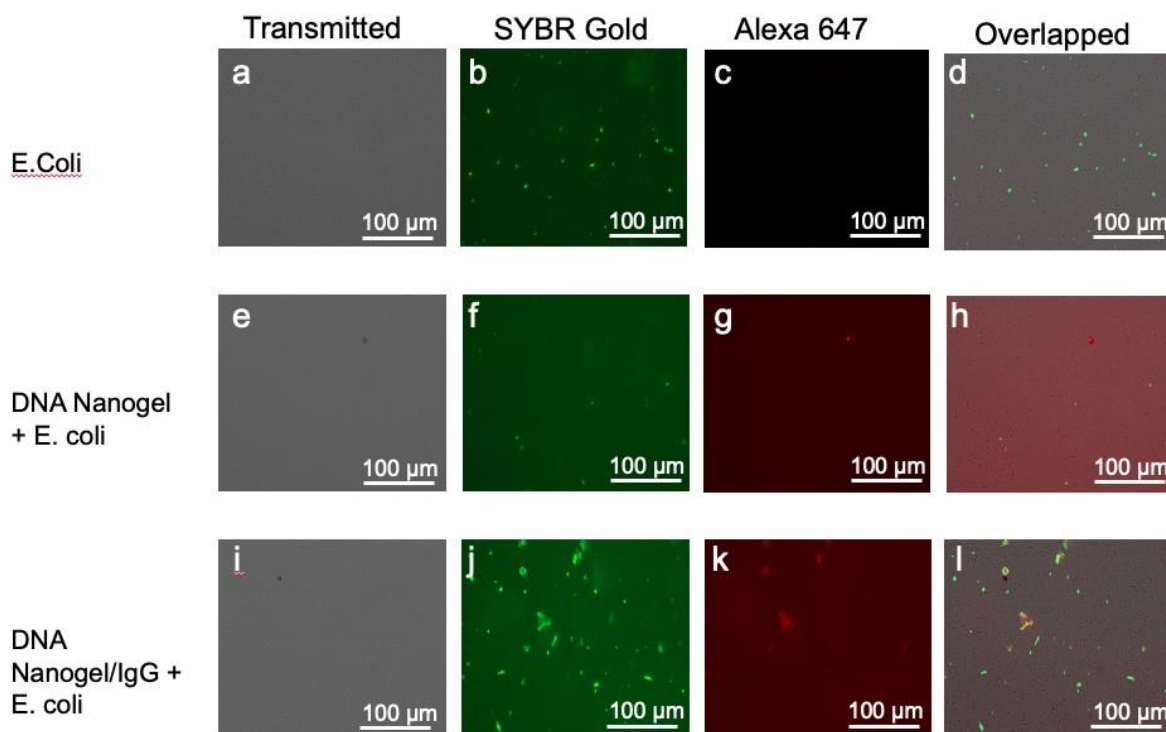
Figure 3.6: Colocalization of protein capsulated DNA nanogel and *E. Coli* under Fluorescence Microscope. (a-d) plain *E. coli*, (e-h) DNA nanogel mixed with *E. coli*, and (i-l) IgG encapsulated DNA nanogel mixed with *E. coli*. First column, bright field; Second column, SYBR Gold stained *E. Coli* (green); Third column, Alexa 647 labelled DNA nanogel (red), Fourth column, overlapped of bright field, SYBR Gold, and Alexa 647 signal. scale bar: 100 µm.

After the demonstrating that we could successfully encapsulate proteins in our nanogel platform, we found that the DNA nanogel has surface charge changed according to the zeta potential results. Preserving protein function is a very important property in protein delivery, so next step we are going to test the protein activity. Leo, *et. al*,[42] reported that the immunoglobulin binding Eib proteins from *Escherichia coli* (*E. coli*) are receptors for IgG Fc. We used *E. coli* to test the function of the protein after encapsulation by DNA nanogel. Colocalization

88

of *E. coli* and DNA nanogels are shown in Figure 3.6, where DNA nanogel was conjugated with Alexa 647, and *E. Coli* was stained with SYBR Gold. Figure 3.6 (a-d) shows the *E. Coli* signal of transmitted, SYBR Gold, Alex 647, overlapped channels, (e-h) shows the mixture of *E. Coli* and plain DNA nanogel signal of transmitted, SYBR gold, Alex 647, overlapped channels; (i-l) shows the mixture of *E. Coli* and IgG loaded DNA nanogel signal of transmitted, SYBR gold, Alex 647, overlapped channels. The green channel shows the SYBR gold signal when it binds on *E. Coli*, the red channel shows the Alexa 647 fluorescence label on DNA nanogel. We can see that in plain *E. coli*, there was no Alexa 647 signal (c). When the Alex 647 labelled DNA nanogel was mixed with *E. coli,* the well-distributed red signal(h) appeared which indicated that the DNA was uniformly distributed and was not binding to *E. Coli*. Noticeably, the IgG encapsulated DNA nanogel showed some red aggregation (k) where the co-localization(l) of red signal and green signals was apparent, which indicated that our IgG encapsulated DNA nanogel had the function to binding *E. coli*. Figure 3.7 (a) is the magnification of Figure 3.6 (l), to visualize in more depth, we observed the mixture of *E. coli* and IgG encapsulated DNA nanogel under SEM (Figure 3.7 b), where we can see our DNA nanogel aggregated around *E. coli*. It is a promising signal that our DNA nanogel platform can maintain protein activity after encapsulation.

To further test if the protein-loaded DNA nanogel preserved the function, we used Keratin-forming tumor cell line HELA cells (KB), we expect the IgG can show targeting function to deliver the nanogel to the cell line. Dox was used to test the cytotoxicity function, which can show the drug delivery efficacy. Figure 3.8 shows the cell viability test with dosage response to the increased concentration of Dox. Black curve shows the cytotoxicity of free Dox, blue curve was the control which is cytotoxicity of physical mixture of random sequence

DNA strands, IgG and Dox, and red curve showed the cytotoxicity of Dox loaded IgG embedded DNA nanogel. The Dox-loaded IgG embedded DNA nanogel showed the similar behavior that the IC50 is over 1µM. Meanwhile, physical mixture of junk DNA, IgG and Dox shows the IC50 around 0.8 µM. The result showed that our IgG-embedded DNA nanogel has improved drug delivery efficacy compared to the physical mixture of IgG and junk DNA, which supported our hypothesis that the IgG still preserved the activity to binding to the cell and caused the improvement of cytotoxicity.

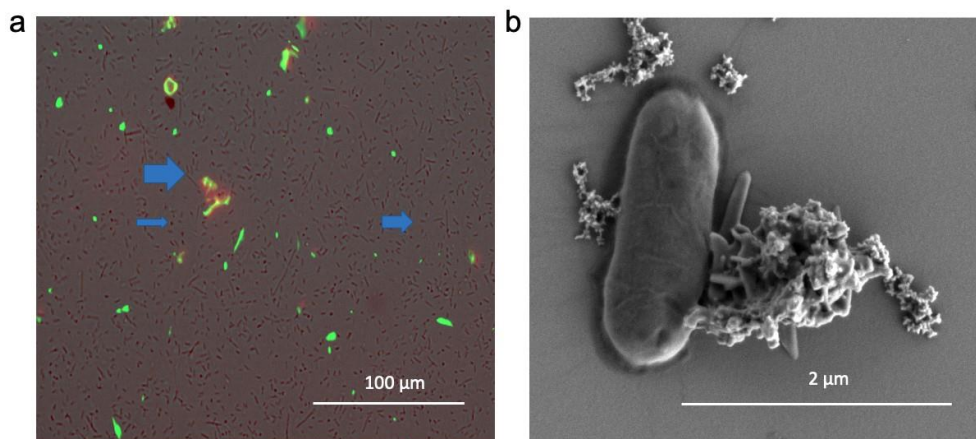**Figure 3.7**: Visualization of nanogel/IgG interacted with E. Coli. (a), Fluorescence image. Green, SYBR Gold stained *E. coli*; Red, Alexa 647 labelled DNA nanogel; (b), SEM image.

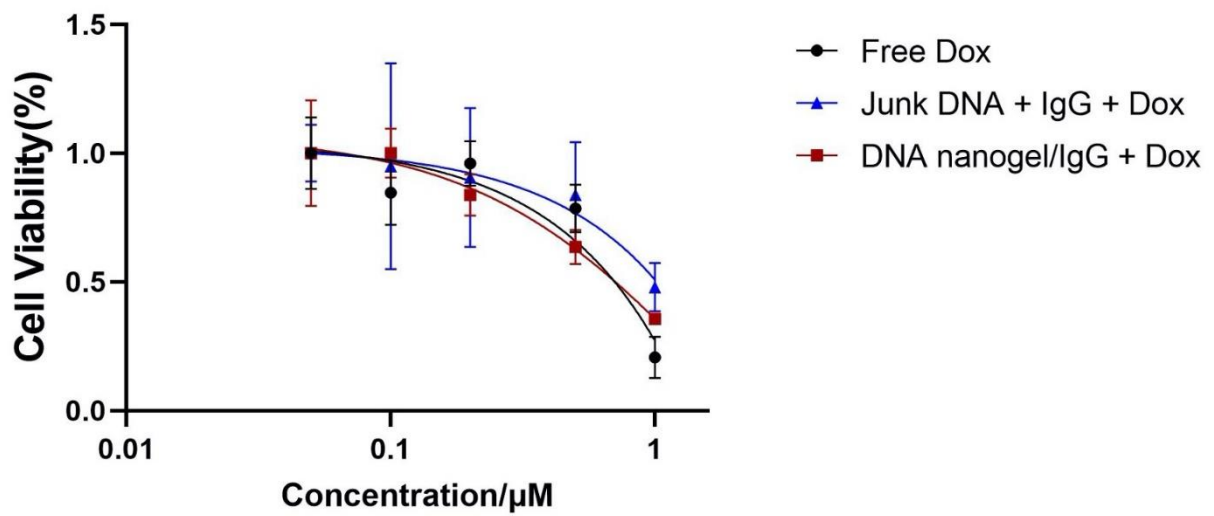**Figure 3.8**: Dose-response cell viability of the Dox-loaded protein embedded DNA nanogel. Black: free Dox; blue: physical mixture of junk DNA, IgG and Dox; red: Dox-loaded IgG embedded DNA nanogel. Cell line: KB cells.

3.4   Conclusion and Further Prospective

We have established a new platform for the next generation of drug delivery systems. The self-assembly DNA nanogel has several advantages such as programmability in response to environmental cues, large surface area to volume ratio, biocompatibility, and addressability on the surface. Due to its simple Watson-Crick base pairing, the DNA nanogel surface can be easily modified with the intended moiety conjugated to 20 Thymine. We have demonstrated that our DNA nanogels can embed functional proteins without any chemical modifications, which preserve the protein structure and function. Therefore, our self-assembly method has overcome the covalent modification strategies. As proof of concept, we have shown that the protein-embedded DNA nanogel has a protein mobility shift on the native agarose gel electrophoresis and the surface charge shift on zeta potential results. In addition, a protein functional assay proved that proteins preserved their function and structure by showing the antigen-antibody conjugation on the *E.coli* surface. The embedded IgG activity was also tested by cytotoxicity experiment, where Dox was loaded into the DNA nanogel, and the IgG tend to target the KB cell Fc receptor. The IC50 was decreased by 20% compared to the physical mixture of DNA, IgG and Dox. However, the IgG was not a good candidate for cell targeting. With the proof of concept, further studies will be exploring the functional therapeutic proteins like CD 44[43] antigen, Her2 inhibiter [44]. Further research also should be done to quantify the amount of the embedded proteins for precise control of delivery *in vitro*. Moreover, the spatial orientation of the embedded proteins onto the DNA nanogel should be controlled. Potentially, we can extend this platform to deliver other therapeutic proteins. Overall, our platform can embed functional proteins onto the DNA nanogel, which can extend to various applications.

3.5   Method

Materials. All DNA strands were purchased from IDT Company. Cyclohexane was purchased from Macron Fine Chemicals (Batch No. 0000142384). Span 80 was purchased from Tokyo chemical industry Co. (CAS 1338-43-8). Solutions were made using Micropure ST (from Thermo Scientific). Tetrahydrofuran (THF) was purchased from Fisher Chemical (T397-500). 1% Agarose gel were made by Agarose LE from Culgene (cat. #C8740) with respective buffers (TBE buffer). Magnesium and potassium were made from Magnesium acetate tetrahydrate (from Alfa Aesar, lot: D26Y034) and Potassium Chloride (from fisher scientific, M- 12445), respectively. Instant Blue was purchased from Expedeon (ISBL 1) and Ethidium Bromide was from Invitrogen (Cat. #15585-001). L-Glutamic acid potassium salt monohydrate was from Sigma Life Science (G1149-100G). Anti-Mouse IgG, antibody produced in goat was from SIGMA Company, (Product Number M5899-2 ML, 058 K 4774). Avidin was from MP Company (Cat. # 100303).

Buffers. TBE with Mg^{2+}, there is 12 mM Magnesium acetate in the buffer. 1x TBE buffer was made from 10 times TBE purchased from Apex (Cat #20-195). 1x TAE was made from 50 times TAE buffer (2M tris base, 1M acetic acid, and 0.1M H2EDTA). PBS pH 7.4 buffer was from Gibco Company by Life technologies (Lot. 1843238).

Synthesis of protein embedded DNA nanogel. First, reverse emulsion was made by 1-min sonication (pulse mode, 70% amplitude, 2s sonication every 3s; the sonic dismembrator model 150 was from Fisher Scientific) of 15ul DNA (20ug DNA in total) in 2ml cyclohexane (with 120mg, span 80). Second, 5ul Protein solution (in 4x 10mM Magnesium acetate and potassium chloride) were added into the reverse emulsion and had another 2-minute

93

sonication. For the Immunoglobulin G (IgG)s capturing, 4x 10mM potassium glutamate was used instead of potassium chloride). After 1-hour reaction, the span 80 and cyclohexane was removed by centrifuge and THF. After dispersed in 1x TBE buffer, the nanogel was characterized using DLS by Zetasizer Nano-ZS90 from Malvern to get size and zeta potential data.

AFM image. Nanogels were dispersed in TAE (with Mg^{2+} and K^+ and 5 µl sample was dropped on the mica, followed by dropping 40 µl 2mM magnesium acetate on it. The liquid was gently blown away. The samples were scanned under tapping mode using Veeco Scanning Probe Microscope (Digital instruments, the controller model was NanoScope IV).

Dynamic light scattering (DLS) and Zeta potential. Nanogel Samples are resuspended in 15 µl 1x TBE buffer. After wash and use water to dilute into DTS1070 disposable folded capillary cell. DLS machine model is Zetasizer Nano Range from Malvern Instruments. Both size and zeta potential are measured by DLS test.

Electrophoresis. 1% agarose gel in TBE buffer was ran under 100V for 50 min. Ethidium bromide was used to stain the DNA bands and Instant blue (Coomassie Blue) was used to stain the protein bands.

Colocalization of protein encapsulated DNA nanogel and *E. coli*. DNA nanogel was modified by 20T-Alexa 647, which shows the red signal under fluorescence microscope. *E. Coli* was cultured in agar plate overnight. Concentrate the *E. coli* by centrifuge under 44000 rpm for 5 min. Re-disperse the *E. Coli* into 6 ml PBS buffer. Seed 500 µl/well *E. Coli* dispersion into 12-well plate. *E. coli* was stained by SYBR gold. Incubate the *E. Coli* with Dox, Dox loaded DNA nanogel, Dox loaded IgG embedded DNA nanogel for 6 hours. Images were taken under Fluorescence Microscope.

SEM image. *E. coli* was concentrated by centrifuge, followed by measuring the OD value (0.9) in PBS buffer. Then *E. Coli* was incubated 30min with desire samples, followed by 10% formalin fixing. After washed with DI water, the *E. coli* was dropped on Si wafer.

Cell Viability Assay. KB cells (7000 cells per well) were seeded on a 96-well plate and cultured for 24 hours. Nanogel/Dox (equal to 0.05-2µmol per well) was added into the cell and incubated for specific hours, followed by medium change with 5mg/ml MTT solution. After 4h incubation, the liquid was removed by a small needle, and the cells were mixed with 100µl of dimethyl sulphoxide (from Macron, Batch No: 0000082524). The absorbance was measured at a wavelength of 540nm by the plate reader.

This Chapter, in full, is a paper under preparation for publication. Xiangyi Dong, Jinhyung Lee, Yi Chen. The dissertation author was the investigator and co-first author with Jinhyung Lee.

3.6 Reference

[1] Manning, M. C.; Patel, K.; Borchardt, R. T. Pharmaceutical Research: An Official Journal of the American Association of Pharmaceutical Scientists. 1989, pp 903–918.

[2] Gu, Z., Biswas, A., Zhao, M. and Tang, Y., 2011. Tailoring nanocarriers for intracellular protein delivery. Chemical Society Reviews, 40(7), pp.3638-3655.

[3] Lo, S.L. and Wang, S., 2010. Intracellular protein delivery systems formed by noncovalent bonding interactions between amphipathic peptide carriers and protein cargos. Macromolecular rapid communications, 31(13), pp.1134-1141.

[4] Peer D, Karp JM, Hong S, Farokhzad OC, Margalit R, Langer R. Nanocarriers as an emerging platform for cancer therapy. Nature nanotechnology. 2007 Dec;2(12):751-760.

[5] Bareford L M, Swaan P W. Endocytic mechanisms for targeted drug delivery. Advanced drug delivery reviews. 2007 Aug 10;59(8):748-58.

[6] Herrera Estrada, L. P.; Champion, J. A. Protein Nanoparticles for Therapeutic Protein Delivery. Biomater. Sci. 2015, 3 (6), 787–799.

[7] Lagassé H A D, Alexaki A, Simhadri V L, Katagiri N H, Jankowski W, Sauna Z E, and Kimchi-Sarfaty C. Recent advances in (therapeutic protein) drug development. F1000Research, 2017, 6.

[8] Asher Mullard. 2020 FDA drug approvals. Nature Reviews Drug Discovery 20, 85-90 (2021).

[9] Anselmo A C, Mitragotri S. Nanoparticles in the clinic. Bioengineering & translational medicine, 2016, 1(1): 10-29.

[10] Frokjaer S, Otzen D E. Protein drug stability: a formulation challenge. Nature reviews drug discovery, 2005, 4(4): 298-306.

[11] Peer D, Karp J M, Hong S, Farokhzad O C, Margalit R, and Langer R. Nanocarriers as an Emerging Platform for Cancer Therapy. In Nano-Enabled Medical Applications. Jenny Stanford Publishing, 2020: 61-91.

[12] Lee, K. Y.; Yuk, S. H. Polymeric Protein Delivery Systems. Prog. Polym. Sci. 2007, 32 (7), 669–697.

[13] Chou, L. Y. T.; Ming, K.; Chan, W. C. W. Strategies for the Intracellular Delivery of Nanoparticles. Chem. Soc. Rev. 2011, 40 (1), 233–245.

[14] Kabanov, A. V; Vinogradov, S. V. NIH Public Access. 2010, 48 (30), 5418– 5429.

[15] Solaro, R. Targeted Delivery of Proteins by Nanosized Carriers. J. Polym. Sci. Part A Polym. Chem. 2008, 46 (1), 1–11.

[16] Tang, R.; Kim, C. S.; Solfiell, D. J.; Rana, S.; Mout, R.; Velázquez- Delgado, E. M.;

Chompoosor, A.; Jeong, Y.; Yan, B.; Zhu, Z. J.; Kim, C.; Hardy, J. A.; Rotello, V. M. Direct Delivery of Functional Proteins and Enzymes to the Cytosol Using Nanoparticle-Stabilized Nanocapsules. ACS Nano 2013, 7 (8), 6667–6673.

[17] Sinha V R, Trehan A. Biodegradable microspheres for protein delivery. Journal of controlled release, 2003, 90(3): 261-280.

[18] Lee K Y, Yuk S H. Polymeric protein delivery systems. Progress in polymer science, 2007, 32(7): 669-697.

[19] Yan M, Du J, Gu Z, Liang M, Hu Y, Zhang W, Priceman S, Wu L, Zhou ZH, Liu Z, Segura T. A novel intracellular protein delivery platform based on single-protein nanocapsules[J]. Nature nanotechnology, 2010, 5(1): 48-53.

[20] Jain Ashish, Jain A, Gulbake A, Shilpi S, Hurkat P, Jain SK. Peptide and protein delivery using new drug delivery systems. Critical Reviews™ in Therapeutic Drug Carrier Systems, 2013, 30(4).

[21] Bennion, B. J.; Daggett, V. The Molecular Basis for the Chemical Denaturation of Proteins by Urea. Proc. Natl. Acad. Sci. U. S. A. 2003, 100 (9), 5142–5147.

[22] Zheng, D.; Giljohann, D. A.; Chen, D. L.; Massich, M. D.; Wang, X.-Q.; Iordanov, H.; Mirkin, C. A.; Paller, A. S. Topical Delivery of siRNA-Based Spherical Nucleic Acid Nanoparticle Conjugates for Gene Regulation. Proc. Natl. Acad. Sci. 2012, 109 (30), 11975–11980.

[23] Lee, H.; Lytton-Jean, A. K. R.; Chen, Y.; Love, K. T.; Park, A. I.; Karagiannis, E. D.; Sehgal, A.; Querbes, W.; Zurenko, C. S.; Jayaraman, M.; Peng, C. G.; Charisse, K.; Borodovsky, A.; Manoharan, M.; Donahoe, J. S.; Truelove, J.; Nahrendorf, M.; Langer, R.; Anderson, D. G. Molecularly Self-Assembled Nucleic Acid Nanoparticles for Targeted in Vivo siRNA Delivery. Nat. Nanotechnol. 2012, 7 (June), 389–393.

[24] Mikkilä, J.; Eskelinen, A. P.; Niemelä, E. H.; Linko, V.; Frilander, M. J.; Törmä, P.; Kostiainen, M. A. Virus-Encapsulated DNA Origami Nanostructures for Cellular Delivery. Nano Lett. 2014, 14 (4), 2196–2200.

[25] Kim, K.-R.; Kim, D.-R.; Lee, T.; Yhee, J. Y.; Kim, B.-S.; Kwon, I. C.; Ahn, D.-R. Drug Delivery by a Self-Assembled DNA Tetrahedron for Overcoming Drug Resistance in Breast Cancer Cells. Chem. Commun. (Camb). 2013, 49 (20), 2010–2012.

[26] Yatsunyk LA, Pietrement O, Albrecht D, Tran PL, Renciuk D, Sugiyama H, Arbona JM, Aimé JP, Mergny JL. Guided assembly of tetramolecular G-quadruplexes. ACS nano, 2013, 7(7): 5701-5710.

[27] Rippe, K.; Fritsch, V.; Westhof, E.; Jovin, T. M. Alternating d(G-A) Sequences Form a Parallel-Stranded DNA Homoduplex. EMBO J. 1992, 11 (10), 3777–3786.

[28] Bang, I. Untersuchungen Uber Die Guanylsaure. Biochemistry 1910, 293- 231, 26.

[29] Gellert, M.; Lipsett, M. N.; Davies, D. R. Helix Formation By Guanylic Acid. Proc. Natl. Acad. Sci. 1962, 48 (12), 2013–2018.

[30] Guo W, Lu CH, Orbach R, Wang F, Qi XJ, Cecconello A, Seliktar D, Willner I. pH-Stimulated DNA Hydrogels Exhibiting Shape-Memory Properties. Advanced Materials, 2015, 27(1): 73-78.

[31] Chen F, Lu Q, Huang L, Liu B, Liu M, Zhang Y, Liu J. DNA Triplex and Quadruplex Assembled Nanosensors for Correlating K+ and pH in Lysosomes. Angewandte Chemie International Edition, 2021, 60(10): 5453-5458.

[32] Idili A, Vallée-Bélisle A, Ricci F. Programmable pH-triggered DNA nanoswitches[J]. Journal of the American Chemical Society, 2014, 136(16): 5836-5839.

[33] Heller I, Hoekstra TP, King GA, Peterman EJ, Wuite GJ. Optical tweezers analysis of DNA–protein complexes. Chemical reviews, 2014, 114(6): 3087-3119.

[34] Hornblower B, Coombs A, Whitaker RD, Kolomeisky A, Picone SJ, Meller A, Akeson M. Single-molecule analysis of DNA-protein complexes using nanopores. Nature Methods, 2007, 4(4): 315-317.

[35] Frykholm K, Alizadehheidari M, Fritzsche J, Wigenius J, Modesti M, Persson F, Westerlund F. Probing Physical Properties of a DNA-Protein Complex Using Nanofluidic Channels. Small, 2014, 10(5): 884-887.

[36] Park S H, Yin P, Liu Y, Reif J H, LaBean T H, Yan H. Programmable DNA self-assemblies for nanoscale organization of ligands and proteins. Nano Letters, 2005, 5(4): 729-733.

[37] Zhu, G.; Zheng, J.; Song, E.; Donovan, M.; Zhang, K.; Liu, C.; Tan, W. Self-Assembled, Aptamer-Tethered DNA Nanotrains for Targeted Transport of Molecular Drugs in Cancer Theranostics. Proc. Natl. Acad. Sci. U. S. A. 2013, 110 (20), 7998–8003.

[38] Chang, M.; Yang, C. S.; Huang, D. M. Aptamer-Conjugated DNA Icosahedral Nanoparticles as a Carrier of Doxorubicin for Cancer Therapy. ACS Nano 2011, 5 (8), 6156–6163.

[39] Ko, S. H.; Liu, H.; Chen, Y.; Mao, C. DNA Nanotubes as Combinatorial Vehicles for Cellular Delivery. Biomacromolecules 2008, 9 (11), 3039– 3043.

[40] Williams, B. A. R.; Lund, K.; Liu, Y.; Yan, H.; Chaput, J. C. Self-Assembled Peptide Nanoarrays: An Approach to Studying Protein-Protein Interactions. Angew. Chemie - Int. Ed. 2007, 46 (17), 3051–3054.

[41] Leirmo S, Harrison C, Cayley D S, et al. Replacement of potassium chloride by potassium glutamate dramatically enhances protein-DNA interactions in vitro[J]. Biochemistry, 1987, 26(8): 2095-2101.

[42] Leo J C, Goldman A. The immunoglobulin-binding Eib proteins from Escherichia coli are receptors for IgG Fc[J]. Molecular immunology, 2009, 46(8-9): 1860-1866

[43] Lee J Y, Lee H S, Kang N W, Lee S Y, Kim D H, Kim S, Yoon I S, Cho H J, Kim D D. Blood component ridable and CD44 receptor targetable nanoparticles based on a maleimide-functionalized chondroitin sulfate derivative. Carbohydrate polymers. Carbohydrate polymers,

2020, 230: 115568.

[44] Kulukian A, Lee P, Taylor J, Rosler R, de Vries P, Watson D, Forero-Torres A, Peterson S. Preclinical activity of HER2-selective tyrosine kinase inhibitor tucatinib as a single agent or in combination with trastuzumab or docetaxel in solid tumor models. Molecular cancer therapeutics, 2020, 19(4): 976-987.

Chapter 4

Reversible DNA Structures

ABSTRACT. Other than the irreversible dissociation structure, in this chapter, we propose reversible DNA structures. In the first half, with a DNA triplex introduced into the DNA nanogel, we developed a new swellable pH-responsive nanogel drug delivery platform. This platform is a DNA nanogel cross-linked using a G-Quadruplex configuration similar to that described in previous chapters. Instead of using an i-motif, we utilized a DNA triplex structure to achieve pH-responsive properties. The nanogel swells under acidic conditions and shrinks back when the pH returns to physiological levels. The swellable DNA nanogel achieved a swelling ratio of 1.66, and its size-reversible conformation change was rapidly responsive to the environmental pH. Upon cell uptake, the pH level decreased, causing a specifically designed DNA double helix to break and form a triplex, followed by swelling inside the endosome, ultimately resulting in drug release. This method also shows promise for enhancing endosome escape. To assess cytotoxicity to cancer cells, we used doxorubicin. The swellable DNA nanogel decreased the IC50 more than threefold compared to a pH-insensitive DNA nanogel. Other than Hoogsteen bonding, in the second section, we investigated a series of reversible 2-dimentional to 3-dimentional DNA structures based on Watson-Crick bonding. We performed DNA simulations for molecular-level visualization of the conformation change of the reversible DNA nanogel triggered by toehold-mediated strand displacement.

4.1   Swellable DNA Nanogel

In previous chapters, we described the successful development of a DNA nanogel system with a G-quadruplex motif. Both small-molecule drugs, such as doxorubicin (Dox), and large drugs, such as proteins, can be loaded onto this nanogel system. We integrated a pH-responsive C-rich motif into the nanogel system to achieve dissociable behavior by decreasing the pH to acidic levels, which enhanced drug release during endocytosis.

Various drug delivery platforms based on low-pH endocytosis have been reported. Other than dissociable systems, swellable systems can also improve the efficacy of drug delivery [1-4]. A reversible polymer-based swelling-shrinking nanogel (NLSC-NG) was reported in 2014 [1]. This nanogel was based on N-lysinal-N'-succinyl chitosan (NLSC) optimized at an isoelectric point of around 6.0 to achieve an acid-triggered charge reversal capability. The nanogel swelled at pH 4.5 in a swelling ratio of 10 compared to pH 7.4 and shrank back when the pH returned to 7.4. The nanogel's swellable properties improved endosome escape and made it reusable, resulting in better penetration into tumor sites. However, the polymer synthesis time was long, and the pH-responsiveness time was 1 h, which is considerably longer than the endosome escape time. The results presented in Chapter 2 showed that our pH-responsive DNA nanogel achieved a rapid response to pH conditions. Our dissociable DNA nanogel released Dox, which was previously loaded onto the double helix, within 5 min. Our system had a synthesis time of 2.5 h, which is a considerable advantage compared to existing pH-responsive drug delivery systems. Other than the i-motif structure, the DNA triplex is another dynamic motif responsive to environmental pH [5], as mentioned in Chapter 1. The transition pH of triplex depends on the GC content of the sequence [6]. The transition pH is 6 when the GC content is 50% and rises to 10 when the GC content is 0%. Notably, the C^+ G-C triplex requires cytosine pronated at a lower

pH, whereas TAT does not. A TAT triplex [7] has been reported to form under a physiological pH when the poly-A to poly-T strand ratio is 1:2, whereas in a ratio of 1:1, the double helix is the preferred structure. Although triplex-based motors have been reported [8-10], as discussed in Chapter 1, no swellable pH-responsive triplex-based DNA nanogel has been reported. Other than irreversible dissociation, reversible features could make it possible to reuse the structure and prolong the active therapy time. This chapter describes a swellable DNA nanogel responsive to pH conditions and has a reversible size when the pH switches between 7.4 and 5.5. For function testing, we used Dox as the delivered drug as well.

4.1.1   Swellable DNA Nanogel Platform

Figure 4.1 shows the swellable DNA nanogel platform. The nanogel forms at a physiological pH. The presence of magnesium allows double helices to form, and potassium cations enable the formation of G-quadruplexes to produce the gel. A triplex structure is introduced into the nanogel platform, which forms a double helix with its complementary strands under physiological conditions and releases the complementary strands to form an intramolecular triplex structure (pink motif at pH 4–6 in Figure 1). Once the double helix dissociates, the distance between two G-quadruplexes increases, causing the DNA nanogel to swell and subsequently release the drug inside the structure. When the pH returns to physiological levels, Hoogsteen bonding in the triplex structure dissociates and forms a double helix. We used DLS to test the nanogel's size reversibility.
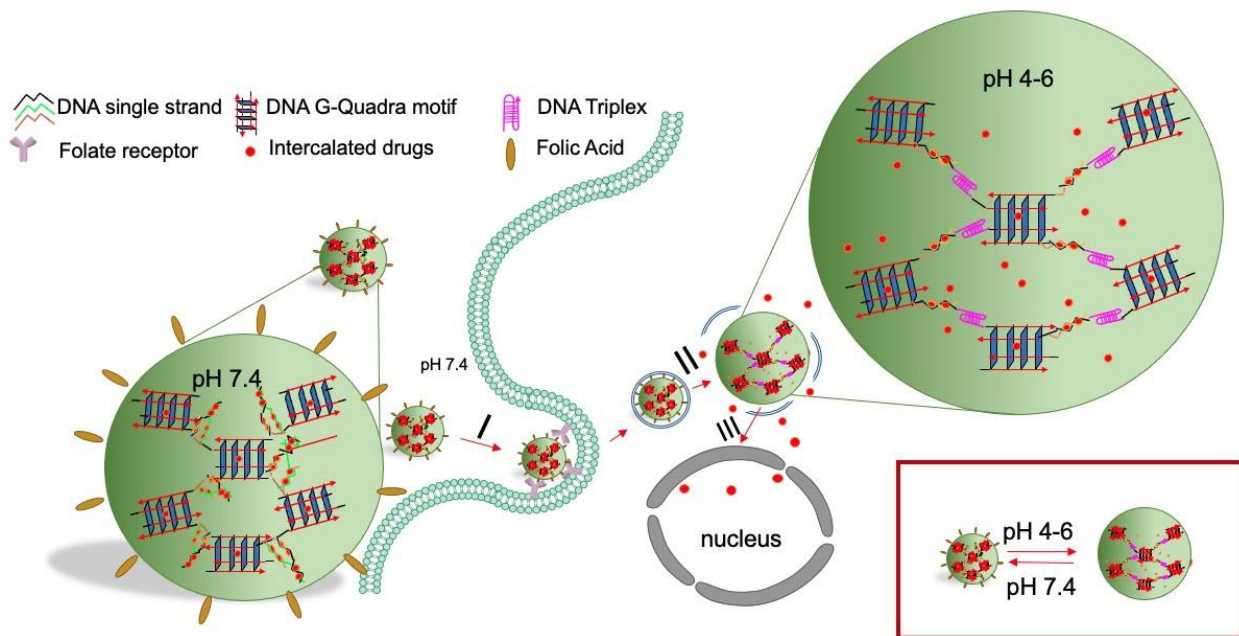
Figure 4.1: Schematic design of the swellable DNA nanogel drug delivery system. I: Specific binding to an overexpressing receptor on tumor cells and triggering of receptor-mediated endocytosis; II: The pH decreases and the nanogel swells, releasing a small-molecule drug; III: Diffusion of the released drug.

We used Dox [33] to test the swellable pH-responsive DNA nanogel platform. When the pH decreased during endocytosis, Dox loaded between base pairings was released because of the dissociation of the double helix.

4.1.2 Swellable DNA Nanogel Designs

As in the case of the dissociable DNA nanogel described in Chapter 2, we used a reverse emulsion system to synthesize the swellable DNA nanogel. The DNA nanogel formed during the inside water phase in the presence of K^+ and Mg^{2+}. To conjugate it, we added folic acid to the system. We then obtained the nanogel by washing away the surfactant after centrifugation. We used Dox to evaluate the cytotoxicity of the nanogel. We used a DNA nanogel without a pH-

responsive design as a control, which did not undergo a conformational change in an acidic pH environment. The next section describes the triplex-based swellable DNA nanogel designs.

4.1.3 Design 1.0
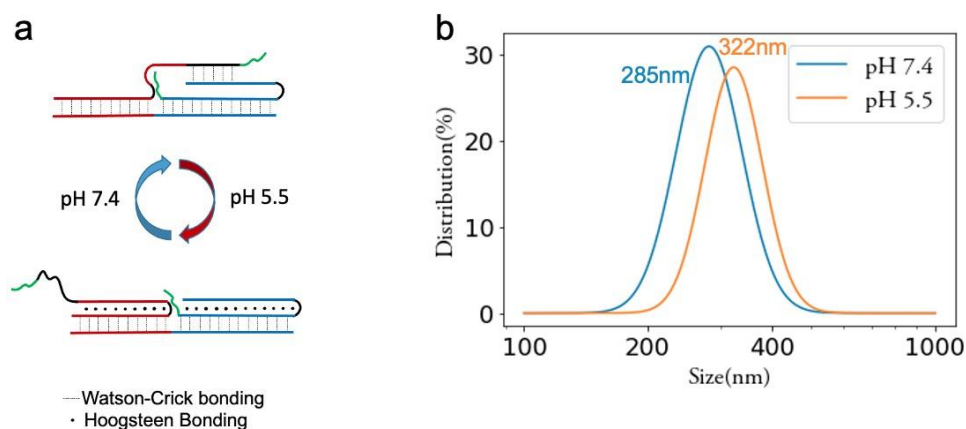
Figure 4.2: Swellable DNA nanogel design 1.0. (a) Single-switch design; the green overhangs are the G-rich sites for cross-linking; the three red and blue domains form a triplex structure under acidic conditions. (b) Size distribution of the nanogel measured by DLS.

Figure 4.2 (a) shows a single switch swellable DNA nanogel design. The three red and blue domains form triplex structures respectively under acidic conditions. The two green overhangs are the G-rich domains designed to form G-quadruplex cross-linking. The distance between the two green overhangs was the same in all swellable design motifs. The top duplex domain at pH 7.4 was six bases (2 nm), while at pH 5.5, the distance between the green domains was expected to be 5 nm (15 nt).

As in the case of the dissociable DNA nanogel described in Chapter 2, after the synthesis of the swellable DNA nanogel, we measured its size using DLS. Figure 4.2 (b) shows the

nanogel sizes at different pH levels. The nanogel swelled from 285 nm at pH 7.4 to 322 nm at pH 5.5. This represented a swelling ratio of 1.13, which was not as high as expected. This was probably because the top red domain was single-stranded and highly flexible. Thus, we could not measure the distance simply based on the base number. Although we obtained a swellable gel, our design required further optimization to achieve a higher swelling ratio and enhance its function.

4.1.4   Design 2.0
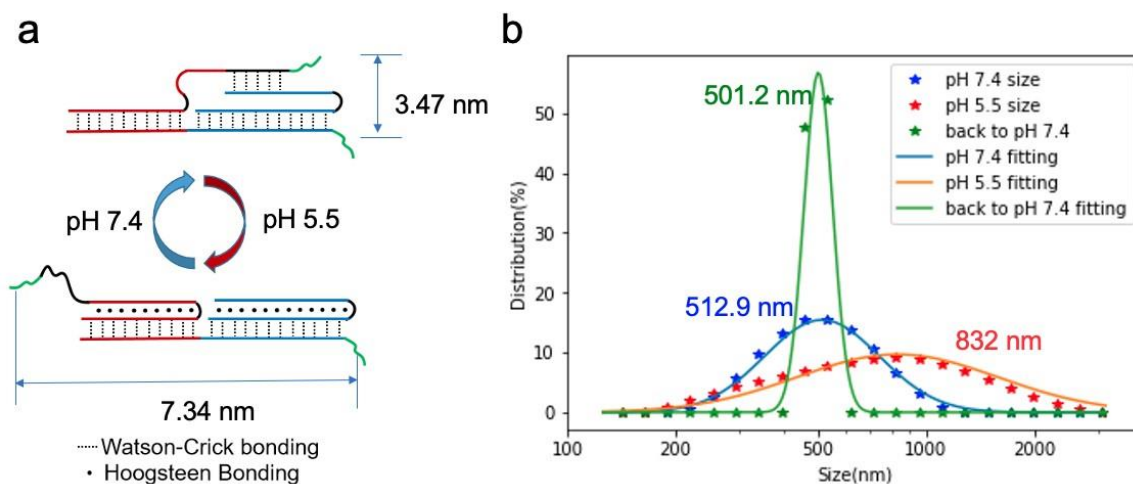
Figure 4.3: Swellable DNA nanogel design 2.0. (a) Single-switch unit. The two green domains are G-rich strands for G-quadruplex cross-linking; the three red and blue domains form two triplex structures under acidic conditions. (b) Size distribution of the nanogel measured by DLS. Blue: original nanogel size at pH 7.4; red: swollen nanogel at pH 5.5; green: nanogel shrunk back at pH 7.4.

Figure 4.3 (a) shows our second design. This design was similar to the first one except that the G-rich domains were changed at the top-right and bottom-right corners to obtain a greater expansion for the single switch. The single switch expanded from 3.47 nm at pH 7.4 to

7.34 nm at pH 5.5, which is comparable to existing expanding DNA structures [1,2].

The DLS data (Figure 4.3 (b)) showed that the second design had reversible properties. We dispersed the swellable nanogel in a PBS buffer. At pH 7.4, its average size was 512.9 nm. When we decreased the pH to 5.5 using HCl, it swelled to 832 nm. When we increased the pH back to 7.4, the size shrank back to 501.2 nm. These results showed that the swellable and reversible DNA nanogel formed successfully and had a swelling ratio of 1.66, which is comparable to existing swellable platforms [1-4].
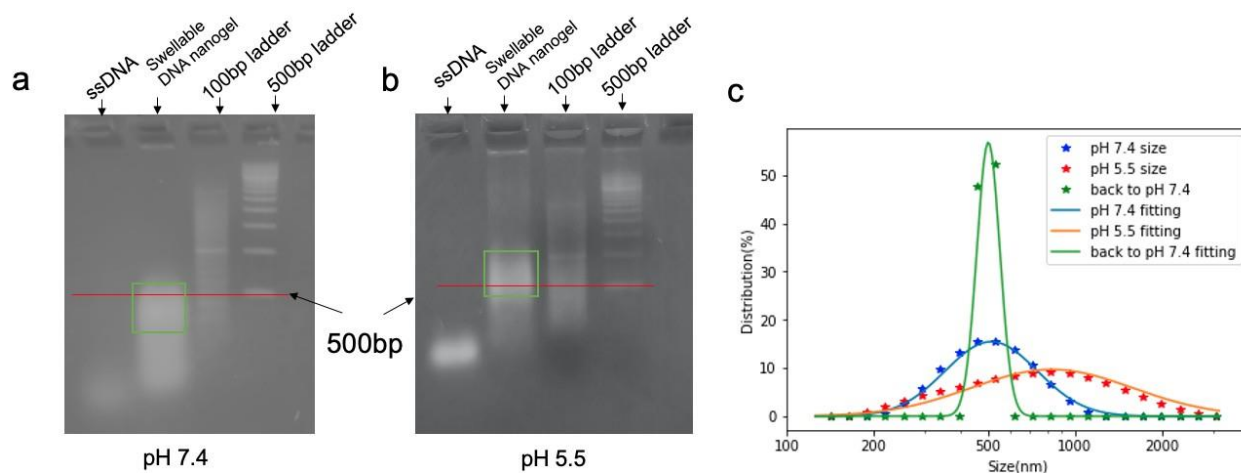
Figure 4.4: Swellable pH-responsive DNA nanogel characterized using a 2% agarose gel. (a) TAE/MES buffer, pH 7.4. (b) MES buffer, pH 5.5. lanes from left to right: single-stranded DNA, swellable DNA nanogel, 100-bp ladder, and 500-bp ladder.

We performed agarose gel electrophoresis to characterize the nanogel's formation and conformation change (Figure 4.4 (a, b)). For each gel, from left to right, the first lane contains single-stranded DNA with the same molecular weight and bases as the single DNA strand that we used to create the nanogel, the second lane contains the swellable DNA nanogel, and the third and fourth lanes are 100- and 500-bp DNA ladders, respectively. At a physiological pH, the

majority nanogel band showed higher mobility than the 500-bp marker, while under acidic conditions, the majority band showed lower mobility. This indicated that the nanogel swelled under acidic conditions. Based on the DLS data, we estimated that the nanogel had a swelling ratio of 1.66 (500 nm to 830 nm). Based on electrophoresis, after a comparison with the strands, we estimated the swelling ratio to be 1.56 (360 bp to 560 bp), assuming that the mobility of the DNA strands was linearly related to the size. The swelling ratios of recently reported swellable systems range from 1.5 to 10. However, synthesis using these methods is time-consuming (ranging from 30 to more than 100 h), and all these systems are characterized by long response times to pH conditions. We obtained our DLS data immediately after adjusting the pH, which suggests that our system underwent a rapid conformation change, which is a considerable advantage for endosome pH drug release.

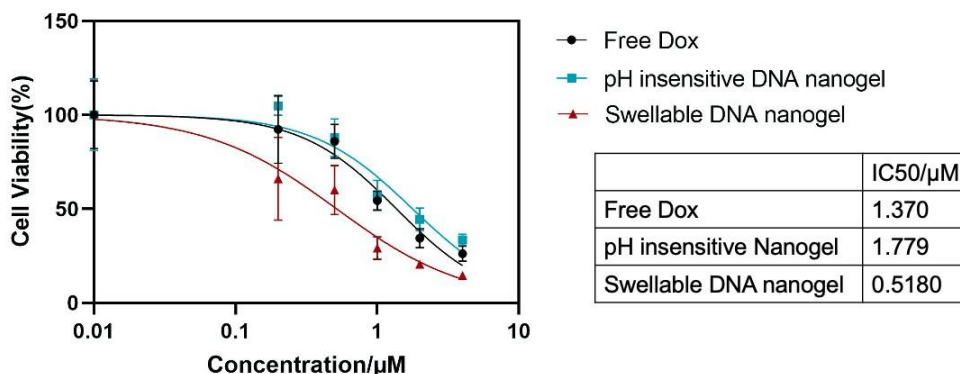|	IC50/µM
Free Dox	1.370
pH insensitive Nanogel	1.779
Swellable DNA nanogel	0.5180

Figure 4.5: Enhanced cytotoxicity of the swellable DNA nanogel. Black: cells treated with free Dox; blue: cells treated with the pH-insensitive DNA nanogel; red: cells treated with the swellable DNA nanogel. Cell line: KB cells. Incubation time: 24 h. The error bars indicate standard deviations (n = 3).

4.1.5　Improved Cytotoxicity of the Swellable DNA Nanogel

We used Dox to evaluate the cytotoxicity of the swellable pH-sensitive DNA nanogel to KB cancer cells, which express the folic acid receptor. For characterization, we performed a 3-(4,5-dimethylthiazol-2-yl)-2,5-diphenyltetrazolium bromide (MTT) assay. The amounts of Dox loaded onto the pH-insensitive and swellable nanogels were the same as that of free Dox (0–4 μM). In Figure 4.5, the black line indicates KB cells treated with free Dox, the blue line indicates cells treated with Dox loaded onto the pH-insensitive nanogel, and the red line indicates cells treated with Dox loaded onto the swellable nanogel. After 24 h of incubation, the swellable DNA nanogel showed higher cytotoxicity, with an IC50 of 0.518 μM, whereas the pH-insensitive nanogel had an IC50 of 1.779μM.

4.1.6　Conclusion

This study is the first to utilize the DNA triplex motif to produce a swellable pH-responsive DNA nanogel, a novel size-reversible platform for drug delivery based on a G-quadruplex configuration. To make the nanogel pH-responsive and size-reversible, we introduced a triplex motif structure with a 50% GC content. We confirmed its conformation change between physiological and acidic conditions using electrophoresis and DLS. The nanogel showed enhanced drug release under acidic conditions. We optimized the largest single-switch extension distance (from 3.47 nm to 7.34 nm) and obtained a nanogel with swelling ratio of 1.66, which is comparable to existing platforms [1-4,11-13]. Moreover, our system has the advantages of easy synthesis (2.5 h at room temperature), a rapid pH response (within 5 min), and a flexible design (overhangs). Furthermore, the swellable DNA nanogel showed higher cytotoxicity, decreasing the IC50 more than threefold compared to the pH-insensitive DNA nanogel. These

properties make our swellable pH-responsive DNA nanogel a promising platform for drug delivery. The swollen size during endocytosis may also facilitate endosome escape. The DNA nanogel platform is a potential candidate for the next generation drug delivery systems. In-vitro and in-vivo pharmacokinetics will be investigated in the future.

4.1.7   Method

Materials. All DNA strands were purchased from IDT. Cyclohexane was purchased from Spectrum (CAS 110-82-7). Span 80 was purchased from Tokyo Chemical Industry Co. (CAS 1338-43-8). Water were made using a MicroPure ST (Thermo fisher Scientific). Tetrahydrofuran (THF) was purchased from EMD (TX0280-6). Agarose gels were made using Agarose LE purchased from Culgene (cat. No. C8740) with the respective buffers. Magnesium and potassium were made from magnesium acetate tetrahydrate (lot No. D26Y034; Alfa Aesar) and potassium chloride (M-12445; Fisher Scientific), respectively. Folic acid–PEG-maleimide was purchased from NANOCS (lot No. 110511). DTT was purchased from MP Biomedicals (cat. No. 856126). Dox was purchased from Fisher Scientific (lot No. 154656). Hydrochloric acid was purchased from J. T. Baker.

Buffers. TAE was made from a 50× TAE buffer (2 M tris base, 1 M acetic acid, and 0.1 M H_2EDTA). The MES buffer was diluted 10 times from a 1 M MES buffer solution purchased from Alfa Aesar. TAE/Mg was made from 12 mM magnesium acetate in a TAE buffer.

Agarose gel electrophoresis. Quantities of 1% agarose gel in TAE/MES (pH 7.4) and MES (pH 5.5) buffers were run at the same time under 100 V for 1 h. Ethidium bromide was added to the gel to stain the DNA bands. After running, the gel was placed under direct UV light to visualize the bands. A camera was used to acquire images.

Conjugation with folic acid. DNA 20T-SH strands were treated with DTT for 1.5 h and then with folic acid overnight. They were then purified using a G-50 Micro Column (29-9034-08; GE Healthcare).

Nanogel synthesis. First, reverse emulsion was performed by 2-min sonication (pulse mode, 70% amplitude, 2-s sonication every 3 s) of 15 μl of DNA (20 μg of DNA in total) in 2 ml of cyclohexane (with 120 mg of Span 80) using a Dismembrator 150 (Thermo Fisher Scientific). Then, 5 μl of salt solution was added to the reverse emulsion, followed by 1-min sonication. After a 1-h reaction, 20T–folic acid was added to the emulsion, followed by 1-min sonication. After a 1-h reaction, Span 80 and cyclohexane were removed by centrifugation and THF washing. The nanogel was then dispersed in PBS (with 10 mM magnesium and 1 mM potassium). The nanogel size was determined using DLS (Zetasizer Nano ZS90; Malvern Panalytical).

Cell culture. KB cells were donated by Dr. Zhang's laboratory and cultured in DMEM (Corning) with 10% (v:v) fetal bovine serum (FBS; HyClone) and 1% Pen Strep (Thermo Fisher Scientific) in an incubator (Thermo Fisher Scientific) at 37°C in a 5% CO_2 atmosphere. The cells were subcultured approximately every two days at 80% confluence using 0.25% (w: v) trypsin at a split ratio of 1:3.

Cytotoxicity. KB cells (7,000 per well) were seeded on a 96-well plate and cultured for 24 h. Dox-loaded nanogels (0.05–4 μmol per well) were added to the cells and incubated for 24 h, followed by medium change with an MTT solution (5 mg/ml). After 4-h incubation, the liquid was removed using a small needle, and the cells were mixed with 100 μl of dimethyl sulfoxide (batch No. 0000082524; Macron). Absorbance was measured at a wavelength of 540 nm using a plate reader.

4.2 DNA Structure Simulation for Reversible Conformation Change by Strand Displacement

4.2.1 Introduction

In addition to pH-responsive motifs, DNA can be used in a diverse range of structures, including two-dimensional arrays, three-dimensional structures, and nanomachines. Among these, dynamic DNA nanostructures show promising abilities in nanometer-scale control. Many approaches have been developed, including strand displacement [14-17], DNA enzymes [18,19], and reconfiguration of arrays from different DNA motifs [20-22]. However, although these systems can sense a variety of physical or chemical cues, they exhibit simple dynamic behaviors in a single unit and small-range changes and cannot undergo dimensional transformation. In this study, we propose a series of 2D-3D transformable DNA nanostructures. By fueling the DNA nanostructure with DNA strands, it can perform a cross-dimensional switch, simulating some of the key aspects of biological processes, such as triskelion protein bending in clathrin patch formation. In this chapter, we describe oxDNA simulations performed to further visualize the DNA structures at the molecular level.

4.2.2 Design of Transformable DNA Nanostructures

To construct the DNA nanostructures, we used short DNA strands as building blocks. As shown in Figure 4.6, we employed a n-point-star DNA motif. It consists of one central strand, three-arm strands, and three end strands with two linker strands on each. The linked strands can partially hybridize with other linker strands on another end strand and leave a single strand with a hairpin domain. A single block strand can hybridize with these single-strand domains to form a

rigid double-strand domain. The overall transformation is controlled by this linker strand. When there is a blocking strand, an extended double-strand domain with a length of 12.2 nm is formed. When a DNA fuel strand, which is fully complementary to the block strands, is introduced, it hybridizes with the blocking strand and extracts it from the DNA nanostructures, with a single-strand domain remaining. This single strand then forms a hairpin structure. The overall length decreases to 6.5 nm (Figure 4.7). Because the linker strand controls the arm distance, to overcome the tension, the DNA nanostructure bends and switches from a flat to a convex form (Figure 4.6 (b)).
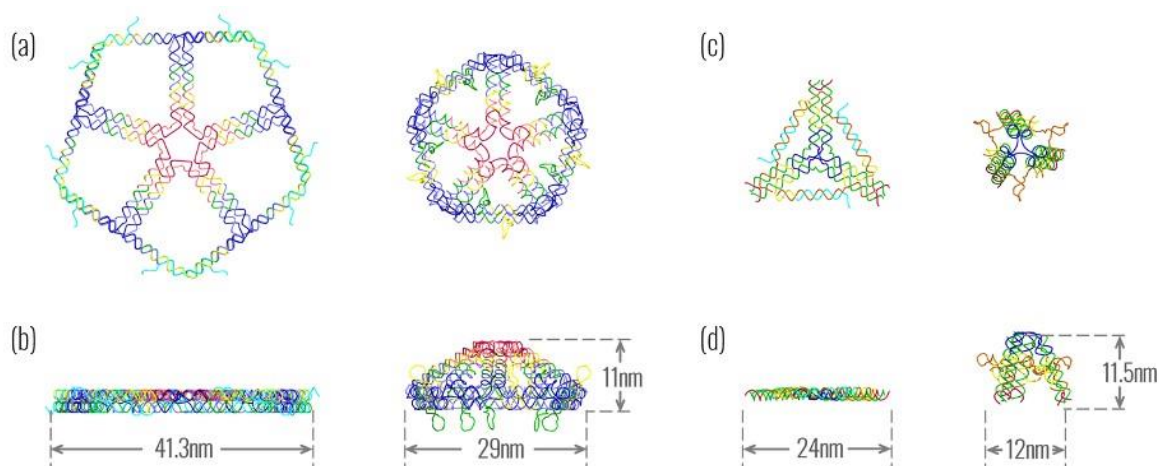

Figure 4.6: Illustration and dimensions of (a, b) five-arm single motifs and (c, d) three-arm array motifs. (a) Top-down view of five-arm 2D (left) and 3D (right) motifs. (b) Side view of five-arm 2D and 3D motifs. (c) Top-down view of three-arm array 2D (left) and 3D (right) motifs. (d) Side view of three-arm array 2D and 3D motifs.
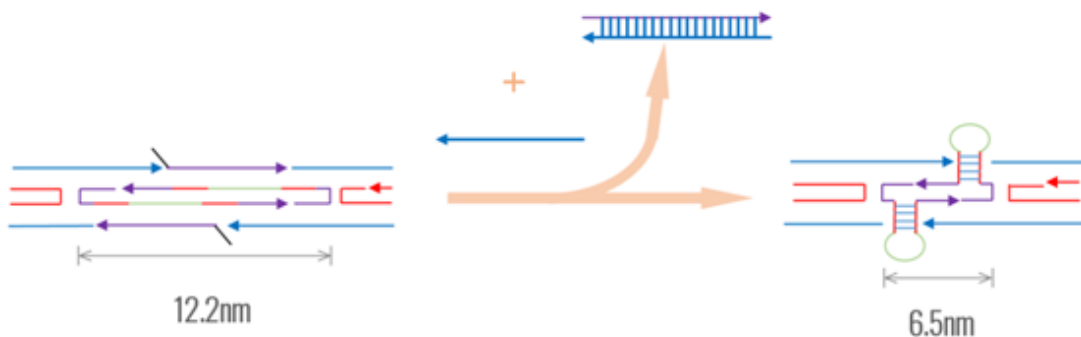
Figure 4.7: Fuel strand–mediated transformation process in single motifs. The fuel strand removes the extension strand, and the single-strand domain that remains is designed to form a hairpin structure, shortening the overall length of the linker.

4.2.3 Experimental Results

The synthesizing work was predominately contributed by Sibai Xie. The transformation of DNA nanostructures was expected to be dictated by the DNA dual strands. To investigate the two reversible states, we first studied the 2D and 3D structures with a five-arm design. We chose this design because five arms are more stable than three arms and have more linker strand domains. The results of native gel electrophoresis of the five-arm design in 2D and 3D formation are shown in Figure 4.8 (Lanes 1 and 2).

In the same gel, we tested the transformation process mediated by the DNA fuel strand. We started with a flat 2D form. After adding the fuel strand, the DNA nanostructure lost the extension strand. The remaining single-strand domain then formed a hairpin structure on the linker strand and forced the flat form to switch to a convex form. As the molecular weight became smaller, so did the size of the cross-section. The structure thus migrated faster in native gel electrophoresis (Figure 4.8, Lane 1). To confirm the results, we added extra fuel strands to exclude the possibility of random hybridization (Figure 4.8, Lanes 5 and 6). We then performed the transformation from 3D to 2D, which showed a similar but reversed pattern (Figure 4.8,

113

Lanes 3 and 4). The upper bands indicate the flat 2D structure because of its rigidity, while the lower bands at ~1 kbp indicate the 3D structure because of its relatively compact structure.
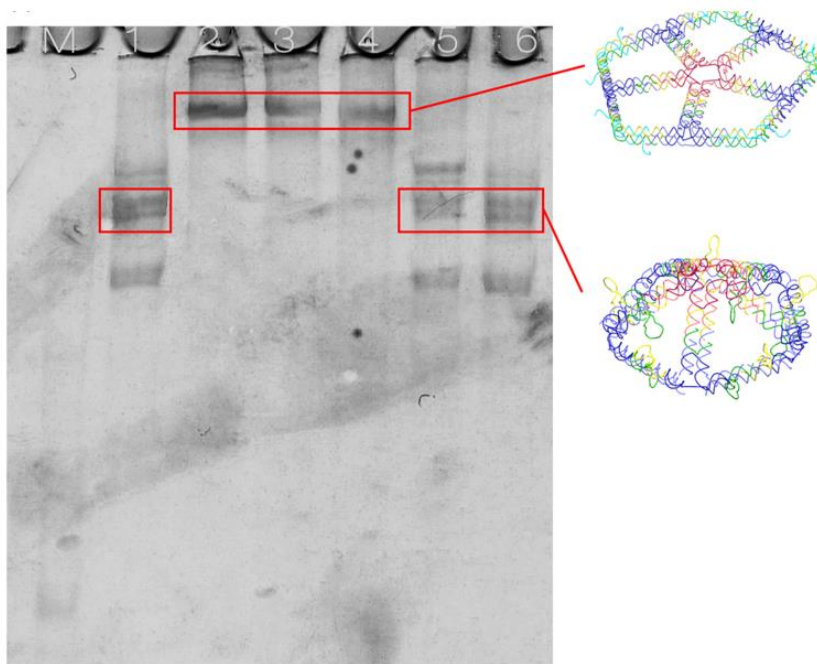
Figure 4.8: A 5% native PAGE gel in TAE/Mg for the conformation change of single 3D and 2D motifs. Lane 1: 3D structure; Lane 2: 3D structure with extension strands added in a 1:1 molar ratio; Lane 3: 3D structure with extension strands added in a 1:3 molar ratio; Lane 4: 2D structure; Lane 5: 2D structure with Fu strands added in a 1:3 molar ratio; Lane 6: 2D structure with fuel strands in a 1:3 molar.

To directly observe the transformation results, we performed AFM measurements. Figure 4.9 (b) (left) shows the 3D form of DNA nanostructures. Each nanostructure was 12 nm in diameter, while the 2D form in the middle panel shows that each unit switched to 25 nm.
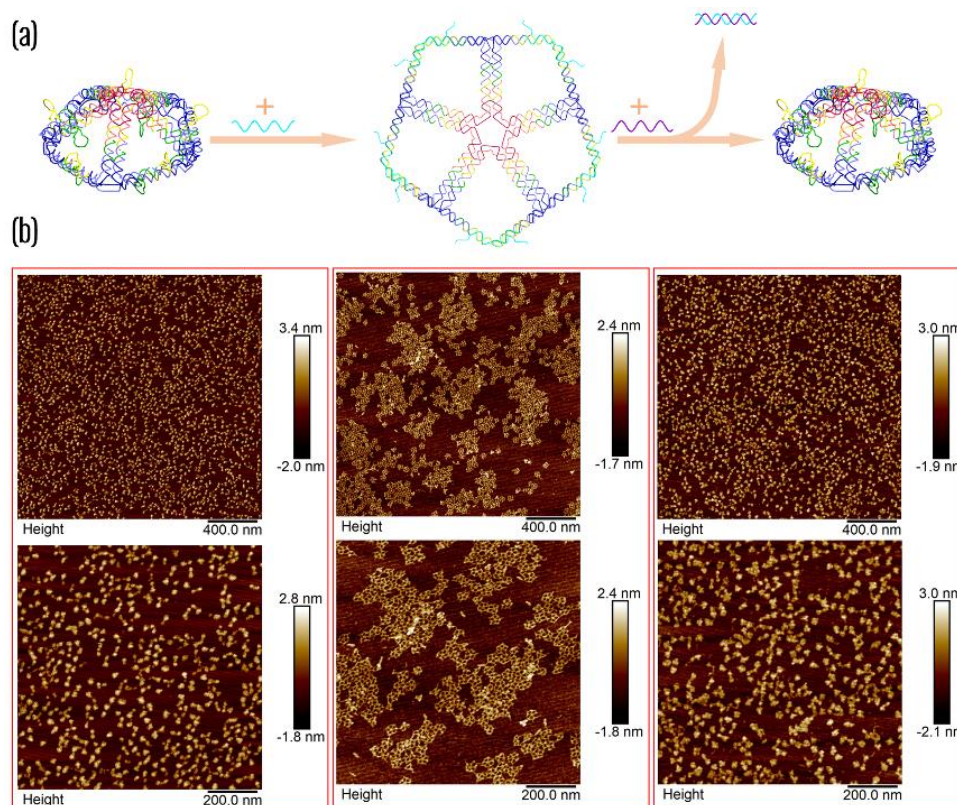
Figure 4.9: Five-arm single motifs' 2D <−> 3D transitions. (a) Transition from 2D to 3D and back. From left to middle: The addition of extension strands makes the hairpin strand expand into a double helix, in turn increasing the distances between the central five-arm vertices. This makes the 3D structure flatten into a 2D structure. From middle to right: The addition of fuel strands extracts the extension strands from the structure, turning the 2D structure back into a 3D structure. (b) AFM images of the respective steps in (a), confirming the formation of the two structures.

We employed similar designs and characterizations for three-, four-, and six-arm motifs as well. Variation in the number of arms offered the system flexibility in terms of tuning the heights and angles of the resulting 3D structures. The predicted changes in height and angles for the different arm numbers are shown in Figure 4.10. Interestingly, AFM showed that the difference between the 3D and 2D states was more prominent in the five- and six-arm motifs than in the three- and four-arm motifs. To determine the cause of this difference, we conducted molecular dynamics simulations of the structures.
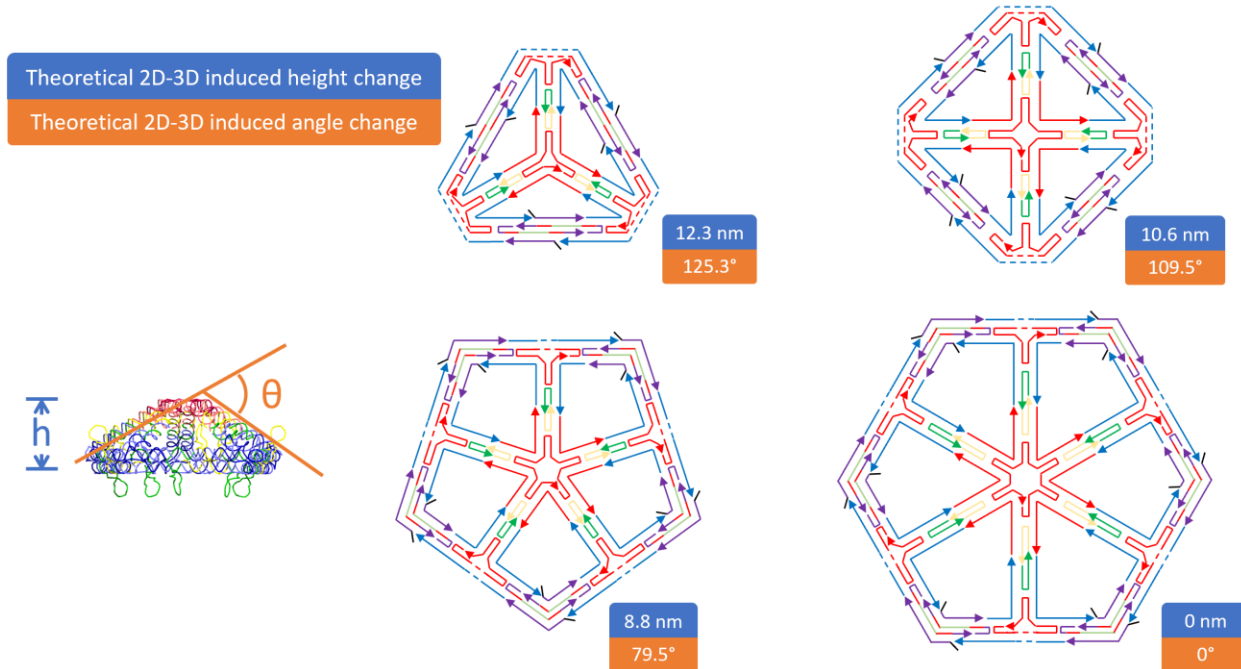
Figure 4.10: Designs of three-, four-, five-, and six-arm motifs and their respective theoretical 2D-3D transformation–induced height and angle changes.

4.2.4 Coarse-Grained Model Simulations

To study the morphology of the structures, we performed DNA simulations using oxDNA [10], a coarse-grained model that offers the possibility of molecular-scale observation. There are also atomic-scale calculation methods, which are computationally extremely expensive. Moreover, on an atomic scale, it is difficult to simulate larger structures, or simulation requires an extremely long time and a heavy computational load. To access longer timescales, mesoscale, or coarse-grained, models have been widely used in the DNA simulation field. These models regard DNA as a simpler consists. OxDNA is a coarse-grained model developed to study the self-assembly and mechanical properties of DNA structures. It regards each nucleotide as a

rigid body with several interaction sites, including the backbone, base repulsion, stacking, and hydrogen boding (Figure 4.11). OxDNA has been shown to produce excellent representations of DNA structures, including 3D structures, DNA origami, and toehold-mediated strand displacement (TMSD). We implemented molecular dynamic (MD) simulations of our TMSD-triggered conformation change in our design. We performed the MD simulations in a monovalent salt concentration of 0.5 M sodium ion at room temperature (298 K). High salt concentrations are widely used for DNA structure simulations to screen repulsive interactions. Because our design greatly depends on the DNA sequence, we used sequence-dependent DNA interaction. We ran each structure at least 10^6 steps to achieve a more realistic state.
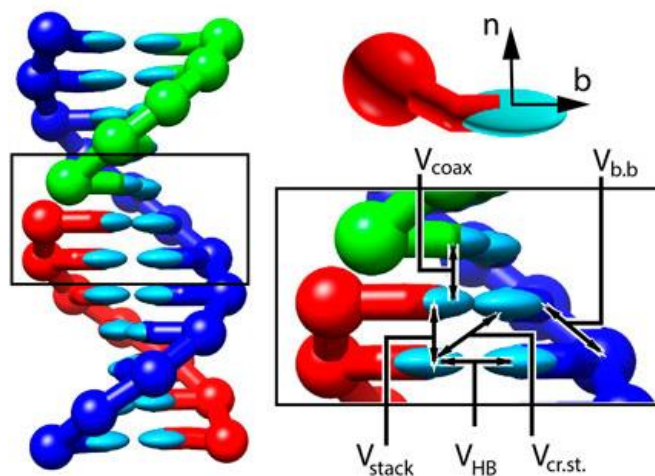
Figure 4.11: OxDNA model of a nicked DNA duplex formed by three DNA strands.

As shown in the simulation images in Figure 4.12, the three-arm structure was strained and was not completely flat in the 2D state. When it was transformed to the 3D state, the change of angle was so sharp that its shape was like in the 2D state. For this reason, the three-arm 2D and 3D states also looked similar in AFM. Conversely, the five-arm 2D motif stretched and expanded into a flat structure, and the 3D state was visibly more compact. This was consistent

with the AFM images. The sizes were also consistent in the simulation results and the AFM images. For the 2D to 3D transition, the circumradius (measured using ImageJ) in AFM changed from 12.9 to 11.9 nm, while the simulation results showed a change from 11.9 to 9.9 nm. The area of the 2D five-arm motif was 1498 nm2 according to AFM and 1556 nm2 according to the simulation results (Table 5.1). The simulation results indicated that the linker length was not optimal for the three-arm structures. It is likely that the strain caused by the double crossover, which was not taken into consideration, ultimately caused the smaller-than-expected linker domain length.
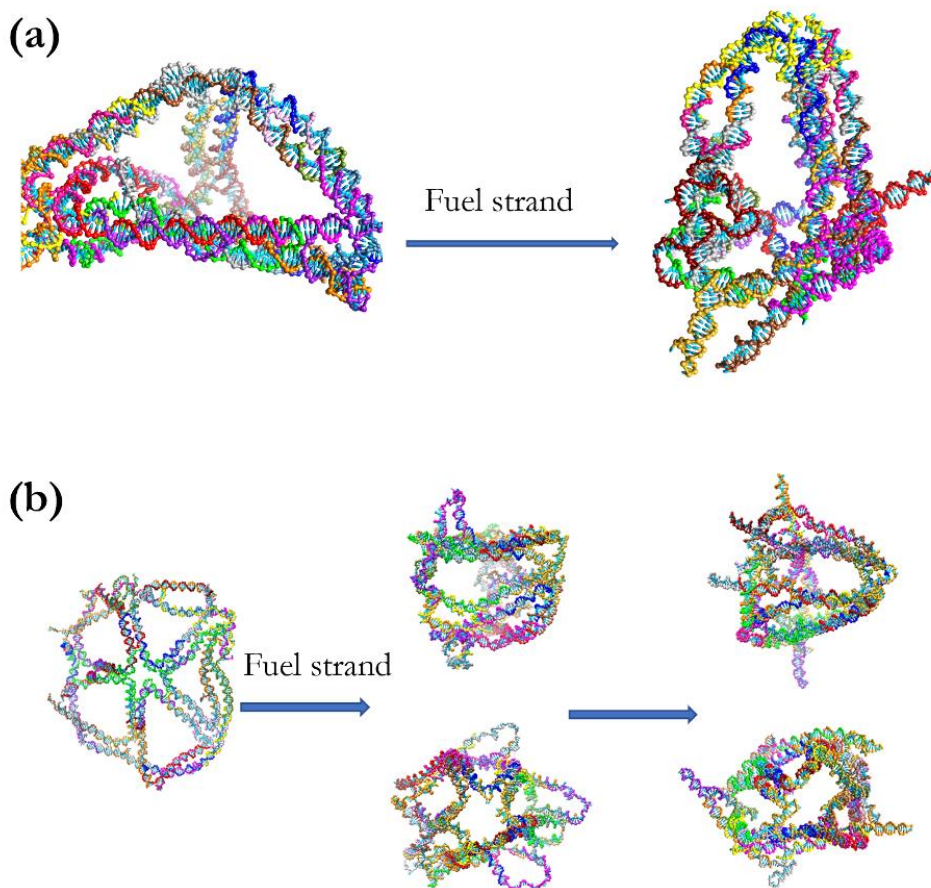
Figure 4.12: Simulation results of the shapes of three- and five-arm motifs. (a) Three-arm motif transformation from 2D to 3D. (b) Five-arm motif transformation from 2D to an intermediate state to 3D.

118

To optimize the structure, the linker length needs to be reassessed. Nonetheless, the goal of this part of the investigation—that is, to design a reversible transformation mechanism with DNA nanostructures—was achieved.

Table 4.1: Statistical Size of oxDNA model and AFM image

Design	oxDNA simulation	AFM
Pentagon	1556.020	1498.321
Triangle 2D	11.861	12.885
Triangle 3D	9.866	11.937

4.2.5   Conclusion

In this study, we developed a general strategy for the construction of transformable DNA nanostructures. A flat nano-object can be transformed into a convex form. We also demonstrated the highly programmable properties of DNA nanotechnology. With an accurate design, the DNA single unit shows a conformational change in nanometers and a controlled, multistep, reversible DNA structure. Furthermore, we performed molecular-level simulations to visualize the details of the structures. Molecular-level simulation can help further understand the design of DNA structures and may become an excellent tool for predicting structures.

4.2.6   Methods

DNA purification. Crude DNA strands were manufactured by Integrated Device Technology (IDT) with a designed sequence. They were further purified using a 20% denaturing PAGE gel in a TBE buffer.

Formation of DNA three-arm motifs. The DNA strands forming the individual three-arm motifs were mixed in a $1\times$ TAE/Mg^{2+} buffer under native conditions. They were then placed in a PCR cycler, heated up to 90°C for 5 min, and then left to slowly cool down to room temperature.

Polyacrylamide gel electrophoresis. A 5% native PAGE gel in TAE/MES (pH 7.4) and MES (pH 5.5) buffers was run at the same condition under 100 V for 50 min. The gel was then stained with stains-all for 30 min, followed by de-staining in water under white light. The gel was then scanned.

Atomic force microscopy. Tapping mode in a liquid was used for the DNA structures. The samples were imaged in a TAE/Mg^{2+} buffer. An SNL-10 tip (Bruker) with a spring constant of 0.24 N/m was used on a multimode AFM instrument (Veecco Metrology). The amplitude setpoint was controlled at the lowest possible value to avoid scratching the structure.

DNA simulations. DNA simulations were performed using oxDNA at a monovalent salt concentration of 0.5 M Na$^+$ at room temperature (298 K). Sequence-dependent DNA interaction was used. Simulation of each structure was run at least 10^6 steps. The length of the edges and distances between corners were measured using a Chimera instrument (UCSF). The average circumradius of 5,000 structures was calculated.

Section 4.1, in its entirety, is a paper prepared for submission to a journal for publication.

Xiangyi Dong and Yi Chen. The author of this dissertation is the investigator and first author of this paper.

Section 4.2, in its entirety, is a part of a paper prepared for submission to a journal for publication. Sibai Xie, Xiangyi Dong, Mingxuan Kai, and Yi Chen. The author of this dissertation is a co-first author of this paper and the main contributor to the simulation study.

4.3   Reference

[1] Ju C, Mo R, Xue J, Zhang L, Zhao Z, Xue L, Ping Q, Zhang C. Sequential intra-intercellular nanoparticle delivery system for deep tumor penetration. Angewandte Chemie. 2014 Jun 10;126(24):6367-72.

[2] Molla MR, Marcinko T, Prasad P, Deming D, Garman SC, Thayumanavan S. Unlocking a caged lysosomal protein from a polymeric nanogel with a pH trigger. Biomacromolecules. 2014 Nov 10;15(11):4046-53.

[3] Jia J, Wang C, Chen K, Yin Y. Drug release of yolk/shell microcapsule controlled by pH-responsive yolk swelling. Chemical Engineering Journal. 2017 Nov 1;327:953-61.

[4] Abandansari HS, Nabid MR, Rezaei SJ, Niknejad H. pH-sensitive nanogels based on Boltorn® H40 and poly (vinylpyridine) using mini-emulsion polymerization for delivery of hydrophobic anticancer drugs. Polymer. 2014 Aug 5;55(16):3579-90.

[5] Rich A. DNA comes in many forms. Gene, 1993, 135(1-2): 99-109.

[6] Idili A, Vallée-Bélisle A, Ricci F. Programmable pH-triggered DNA nanoswitches. Journal of the American Chemical Society. 2014 Apr 23;136(16):5836-9.

[7] Yoon K, Hobbs CA, Koch J, Sardaro M, Kutny R, Weis AL. Elucidation of the sequence-specific third-strand recognition of four Watson-Crick base pairs in a pyrimidine triple-helix motif: T. AT, C. GC, T. CG, and G. TA. Proceedings of the National Academy of Sciences. 1992 May 1;89(9):3840-4.

[8] Gao W, Zhang L, Zhang YM, Liang RP, Qiu JD. DNA colorimetric logic gates based on triplex–helix molecular switch. The Journal of Physical Chemistry C. 2014 Jul 3;118(26):14410-7.

[9] Chen Y, Lee S H, Mao C. A DNA nanomachine based on a duplex–triplex transition[J]. Angewandte Chemie International Edition, 2004, 43(40): 5335-5338.

[10] Liu Z, Li Y, Tian C, Mao C. A smart DNA tetrahedron that isothermally assembles or dissociates in response to the solution pH value changes. Biomacromolecules. 2013 Jun 10;14(6):1711-4.

[11] Zhou T, Chen P, Niu L, Jin J, Liang D, Li Z, Yang Z, Liu D. pH-Responsive Size-Tunable Self-Assembled DNA Dendrimers. Angewandte Chemie International Edition. 2012 Nov 5;51(45):11271-4.

[12] Zhou L, Gao M, Fu W, Wang Y, Luo D, Chang K, Chen M. Three-dimensional DNA tweezers serve as modular DNA intelligent machines for detection and regulation of intracellular microRNA. Science advances. 2020 May 1;6(22):eabb0695.

[13] Cangialosi A, Yoon C, Liu J, Huang Q, Guo J, Nguyen TD, Gracias DH, Schulman R. DNA sequence–directed shape change of photopatterned hydrogels via high-degree swelling. Science. 2017 Sep 15;357(6356):1126-30.

[14] Yurke B, Turberfield AJ, Mills AP, Simmel FC, Neumann JL. A DNA-fuelled molecular machine made of DNA. Nature. 2000 Aug;406(6796):605-8.

[15] Yan H, Zhang X, Shen Z, Seeman NC. A robust DNA mechanical device controlled by hybridization topology. Nature. 2002 Jan;415(6867):62-5.

[16] Liu M, Fu J, Hejesen C, Yang Y, Woodbury NW, Gothelf K, Liu Y, Yan H. A DNA tweezer-actuated enzyme nanoreactor. Nature communications. 2013 Jul 3;4(1):1-5.

[17] Ke Y, Meyer T, Shih WM, Bellot G. Regulation at a distance of biomolecular interactions using a DNA origami nanoactuator. Nature communications. 2016 Mar 18;7(1):1-8.

[18] Sherman W B, Seeman N C. A precisely controlled DNA biped walking device[J]. Nano letters, 2004, 4(7): 1203-1207.

[19] Yin P, Yan H, Daniell XG, Turberfield AJ, Reif JH. A unidirectional DNA walker that moves autonomously along a track. Angewandte Chemie. 2004 Sep 20;116(37):5014-9.

[20] Omabegho T, Sha R, Seeman N C. A bipedal DNA Brownian motor with coordinated legs[J]. Science, 2009, 324(5923): 67-71.

[21] Yin P, Choi HM, Calvert CR, Pierce NA. Programming biomolecular self-assembly pathways. Nature. 2008 Jan;451(7176):318-22.

[22] Lund K, Manzo AJ, Dabby N, Michelotti N, Johnson-Buck A, Nangreave J, Taylor S, Pei R, Stojanovic MN, Walter NG, Winfree E. Molecular robots guided by prescriptive landscapes. Nature. 2010 May;465(7295):206-10.

[23] Doye JP, Ouldridge TE, Louis AA, Romano F, Šulc P, Matek C, Snodin BE, Rovigatti L, Schreck JS, Harrison RM, Smith WP. Coarse-graining DNA for simulations of DNA nanotechnology. Physical Chemistry Chemical Physics. 2013;15(47):20395-414.

Chapter 5

Summary and Prospective Research

Directions

In this dissertation, dynamic DNA structures were investigated to unveil their potential as a next-generation drug delivery system. We presented a DNA nanogel system and showed that dynamic DNA structures could be used for drug release. Through accurate design, we could obtain the desired DNA structures and mechanisms that can be used to create drug delivery carriers with pH-responsive release properties. The DNA nanogel system could successfully reduce the IC50 and release more drugs under acidic conditions. The system can carry both small-molecule drugs as well as proteins. Strand displacement-based dynamic structures were designed to achieve a series of reversible 2D-3D structures. Coarse-grain DNA model molecular dynamic simulation was applied using OxDNA software to visualize the morphology of the designed structures further, and it showed potential power in predicting the stability of DNA drug delivery system designs.

5.1 DNA Dynamic Structures

Nanotechnology has been developed to overcome inherent difficulties within the domain of traditional medicine. Various nanoparticle drug delivery platforms have been investigated, such as inorganic particles that can provide external trigger release like magnetic fields. Liposomes have been widely developed and account for the majority of approved nanoparticle formulations. Polymer-based nanoparticles like PEG conjugations can prolong the circulation time, while antigen conjugation can improve the targeting effect to enhance drug delivery and eradicate side effects. However, challenges still exist in current drug delivery systems. For instance, toxicity should be removed from inorganic particles and liposomes still need to be developed further to improve their loading efficacy without increasing their toxicity (e.g., cationic liposome particles enhance the RNA loading efficacy, but high concentrations of cationic liposomes cause toxicity to the body). In addition, polymer-based nanoparticles involve complex manufacturing procedures and have biocompatibility limitations. All pre-existing nanoparticle systems have low-programmable designs, which cause non-uniform size, complexity of functional design, and difficulty in achieving multifunctionality. DNA nanotechnology has developed in the past 30 years, and the specific bonding of base pairs can be used to form structures by self-assembling with accurate sequence design. Moreover, DNA nanotechnology can provide a dynamic function that can achieve a targeting effect and trigger release and surface modification using pure DNA without any modification. Chapter 1 summarized the previously reported DNA dynamic motifs, including strand displacement motors, DNAzyme motors, i-motif motors, triplex-based motors, and G-quadruplex/aptamer motors. In this dissertation, we proposed and constructed dynamic DNA nanogel structures for application in the drug delivery field.

5.1.1 Dissociable DNA Nanogel

During endocytosis, the pH of endosomes decreases from 7.4 to approximately 5. In some viruses such as human influenza, the virus travels along the endocytic system, and the acidic pH causes a conformation change in the HA to enhance envelop fusion, followed by viral core disassembly in the cytosol and viral RNAs entering the nucleus. Inspired by the acid-dissociation properties of viruses, we proposed a dissociable DNA nanogel. In Chapter 2, we demonstrated a dissociable DNA nanogel whose most important building unit is its crosslinker design. Previously reported DNA hydrogels have mainly focused on the duplex-based Watson–Crick bonding. The G-quadruplex is a specific DNA motif in which four G bases form a square planar structure, and each G interacts with two adjacent Gs through Hoogsteen binding. A monovalent cation is required to occupy the central position between the G-4 stacks, especially potassium. Notably, the G-quadruplex structure forms instantaneously and shows biostability, which improves heat and denaturation resistance. In the DNA nanogel established, the G-quadruplex was used as the crosslinker. The G-quadruplex-based DNA nanogel was confirmed through electrophoresis and DLS size measurement. We also designed the surface modification sites on the surface of the DNA nanogel. Un-hybridized 20A base overhangs can be found on the surface of DNA nanogel. The 20A overhang can later hybridize with the 20T strands through self-assembly. We only have to modify the 20T strands according to the purpose of each disease. In this dissertation, to achieve folic acid-targeting effect, we modified the 20T strands with PEG-folic acid. After the nanogel formation, the overhang 20A strands on the surface of DNA nanogel will be hybridized with the modified 20T.

To achieve the virus-mimicking pH-dissociation property, we induced an i-motif sequence into the building blocks. The i-motif sequence, which contains poly-cytosine, tends to

form quadruplex structures under acidic conditions due to the protonation of the cytosine bases. Meanwhile, under physiological conditions, the C bases tend to hybridize with the complementary G bases. Under acidic condition, cytosine pronation makes the energy more conducive to the formation of Hoogsteen bonds with cytosine (C:C+) to form a quadruple structure instead of a hybridized duplex structure. Then, the DNA nanogel dissociates. After the drug is loaded in the nanogel, it is released. The dissociable DNA nanogel was confirmed through electrophoresis, AFM, and DLS size measurement. Results indicate that the dissociable DNA nanogel size decreases by half and has a higher mobility under pH 5.5 compared with a pH that is under 7.4.

Doxorubicin was used as a test drug not only because it is a widely used cancer drug that can intercalate into the DNA duplex but also because of its intrinsic fluorescence property. When Dox is intercalated into the DNA duplex, the Dox signal is quenched by Froster energy transfer between Dox molecules, whereas the dissociation of a Dox-loaded duplex causes the release of Dox. Under pH 7.4, when DNA nanogel is added into the Dox solution, the Dox signal will be quenched, which indicates that the Dox was loaded into the duplex. When the pH is adjusted to 5, pH-insensitive DNA nanogel showed 16% fluorescence signal recovery due to the pronation of Dox, which makes it easier to diffuse. By contrast, dissociable DNA nanogel showed 56.5% fluorescence signal recovery. The fluorescence signal recovery indicates that Dox was released from the duplex, which means our dissociable DNA nanogel releases threefold more Dox compared with the pH-insensitive DNA nanogel. Release from a membrane system was mimicked by dialysis against the membrane. The dissociable DNA nanogel showed 20% more release within 4 hours compared to the pH-insensitive DNA nanogel and a further 10% after 20 hours.

Cell-based assay was used to further investigate the dissociable DNA nanogel system. Co-localized Dox fluorescence and DAPI-stained cells confirmed Dox accumulation at the nucleus. The Dox-loaded dissociable DNA nanogel showed higher cytotoxicity (15% cell viability) to the targeted cancer cell lines (MCF-7 and MDA-MB-231) after 12 hours of incubation compared with the pH-insensitive DNA nanogel. Dosage response was operated on KB cell lines. The dissociable DNA nanogel decreased the IC50 to 0.5 μM from 1. 78 μM (pH-insensitive DNA nanogel).

The results underscore that we successfully established a G-quadruplex-based DNA nanogel. By changing the sequence to i-motif design, we achieved an acid-dissociated DNA nanogel. Small-molecule drug Dox was tested in the system, and enhanced delivery efficacy to cancer cells was achieved. To further develop the DNA nanogel, we proposed using the DNA nanogel system to load proteins.

5.1.2 Protein Encapsulation

Therapeutic proteins are showing more significant contributions to novel drug development. They are widely used in immunology, infectious diseases, genetic diseases, and other fields. However, the manufacturing of therapeutic protein is complex because in achieving the targeting effect and release mechanism, it is highly challenging to maintain the complex protein conformation. During the process, there are multiple parameters that could affect the final protein products, including culture condition, conjugation environment, and unexpected conformation changes. There are different nano-carriers for protein delivery. However, it is still a major challenge to use conventional nano-carriers to deliver unmodified, functional proteins

with their active conformation and functions to the sites of interest. The nano-carriers used to deliver protein, including the covalent binding of the proteins to the vehicle, will apply irreversible modifications on the structural conformation and function, including some DNA–protein complexes. Since the DNA nanostructure is formed through self-assembled hydrogen bonding, in this chapter, we expanded the DNA nanogel system to encompass protein encapsulation.

After replacing the potassium chloride with potassium glutamate, the interaction between the DNA and the protein improved. Both negatively charged protein-like IgG and positively charged protein-like Avidin were successfully loaded into our DNA nanogel system, which makes our platform a potential benchmark for various drug deliveries. Electrophoresis and AFM images were used to confirm the encapsulation. The co-localization of the protein-stained signal and the DNA-stained signal demonstrated the encapsulation of protein. The AFM images also showed that the protein-encapsulated DNA became larger than the pure DNA nanogel. By measuring the zeta potential, we noted that the surface charge of the DNA nanogel was changed by the loaded protein, which indicates that there are some protein sites on the DNA surface.

To test the activity of protein after it was encapsulated by DNA, we used *E. coli* to test the IgG Fc binding ability because it has been reported that *E. coli* expresses the Fc receptor. *E. coli* was stained by SYBR gold and the DNA was labeled by Alex 647. We observed the aggregation of both SYBR gold and Alex 648 only in the mixture of *E. coli* and IgG-embedded DNA. The physical mixture of DNA nanogel, IgG, and Dox showed a well-distributed DNA signal. The co-localized signal indicates that the DNA nanogel was brought to the *E. coli* because of the Fc-receptor binding between *E. coli* and the encapsulated IgG. The aggregation of *E. coli* and the IgG-embedded DNA nanogel was also observed under SEM, which is consistent

129

with the fluorescence observation. The result supports that the self-assembled protein-embedded DNA preserves the binding ability of IgG. Dox was loaded in the IgG-embedded DNA nanogel, and it was loaded to the KB cells which express the Fc Gamma receptors. The cytotoxicity test showed that the IgG-embedded DNA nanogel has a 20% lower IC50 compared with the physical mixture of IgG, DNA, and Dox.

Therefore, we successfully proved that our DNA nanogel system can be extended to protein encapsulation. Further research should be developed focusing on the quantity of the embedded protein, the spatial orientation of the embedded protein, as well as therapeutic proteins like CD 55 antigen and Her2 inhibiter instead of IgG.

5.1.3 Reversible DNA Nanogel

Aside from dissociable drug delivery systems, a swellable system can also improve the efficacy of drug delivery. Swellable systems usually show reversible conformation change, which makes them reusable and results in sustained drug delivery, deep penetration, and possible dosage reduction.

The triplex DNA structure exhibits conformation change under different pH. We designed a reversible switch unit to achieve close and expanded conformation. By optimizing the design, we achieved a swellable DNA nanogel with a swollen ratio of 1.66, which is comparable to existing swollen platforms. Noticeably, most of the existing swollen platforms require long pH response times, while our reversible DNA nanogel changes immediately after pH change. The cytotoxicity investigation also supports that our swellable DNA nanogel can improve the drug delivery efficacy. After 24 hours of incubation with the targeted cancer cell

line, the swellable DNA nanogel showed an IC50 of 0.5 µM, whereas the pH-insensitive DNA nanogel had an IC50 of 1.8 µM.

This study is the first to utilize the DNA triplex motif to produce a swellable pH-responsive DNA nanogel based on a G-quadruplex structure for drug delivery. We tested the conformation change under different pH through electrophoresis and DLS size measurement. The improved drug delivery property was confirmed by a cytotoxicity test. The mechanism through which the swellable DNA nanogel releases drugs from the endosome still needs further investigation. It is highly possible that the reversible and reusable conformation change can achieve deep penetration. Furthermore, the drug-releasing formulation on the reversible carrier would be of interest in future research. Different from the dissociable DNA nanogel in which all the drugs loaded in the nanogel pore are released upon dissociation, the swollen nanogel only releases the drugs loaded in the duplex, while the drugs loaded inside the pore are released by diffusion. Thus, it is highly possible to preserve the drugs that are not necessary for use. After cell apoptosis, the pH will change back to pH 7.4, the nanogel will shrink, and the drug that has not been used can again be loaded into the shrunken nanogel. Thereafter, the nanogel can target the next cell, thereby increasing penetration and decreasing the clinical recommended dosage.

5.1.4 Simulation of DNA Dynamic Structure

In addition to pH-responsive motifs, other DNA structures include nanomachines, 2D arrays and 3D structures. The reported dynamic DNA structures can sense a variety of physical or chemical cues, but they only exhibit dynamic behaviors in a single unit and small-range changes and cannot undergo dimensional transformation. Chapter 4.2 presented a series of 2D-

3D reversible structures that achieved conformational change through toehold-mediated strand displacement. The series of 2D-3D structures were built with repeatable units that formed three-arm, four-arm, five-arm, and six-arm structures.

Electrophoresis and AFM images confirmed the reversible behavior. However, we were unable to conduct an in-depth examination of the structure to understand why the three-arm design shows negligible particle size change under AFM, while the five-arm design manifests a larger change. A coarse-grain DNA model was used to perform MD simulation and obtain a better visualization of the DNA base-level structures. This helped establish that the design problem on the three-arm was that the linker length was not optimal due to the strain caused by the double crossover on the edge. To optimize the structure, the linker length needs to be re-assessed. In the future, it would be possible to utilize the model to predict the structure morphology.

5.2 Prospective Research Directions

5.2.1 Next-generation Drug Delivery System

Their advantages of programmable design for accurate control, self-assembly for non-covalent bonding, and easy design for modification make DNA nanostructures a potential next-generation drug delivery system.

When considering oligonucleotide delivery, the DNA structure has an irreplaceable advantage. Oligonucleotide drugs have attracted much attention in the past 10 years. Before 2013, only two oligonucleotide drugs were approved by the FDA. However, since 2013, 12 oligonucleotide drugs have been approved. With the sequence-dependent complementary design approach, the DNA nanostructure is very promising for oligonucleotide drugs. Among the approved drugs, eight are antisense oligonucleotides and three are siRNAs. We can modify our structure to load siRNA or antisense oligonucleotide and compare them to existing formulations (oligonucleotide injection, GalNAc, liposome, etc.).

Moreover, we can integrate the antisense drugs into our carrier as a component so that the carrier could be a targeting carrier before it reaches the site of interest and dissociate using different mechanisms (pH change, enzyme concentration, etc.) to serve as the drug. By knowing the existing sequences of oligonucleotide drugs, we can specifically design to built up a carrier with the active pharmaceutical ingredient (API) sequence. For modified API like morpholino, where DNA phosphate backbone was modified to neutral charged, we should take the neutralized backbone into consideration.

5.2.2 DNA Nanogel System Benchmark

We established a DNA nanogel system that has the ability to load small-molecule drugs like Doxorubicin (~600 Da) and large drugs like Avidin (68 kDa) and IgG (~150 kDa). To establish the DNA nanogel system benchmark, further studies should focus on therapeutic drugs with different molecular weights. Drug loading, release, and delivery to the cell should be tested as well.

In this dissertation, we used folic acid to modify the surface. We can also test other functional candidates like aptamers and CD 44 receptors, as well as the RGD and LNX. The modification percentage also needs to be calibrated, followed by testing the targeting efficacy after surface modification.

The swellable DNA nanogel, we expected the swollen behavior may improve the endosome escape and tumor site penetration. The *in vitro* and *in vivo* pharmacokinetics and endosomal tracing experiment will be the next step.

We tested the in vitro behavior of the Dox-loaded DNA nanogel. After the in vitro test, in vivo experiments will be the next step. We can use fluorescence-labelled DNA strands to manufacture the DNA nanogel, and the in vivo bio distribution will be investigated. For example, we can use a Cy5.5-labelled drug-loaded DNA nanogel for testing in tumor-bearing mice, then near-infrared optical imaging technique can be leveraged to detect the bio-distribution of the DNA nanogel. Drug accumulation in different tissues, as well as tumors, will also be studied, followed by testing tumor growth inhibition and toxicity. The elimination half-time and mean residence time of the drug-loaded DNA nanogel can be investigated by analyzing the plasma concentration versus the time curves.

5.2.3 Behavior-driven DNA Molecular Structure Design

Many experimental measurements (e.g., electrophoresis, AFM, SEM, DLS) can be utilized to understand the dynamics of DNA molecules at specific conditions, including salt concentration, pH value, and replacement strand presence. However, carrying out a direct observation of DNA transformation or reaction is still difficult, thus setting a high barrier to understanding the reaction dynamics. In the field of drug delivery, the DNA is one of the most promising candidates in next-generation delivery systems. The dynamics of the DNA structure in loading and releasing drugs are critical to guide the development of a DNA drug delivery system.

Computational simulations for nucleotides have been widely used. For example, Schreck et al. used the OxDNA model to simulate large nanoprisms that are composed of multi-arm star tiles. The OxDNA model predicts equilibrium structures for different designs that are consistent with cryo-TEM results. Similarly, we applied molecular dynamics technique in the ongoing work to visualize the structure change. As a result, the computational simulations not only reproduced the morphology we observed using AFM but also revealed the reaction path in which the 2D structure evolves into the final 3D structure. This simulation took about 24 hours, running in parallel on a 16-core node. Considering the inexpensive computing cost and inspired by the insightful findings, we could reasonably extend the current work to a more general scope.

Enumeration is a method that is widely applied in chemistry and solid-state physics to generate a group of possible structures from a disordered source. With the advancements in computing power and the advent of structure-generating codes, high-throughput materials design is now a reality, which has greatly hastened the discovery of new materials. We can borrow this

concept and apply similar techniques to generate DNA molecules of interest, but at the coarse-grain level instead of at the atomic level. For dynamic DNA structures, the critical issue is how to design a carrier candidate that fits our needs, for example, a 2D-3D reversible structure. Experiments usually start with a design, which goes through endless trials and errors of modifications until, finally, the appropriate candidate is determined. This process may take years and, even then, success is not guaranteed. Fortunately, the properties of DNA bases are quite well known, and our focus is more on the topological structure and transformation between different states, which makes molecular dynamics a perfect tool to carry out this investigation.

Here, I present a conceptual outline of my potential work. We could start with a set of prototypical structures that are of great interest in current drug delivery, including 2D-3D structures. A few possible modifications can be undertaken, such as changing the length of crossovers or sequence arrangements. Molecular dynamics will be able to reveal the structural transformation triggered by pH change and the comparable stability of the structure. It is known that computational and experimental results are not exactly matched since a simulation mimics the performance in an ideal environment. However, it is sufficient to capture the trend and can contribute to shortening the lab research time.